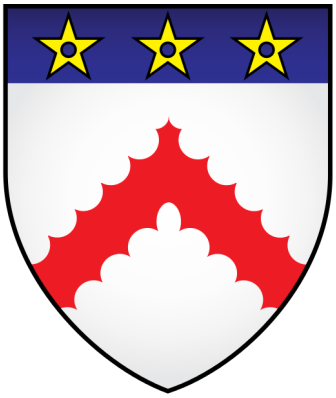

Investigation and Validation of The Functional Role of sMEK1 Acetylation in DNA Damage Repair and HDACi-mediated Radiosensitisation

MSc by Research Thesis

Supervised by
Prof Anne Kiltie

Xin Ying Yeo

Keble College

CRUK/MRC Oxford Institute for Radiation Oncology
Department of Oncology
University of Oxford

Trinity Term 2018

ACKNOWLEDGEMENTS

I would like to express my gratitude to the supervisor, Professor Anne Kiltie, for giving me this golden opportunity to conduct exciting research in her lab, particularly in the area of understanding the molecular mechanism of potential radiosensitiser(s) to improve the treatment outcome of bladder cancer patients. Anne's enthusiasm, her lively and energetic presence as well as the love for science are highly contagious and have had a positive influence on my work throughout this degree. I am also grateful for many of her insightful discussions and guidance that have shaped me strongly as a young independent scientist.

Besides, I will always be immensely thankful to the postdoctoral researchers in the group, Dr Judith Nicholson and Dr Juri Na, who were assigned as my co-supervisors during the year. Both of them are excellent scientists with extensive experience in the field of cancer research, and most importantly offered me their support, assistance and invaluable feedback on how to better improve my experimental planning. They have been of enormous help in building my inquisitive and critical thinking skills to accurately analyse the data obtained. A special shout-out also goes to Jude for carrying out the preliminary mass spectrometry acetylome screen to identify the target proteins with a known role in the DNA damage response, which had provided the foundation for further research work and eventually led to my project!

Furthermore, I thank all the other members in the Kiltie's group: Jia-Ling Ruan, Edward Ottley, Salome Paillas, Susan Kilgas and Jessica Gorrill. It was a wonderful experience to be working alongside and sharing the laboratory with them. Apart from learning a lot about effective team work, they also provided me with the friendship which I will

continue to cherish for the many years to come. I wish them all the best in their careers and hope our paths will cross again in the near future!

Last but not least, I would like to thank my family and friends for their emotional support as well as the Malaysia government for making this a dream came true to study in the University of Oxford.

DECLARATION

This dissertation is submitted for the degree of Master by Research in Oncology. I hereby declare that the results presented in this thesis are all of my own. The dissertation does not exceed the prescribed word limit.

ABSTRACT

Muscle-invasive bladder cancer (MIBC) most commonly affects the elderly with more than half of new diagnoses in the over 75-year age group. This means there is a need for less toxic treatments to improve treatment outcomes. Histone deacetylase inhibitors (HDACi) have emerged as effective, low toxicity radiosensitising agents, although the mechanism of radiosensitisation is not fully defined. This study investigates the radiosensitising effects of the HDAC inhibitor panobinostat (PAN) via a mechanism involving increased acetylation of non-histone proteins.

This project aimed to validate acetylation sites in non-histone proteins which were identified in a mass spectrometry screen following PAN treatment, and to investigate their functional roles in radiosensitisation. I hypothesised that specific acetylation sites in non-histone proteins could have vital roles in the DNA damage response (DDR). Of the identified acetylated non-histone proteins, suppressor of MEK1 (sMEK1), the regulatory subunit of serine/threonine-protein phosphatase 4 complex, was the primary focus, as it can act as a phosphatase for gamma H2A.X (γH2AX) upon completion of DNA repair. Cell lines were transfected with sMEK1 and subjected to PAN treatment and/or ionising radiation (IR) to detect time-course changes of DDR protein markers. A delayed DDR was observed in PAN-treated cells with persistently increased levels of phospho-ATM and γH2AX at 4 hours after recovery from IR, consistent with the radiosensitising activity of PAN. Endogenous sMEK1 protein was downregulated independent of PAN concentration between 8-24 hours, potentially through the regulation of mRNA expression. Reciprocal co-immunoprecipitations using anti-acetyl lysine and anti-HA antibodies confirmed the acetylation status of sMEK1 following PAN treatment. A transient interaction with the most abundant bromodomain protein, BRD4, was also detected in the chromatin compartment. Subcellular fractionation

indicated significant nuclear localisation of sMEK1 immediately after IR in control DMSO cells, followed by migration to the chromatin fraction 4 hours later for γH2AX elimination. However, this was disrupted by PAN which resulted in less chromatin localisation at 4 hours after IR and higher levels of γH2AX than control. Downregulating endogenous sMEK1 in the cells via siRNA transfection not only resulted in an increase in radiosensitivity, but also a delay in the induction of the DDR, as indicated by a slower γH2AX signal intensity achieved at 2 hours. This supports the hypothesis of sMEK1 being a key protein in PAN radiosensitisation through its loss-of-function in the DDR pathway and changes in subcellular localisation.

In conclusion, I have shown that sMEK1 is regulated by PAN treatment and is acetylated. sMEK1 could therefore represent a clinically promising new radiosensitising drug target or biomarker to be further validated.

TABLE OF CONTENTS

1. INTRODUCTION

1.1 Overview

The molecular mechanism of histone deacetylase inhibitor (HDACi)-mediated radiosensitisation is an interest of our group, and we have so far investigated panobinostat (PAN), which is a pan-HDAC inhibitor. We are interested in identifying potential radiosensitising agent(s) with high tumour selectivity to minimise the systemic toxicity of chemoradiation in elderly patients diagnosed with muscle-invasive bladder cancer (MIBC). HDAC inhibition is a promising approach. A number of non-histone targets differentially regulated by PAN treatment and ionising radiation (IR) with known roles in the DNA damage repair pathway were discovered from a mass spectrometry screen. These included the suppressor of MEK1 (sMEK1) that acts as a regulatory subunit of serine/threonine-protein phosphatase PP4 complex, involved in γH2AX resolution during the late phase of the DDR. Investigating potential roles for sMEK1 in the DDR provided the basis for this research project.

1.2 Muscle-invasive bladder cancer (MIBC)

Bladder cancer is the tenth most common cancer in United Kingdom with approximately 10,300 new diagnoses annually, accounting for 3% of the total cases across all cancer types (Cancer Research UK, 2015). Many risk factors have been identified to date, including age, carcinogens like tobacco, occupational exposures, family history, genetic mutations of HRAS/Rb1/PTEN and chronic inflammation (Lindor et al., 2008; Gallagher et al., 2010). It has been demonstrated that smokers with less functional polymorphisms of N-acetyltransferase-2 (NAT2) slow acetylator

phenotype possess reduced ability to detoxify carcinogens, and this correlates to a higher risk of bladder cancer (Brennan et al., 2001; Kirkali et al., 2005).

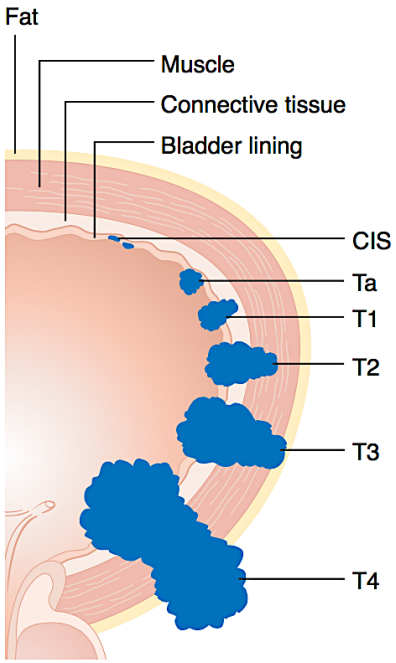

Figure 1-1. Human urinary bladder system showing the T stages of bladder cancer. Specialised mucous membrane, transitional epithelium otherwise known as urothelium forms the lining from the renal pelvis to the proximal urethra, which upon mutations can result in the development of urothelial (transitional cell) carcinoma anywhere along this pathway. There are five main T stages of bladder cancer:
Ta - cancer affects the innermost layer of the bladder lining;
T1 - cancer has grown into the connective tissue beneath the bladder lining;
T2 - cancer has grown into the muscle layer of the bladder;
T3 - cancer has grown through the muscle layer;
T4 - cancer has grown outside the bladder or into neighbouring organ(s) or into the wall of the pelvis.
Abbreviations: CIS, carcinoma in-situ; T, tumour. The figure is adapted from Cancer Research UK (CRUK, 2015).

In addition to urothelial carcinoma formation as outlined in Figure 1-1 representing the major histological subtype, squamous cell carcinomas, adenocarcinomas, small cell carcinomas and sarcomas are also found in the bladder. Bladder cancer can be further divided into muscle-invasive and non-muscle-invasive disease based on the extent of invasion of the muscularis propria embedded deep in the bladder wall.

Current therapeutic options are neoadjuvant chemotherapy followed by surgical removal of the bladder (cystectomy) and pelvic lymph node dissection, or bladder-preserving treatment consisting of transurethral tumour resection and radiotherapy with or without concurrent chemotherapy (Stenzl et al., 2011). Ionising radiation (IR) induces DNA damage, especially double-strand breaks (DSBs) which are toxic to the cells, and failure to repair such lesions prevents cells from dividing correctly and even leads to apoptotic cell death. Since more than half of the new cases are in over 75-year

age group, many are neither suitable for radical cystectomy nor able to tolerate nephrotoxic chemotherapy. Therefore, there is an urgent rising need to find less systemically toxic radiosensitising agents with minimal exacerbation of the local toxicity of radiation in surrounding normal tissues, to widen the treatment options and improve survival outcomes among the increasingly elderly patient population (Kotwal et al., 2008; James et al., 2012).

1.3 Genomic instability in cancer

Genomic instability is a double-edged sword: a source of genetic variation beneficial for natural selection and evolution, which can result in age-related illnesses including cancer. Genomic instability is inherent in most, if not all, cancer types and known to be the fundamental enabling characteristic of other cancer hallmark capabilities (Hanahan and Weinberg, 2011). It is defined as a sequential accumulation of mutations combined with clonal selection and expansion, that originates from many different pathways like telomere damage, centrosome amplification and epigenetic modifications as well as DNA insults from intrinsic or extrinsic agents (Ferguson et al., 2015). In the process of carcinogenesis, an accelerated rate of temporary or permanent alteration occurs spontaneously within the genome either at the level of nucleic acid sequences (insertion, deletion, frameshifts, missense and nonsense mutations) or chromosomal rearrangements (gain or loss of the whole chromosomes, end-to-end fusion, deletion, inversion, duplication and translocation of large segments).

Large-scale sequencing and bioinformatic approaches in the Cancer Genome Project and the Cancer Genome Atlas have uncovered specific mutational signatures of DNA damage and errors in DNA repair, out of a remarkable diversity of somatic mutations in various human cancers. A direct causal link is also identified between several DNA

damage response (DDR) genes and cancer susceptibility disorders such as Ataxia-telangiectasia, Bloom syndrome, Lynch syndrome (hereditary non-polyposis colorectal cancer) and Werner syndrome (Lessel et al., 2014; Pearl et al., 2015). A significant proportion of hereditary cancers like breast and ovarian cancers have mutated *BRCA1* and *BRCA2* genes, with compromised double-strand break (DSB) repair by homologous recombination (HR). In most cases however, specific DDR defects are poorly established.

As postulated by the classic mutator hypothesis (Loeb et al., 1974; Nowell, 1976), mutation rates at other genomic sites are elevated as a consequence of defective or loss of DNA repair and maintenance genes, subsequently causing cellular transformation. Constitutive activation of oncogenes such as MYC and RAS, promotes high cellular proliferation and transcriptional activity. Constant firing of replication forks stimulated from origins leads to replication stress, fork collapse and the formation of DSBs due to exhausted pools of deoxynucleotide triphosphate (dNTP). Despite an activated DDR, the damage is not always correctly resolved due to dysfunctional DDR components. Simultaneous disruption of tumour suppressor genes such as p53 and retinoblastoma (RB) protein allows evasion of the damage checkpoint controls in order to proceed through cell cycle, divide and undergo mutagenesis due to unrepaired DNA (Halazonetis et al., 2008).

1.4 DNA damage response pathways

Approximately 70,000 individual molecular lesions occur per day in each of the ~10^{13} cells in the human body (Lindahl and Barnes, 2000), of which 75% are largely single-strand breaks (SSBs). Since DNA is an exclusive permanent repository of the cellular genetic information, cells have acquired enzymes to initiate a highly coordinated

cascade of events, collectively termed as the DNA damage response (DDR), to sense DNA anomalies and mediate repair via inter-connected complex signalling pathways. This ensures faithful maintenance and transmission of the genetic material into daughter generations of cells following mitosis. The vast majority of damage is of endogenous origin during metabolic processes: mis-incorporation of bases by replicative DNA polymerases at a rate of 10^{-4} to 10^{-6} during synthesis (McCulloch and Kunkel, 2008), and spontaneous chemical changes occurring in the DNA such as deamination, depurination and oxidation. Environmental DNA damage can also come from exposure to chemicals and radiation, which result in the formation of pyrimidine dimers, alkylation and mainly cytotoxic double-strand breaks (DSBs). Consequently, human cells have adapted to respond to each type of damage in a very specific manner.

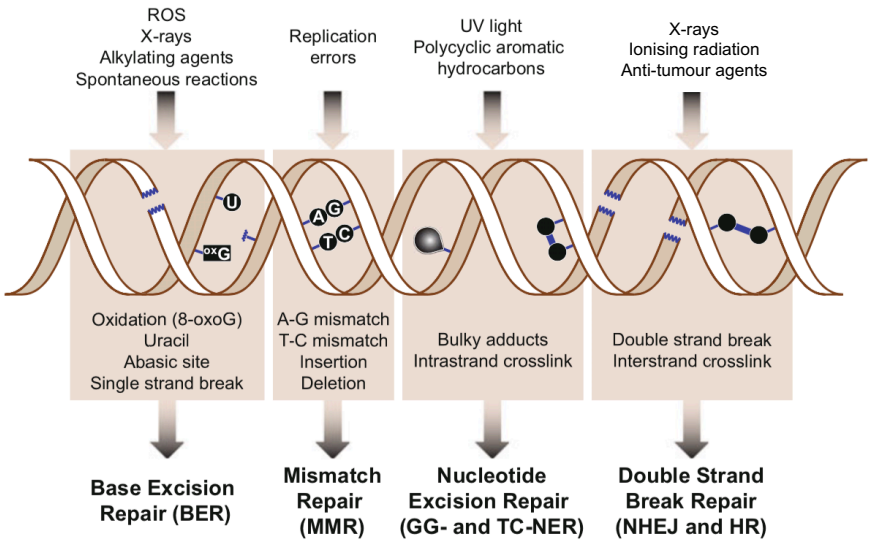

Figure 1-2. Overview of the main DNA lesion types originating from various endogenous or exogenous sources and the corresponding repair mechanisms. The variety of genotoxic lesions present in a cell is matched by the complexity of DNA repair mechanisms. For instance, simple lesions such as base alkylation can be repaired by direct reversal through an enzymatic reaction, while complex damage requires a series of proteins and enzymes for excision repair. DNA double-strand breaks (DSBs) are the most cytotoxic and are resolved by two major pathways: NHEJ and HR.
Abbreviations: ROS, reactive oxygen species; UV, ultraviolet; NHEJ, non-homologous end joining; HR, homologous recombination. The figure is adapted from Boland et al., 2005; Dexheimer, 2013.

All the repair mechanisms illustrated in Figure 1-2, are crucial to correct DNA damage before undergoing replication so that only undamaged DNA is used as template to

transmit genetic information to the next cellular generation. Simple alterations like base alkylation can be stoichiometrically reversed by the enzyme O^6-Methylguanine DNA methyltransferase (MGMT) (Mishina et al., 2006), whereas base deamination and oxidative lesions caused by reactive oxygen species are repaired by lesion-specific DNA glycosylases in base excision repair (BER). Specific proteins can also slide along the surface of DNA molecules, pausing at bulges or irregularities in the double helix shape to recognise a wide spectrum of chemical adducts that distort the local B-DNA structure such as UV-induced pyrimidine dimers and cisplatin-DNA intrastrand crosslinks, and remove bulkier lesions by nucleotide excision repair (NER). Mismatches not removed by the 3'-5' proofreading exonuclease activity of DNA polymerase during replication are corrected by mismatch repair (MMR) machinery that scans the newly synthesised DNA strand to recognise mis-incorporated bases and corrects insertion/deletion loops (IDLs) arising from polymerase slippage when repetitive DNA sequences are replicated. Post-replication repair exists as an alternative pathway to deal with DNA damage at the replication fork.

The repair of DSBs is critical for cell survival and maintenance of genomic integrity. DSBs are constantly formed and repaired during physiological processes, for example in chromosomal crossover in meiosis and V(D)J recombination during lymphocyte maturation for somatic hypermutation or class-switch recombination. The main exogenous sources of damage are ionising radiation (IR) and chemotherapeutic drugs. Cells use one of the two major pathways to repair DSBs - homologous recombination (HR) and non-homologous end joining (NHEJ) (Alt et al., 2013; Khanna and Jackson, 2001); the pathways have differences in the requirement for a homologous template DNA as well as in DSB repair fidelity.

One of the initial important signalling events after DSB formation is phosphorylation of the histone variant H2AX, constituting about 10% of the H2A histones in human chromatin, by multiple protein kinases from the phosphatidylinositol 3-like family including ataxia telangiectasia mutated (ATM) and DNA dependent protein kinase (DNA-PK) (Wang et al., 2005; Rogakou et al., 1998). The addition of a phosphate group on the Serine 139 residue at the histone carboxyl terminus can be detected as soon as 20 seconds after IR-induced DSBs, and the half maximum accumulation of γH2AX occurs by 1 minute when the phosphorylation waves have spread one or more megabases around the DNA break sites (Rogakou et al, 1998). Gamma H2AX (γH2AX) formation is not only involved in the early steps leading up to chromatin decondensation, but it also acts as a major recruitment signal for downstream repair and signalling factors to the nuclear foci as shown in Figure 1-3. Thus, phosphorylated H2AX is widely used as a surrogate marker of DNA damage in experimental methods.

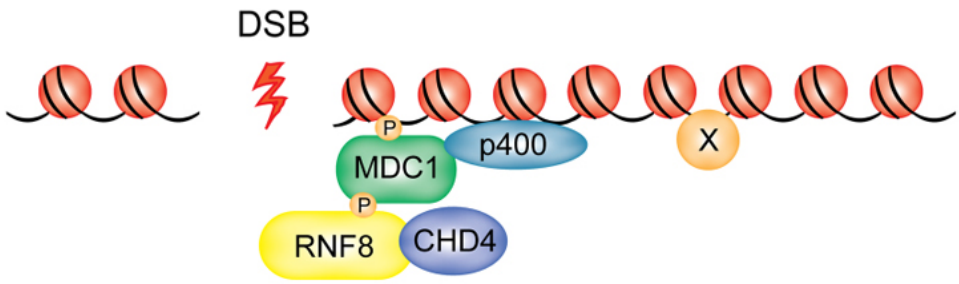

Figure 1-3. The role of γH2AX in chromatin decondensation at DSBs. Within 30 seconds of irradiation, the E3 ubiquitin ligase enzyme ring finger protein 8 (RNF8) is found in association with γH2AX and mediates extensive chromatin relaxation through its interactions with CHD4, a component of the nucleosome remodelling and deacetylase complex (NuRD) (Mailand et al., 2007; Luijsterburg et al., 2012). The figure is obtained from Bartocci and Denchi, 2013.

1.4.1 Double-strand break repair: Homologous recombination (HR)

HR is considered to be the most effective error-free DSB repair with high fidelity, but is restricted to late-S and G2 phases of the cell cycle because it requires the presence of an undamaged sister chromatid as a repair template for the genetic exchange of equivalent

regions of DNA between homologues. In Figure 1-4, HR is initiated by the displacement of the Ku complex and recruitment of the heterotrimeric MRN complex (MRE11-RAD50-NBS1) for DSB recognition (Lee et al., 2016). This allows the meiotic recombination 11 (MRE11) protein to initiate end-trimming and process the DNA ends surrounding the break site with its 3'-5' exonuclease activity. CtBP-interacting protein (CtIP) then performs DNA resection in a 5'-3' direction to generate 3' single-stranded overhangs (Sartori et al., 2007). A combined action of Bloom syndrome RecQ helicase-like (BLM helicase) and 5'-3' exonuclease EXO1 results in subsequent end resection, producing long stretches of single-stranded DNA (ssDNA) which are bound and protected by replication protein A (RPA) (Nimonkar et al., 2008). In conjunction with other mediator proteins such as RAD52 and RAD51 paralogs (RAD51B, RAD51C, RAD51D, XRCC2, XRCC3), RPA1 is then replaced by DNA repair protein RAD51 homologue 1 through the interaction with breast cancer type 2 susceptibility protein (BRCA2) (Forget and Kowalczykowski, 2010; Liu et al., 2014).

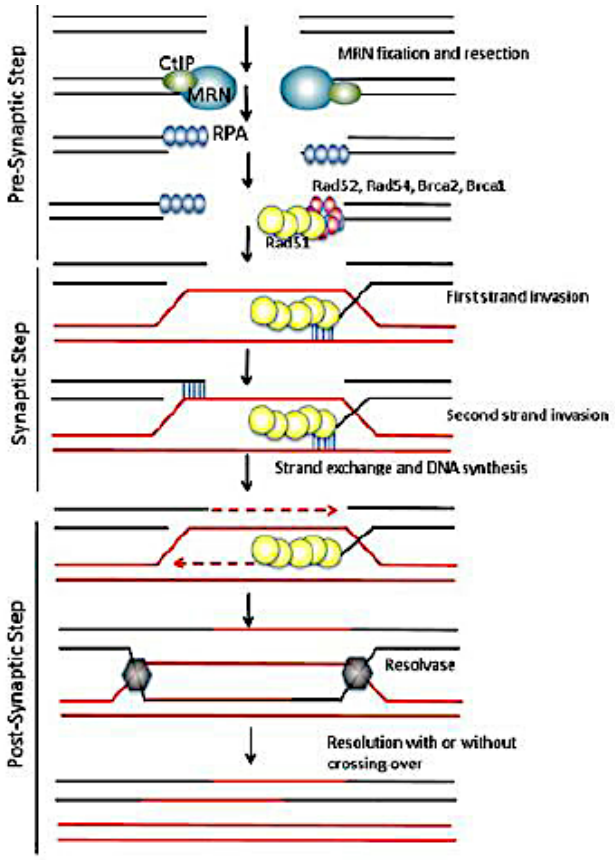

Figure 1-4. Double-strand break repair by homologous recombination. HR can be divided into three stages, namely pre-synaptic, synaptic and post-synaptic. RPA binding essentially removes disruptive secondary structures of the DNA that will otherwise obstruct the binding of RAD51 recombinase. Localisation of BRCA2 to the damage sites occurs via BRCA1 and partner and localiser of BRCA2 (PALB2), by mediating the interaction between BRCA2 and RAD51 (Zhang et al., 2009). **Abbreviations:** MRN, MRE11-RAD50-NBS1; CtIP, CtBP-interacting protein; RPA, replication protein A; BRCA, breast cancer susceptibility protein. The figure is taken from Renodon-Cornière et al., 2013.

Following BRCA2 replacement by RAD51, the RAD51-coated ssDNA tail, also referred to as the RAD51 nucleoprotein filament, is formed to carry out a DNA sequence homology search. Upon successful recognition of the homologous sequence, the ssDNA filament undergoes strand invasion mediated by RAD51. Formation of a displacement loop (D-loop) signifies the crucial stage whereby the damaged strand has completely invaded the template DNA duplex of the sister chromatid and formed heteroduplex DNA (hDNA). Next, DNA polymerase ε/η is responsible for catalysing strand synthesis from the 3' end of the invading strand and successive ligation by DNA ligase I, forming an intermediate structure of a four-way junction known as the "Holliday junction" (McIlwraith et al., 2005). This can be effectively resolved in one of the three ways: dissolution mediated by BLM-TopIIIα complex, asymmetrical or symmetric cleavage by structure-specific endonucleases (Ip et al., 2008; Mimitou and Symington, 2009; Seki et al., 2006). The error-free repair of a DSB is finally completed once RAD51 is removed from hDNA structure by RAD54 (Wright and Heyer, 2014).

Cells with impaired BRCA2 and/or RAD51 function, lose the capability of performing conventional HR but are directed to use single strand annealing (SSA), which results in a deletion-rearrangement event of one of the tandem repeats and its intervening sequence flanking the DSB (Stark et al., 2004). One of the pivotal steps in this alternative highly mutagenic pathway is CtIP-mediated 5'-3' end resection (Escribano-Diaz et al., 2013; Munoz et al., 2012). Generation of ssDNA by the actions of multiple nucleases and helicases initiate RAD52 binding to the 3' ssDNA tails and annealing of these repeat sequences to form a synapsed intermediate. Overhanging flap structures are later digested by ERCC1-ERCC4 endonuclease complex (Gottlich et al., 1998; Motycka et al., 2004; Rothenberg et al., 2008). Broken ends are ligated by LIG3 to seal the DNA backbone following polymerase filling of any gaps.

1.4.2 Double-strand break repair: Non-homologous end joining (NHEJ)

NHEJ is the main DSB repair pathway in mammalian cells due to its availability in all phases of the cell cycle. DSBs are eliminated by DNA end-trimming and direct re-ligation of short microhomologies present on the single-stranded tails, so repair is error-prone with insertions or deletions (INDELs) commonly found at the breakpoint. Initial recognition step entails binding of the Ku70/Ku80 heterodimer (Ku complex) to the exposed DNA termini within seconds after DSB formation, as described in Figure 1-5. The Ku complex then adopts a preformed ring-shaped structure to completely encircle the DNA duplex in a sequence-independent manner (Walker et al., 2001). Catalytic subunit of DNA-dependent protein kinase (DNA-PKcs) is recruited to the damage site, forming a DNA-PK holoenzyme which exhibits protein kinase activity. As a result, inward translocation of the Ku complex along the DNA is induced and DNA-PKcs gains contact with the free DNA termini (Yoo and Dynan, 1999). Upon DNA-PKcs binding to opposing DSB ends, synapsis is promoted to bridge and tether the two DNA molecules, after which its autophosphorylation increases the accessibility to downstream repair proteins (DeFazio et al., 2002).

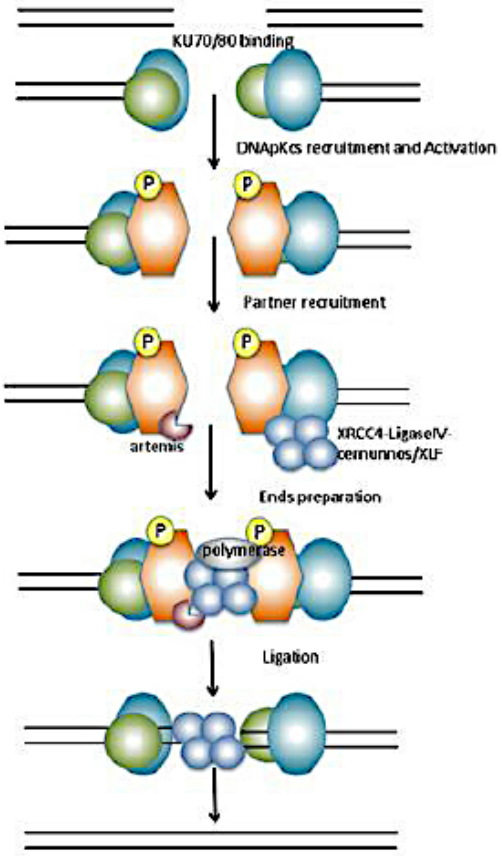

Figure 1-5. Double-strand break repair by non-homologous end joining. The molecular mechanism of NHEJ is mediated by the sequential recruitment of a relatively small number of essential factors. Depending on the type and complexity of DSB break, extra modifications may be required prior to ligation. For instance, single-stranded overhangs are made ligatable through DNA polymerase-mediated strand-filling or NHEJ-specific nucleolytic resection. This can be achieved via members of the X-family DNA polymerases, specifically Pol μ and Pol λ for the resynthesis of missing nucleotides (Lieber et al., 2008). Likewise, nuclease Artemis when phosphorylated, acquires DNA-PK independent 5'-3' exonuclease and DNA-PK dependent endonuclease activities to excise 3' single-stranded phosphoglycolate overhangs (Jeggo and O'Neill, 2002).
Abbreviations: DNAPKcs, DNA-dependent protein kinase catalytic subunit; XRCC4, X-ray repair cross-complementing group 4. The figure is taken from Renodon-Cornière et al., 2013.

Most candidates participating in end-processing, inclusive of lesion-specific BER enzymes like APE1 and polynucleotide kinase 3'-phosphatase (PNKP) are responsible for misrepair of overhangs as well as the gain or loss of nucleotides (Chappell et al., 2002). The final ligation step is carried out by DNA ligase IV (LIG4) in complex with its binding cofactor X-ray repair cross-complementing group 4 (XRCC4). XRCC4-like factor (XLF) also interacts with the XRCC4-LIG4 complex to promote DNA ligation (Ahnesorg et al., 2006). The paralog of XRCC4 and XLF (PAXX) facilitates DNA ligation *in vitro* and assembly of NHEJ factors in a Ku-dependent manner, whereas aprataxin and PNK-like factor (APLF) acts a scaffold protein to bring XRCC4-LIG4 and XLF together at the site of repair (Ochi et al., 2015; Grundy et al., 2013).

The choice of repair pathway between HR and NHEJ is based upon the antagonistic relationship between BRCA1 and p53 binding protein 1 (53BP1). 53BP1 protein is

present continuously throughout the cell cycle, in which it restricts end-resection by the MRN complex thus favouring the less accurate NHEJ (Bunting et al., 2010; Xie et al., 2007). In contrast, BRCA1 inhibits the function of 53BP1 during the late S/G2 phase of the cell cycle, and so favours HR.

1.4.3 Double-strand break repair: Alternative non-homologous end joining (alt-NHEJ)

Alternative NHEJ (alt-NHEJ), also known as microhomology-mediated end joining (MMEJ) is a mutagenic form of DSB repair often accompanied by deletion of DNA sequences (Decottignies, 2013). It starts with short-range end resection by MRE11 and/or CtIP nucleases on either side of a DSB to expose microhomologous regions (Truong et al., 2013), but this can be inhibited by the Ku heterodimeric complex. Poly (ADP-ribose) polymerase 1 (PARP1) is also required in the early stage to act as a break sensor and signal transducer for the recruitment of further downstream factors such as the MRN complex, XRCC1 and LIG3 (Audebert et al., 2004; Haince et al., 2008; Sharma et al., 2015). EXO1 and BLM may continue to perform extensive end-resection if necessary. After pairing of short homologous repeats flanking the DSBs, the enzyme flap structure-specific endonuclease 1 (FEN1) is recruited to remove overhanging flaps. DNA polymerase γ potentially fills in any existing gap (Nick McElhinny et al., 2005), and XRCC1-LIG3 or LIG1 is recruited to the damage site for end-ligation, with intact DNA as the final end product (Paul et al., 2013).

1.5 Deregulated expression of histone deacetylases (HDACs)

Among all post-translational modifications on histone proteins, acetylation has been extensively studied with a crucial role in regulating chromatin compaction and its overall structure. Acetylation, as illustrated in Figure 1-6, is a dynamic process

controlled by the antagonistic actions of acetyltransferases (HATs) and deacetylases (HDACs) to add or remove an acetyl group on ε-amino functional side chain of lysine residues, respectively. The HDAC family consisting of 18 genes, can be subdivided into four distinct classes in Table 1-1 based on amino acid sequence homology in the enzyme catalytic domain (de Ruijter et al., 2003; Bolden et al., 2006).

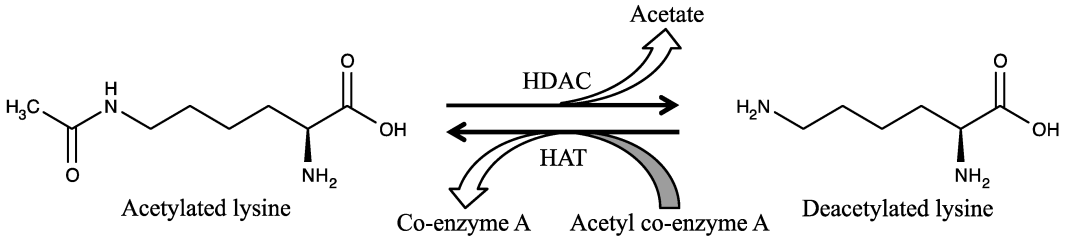

Figure 1-6. Acetylation-deacetylation equilibrium on lysine amino acid residues. Using acetyl co-enzyme A as an acetyl group donor, the acetylation reaction is catalysed by histone acetyltransferases (HATs). Histone deacetylases (HDACs) catalyse deacetylation, i.e. the removal of acetyl group from the amino (-NH_2) side chain. The figure is obtained from Losson et al., 2016.

Table 1-1. Different classes of histone deacetylases (HDACs) with diverse cellular functions and cell-type specific expression patterns.

Class	Members	Tissue distribution	Subcellular localisation	Roles
I	HDAC1 HDAC2 HDAC3 HDAC8	Ubiquitous	Nucleus only	Regulation of cell proliferation, differentiation, cell-cycle progression and apoptosis
II - IIa	HDAC4 HDAC5 HDAC7 HDAC9	Tissue-specific	Nucleus/ cytoplasm	Maintenance of cardiac and vascular integrity, chondrocyte differentiation
- IIb	HDAC6 HDAC10		Mostly cytoplasm	
III	NADH-dependent Sir family of deacetylases	No information	No information	Unknown
IV	HDAC11	Tissue-specific	Nucleus/ cytoplasm	Unknown

HDACs generally function as transcriptional corepressors to regulate gene expression. In methylation-associated gene silencing, HDACs are recruited to methylated foci by DNA methyltransferases and methyl-CpG-binding proteins to form a transcriptionally repressed compact chromatin state. Enzyme-catalysed deacetylation gives rise to a positively charged amino group on conserved lysine residues at the free N-terminal of the histone tails, which bind tightly to negatively charged DNA. As a result, this renders DNA less accessible to transcription factors and other proteins necessary for gene transcription. HDACs can also act on non-histone targets and deacetylate transcription factors, transcription co-regulators and signalling mediators as well as proteins involved in cell cycle progression, apoptosis and DNA repair (De Schutter and Nuyts, 2009).

Due to their participation in a diverse range of cellular functions, deregulated expression of HDACs has been implicated in tumorigenesis, particularly regarding the gene deregulation required for cancer initiation and progression during neoplastic transformation (Glozak and Seto, 2007; Marks et al., 2001). It was proposed that HDAC-mediated gene repression may result in sustained proliferation and uncontrolled cell growth by suppressing the transcription of cyclin-dependent kinase (CDK) inhibitors like p21 and p57 (Lagger et al., 2002; Yamaguchi et al., 2010), as well as regulating migration-related genes such as integrins and matrix metalloproteinase 2 (Lin et al., 2005). This is further corroborated by various findings on the aberrant expression of specific HDAC isoenzymes in several human cancers, for instance deregulated class I HDACs in colorectal, gastric and prostate tumours (Weichert et al., 2008). Specifically in urothelial cell carcinoma of the bladder, upregulated mRNA transcript levels of all members of the class I HDACs family are commonly detected in both low-grade and stage tumours in comparison to the normal mucosa and benign controls (Junqueira-Neto, 2015). For instance, HDAC8 is significantly upregulated in 11 out of 18 urothelial

cancer cell lines whereas HDAC2 upregulation only occurs in a small subset of tumours. Decreased mRNA expression of class IIa HDACs such as HDAC4, HDAC5 and/or HDAC7 were also found in 15 of the 18 cell lines used (Niegisch et al., 2013). This suggests an oncogenic role of the class I HDACs in bladder carcinogenesis, which represent putative therapeutic targets exploitable for drug design.

1.5.1 Therapeutic application of inhibiting histone deacetylases (HDACs)

Following siRNA functional experiments which demonstrated decreased cell viability and motility with increased apoptosis after knocking down HDACs in bladder (Junqueira-Neto, 2015), breast (Senese at al., 2007), colon (Weichert et al., 2008) and lung (Jung et al., 2012) cancers, HDAC inhibitors (HDACi) of specific or broad-spectrum were identified as promising radiosensitising agents for treatment of MIBC. The DNA damage response (DDR) is an attractive target for radiosensitising drugs to increase the efficacy of radiotherapy by inhibiting DNA repair in cancer cells, thus resulting in an increased therapeutic window compared to radiation alone (James et al., 2012). At the molecular level, HDAC inhibition results in a global hyperacetylation of histone and non-histone proteins, leading to gene transcriptional changes that mediate most of the pleiotropic effects as summarised in Figure 1-7. This essentially reverses gene silencing and permits re-expression of the epigenetically silenced genes.

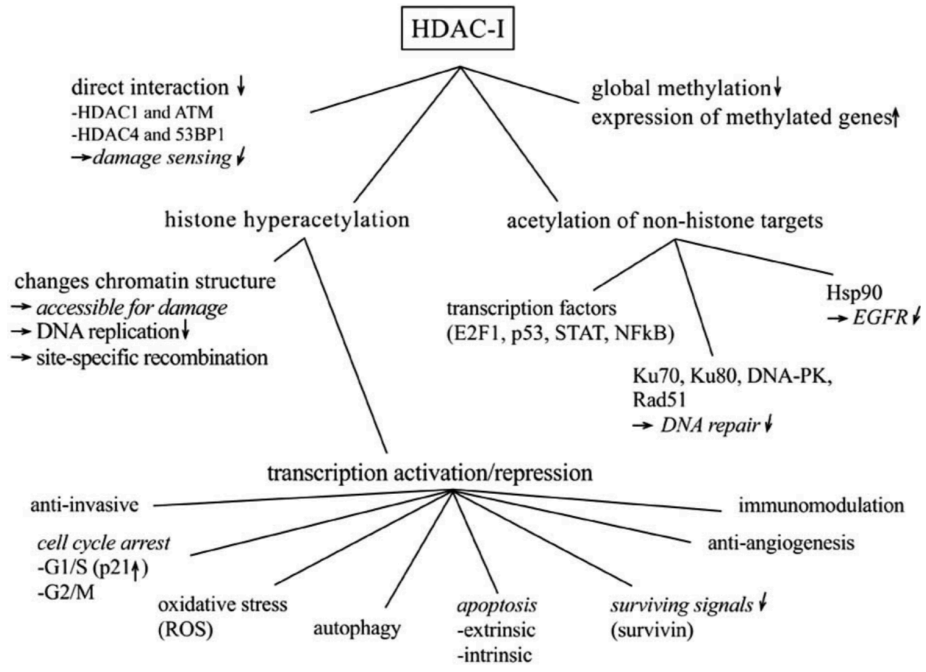

Figure 1-7. General overview of the pleiotropic effects of HDAC inhibitors (HDACi). HDACi influence two or more seemingly unrelated phenotypic traits by modulating gene transcriptional changes and primarily induce apoptosis, cell cycle arrest and differentiation. They serve as selective radiosensitisers with preferential cytotoxicity for tumour cells. The figure is adapted from De Schutter and Nuyts, 2009.

Combined treatment with HDACi and ionising radiation (IR) can result in higher cell death due to the synergistic effects of different cytotoxic mechanisms associated with each modality. In cancer cells, increased apoptosis, cell cycle arrest, senescence and cellular differentiation have been reported as a result of decreased NHEJ, one of the major pathways to repair double-strand breaks (DSBs); whilst healthy non-tumour cells do not undergo cell death (Lee et al., 2010). This implies that normal tissues can be spared the radiosensitising effects of HDACi despite enhanced tumour cell kill. The molecular mechanism of HDACi-mediated radiosensitisation occurs via two main routes. Firstly, histone hyperacetylation promotes an open chromatin structure and allows greater accessibility for DNA-damaging agents to induce potentially lethal DSBs. Secondly, it is increasingly recognised that HDACi can directly disrupt interaction of HDAC enzymes with the damage sensor proteins ATM and 53BP1 (Kim et al., 1999; Kao et al., 2003), as well as alter the acetylation status of proteins involved

in both the HR and NHEJ repair pathways, although many of these are neither functionally characterised nor systematically investigated to date. Non-histone targets of HDACi also include transcription factors that orchestrate the DDR, for example E2F1 exhibits increased acetylation and altered function in response to HDAC inhibition (Martinez-Balbas et al., 2000), while p53 is acetylated upon IR (Gu and Roeder, 1997; Falkenberg and Johnstone, 2014).

The HDACi panobinostat (PAN) is a promising radiosensitiser *in vitro* and FDA-approved for use in multiple myeloma. It is currently in clinical trials for a range of solid tumours (www.clinicaltrials.gov). Previous work from the laboratory has demonstrated that PAN treatment on MIBC cell lines with defective NHEJ repair results in radiosensitisation through downregulation of the HR DNA repair pathway (Groselj et al., 2013). This is partly achieved by post-transcriptional downregulation of the DNA repair protein MRE11 (Martin et al., 2014), which can be predictive of treatment outcome after radiotherapy in MIBC (Choudhury et al., 2010), via E3 ligase cellular inhibitor of apoptosis protein 2 (cIAP2)-mediated degradation of a C-terminally truncated intermediate in Figure 1-8, which compromises the cancer cells' ability to repair DNA damage (Nicholson et al., 2017).

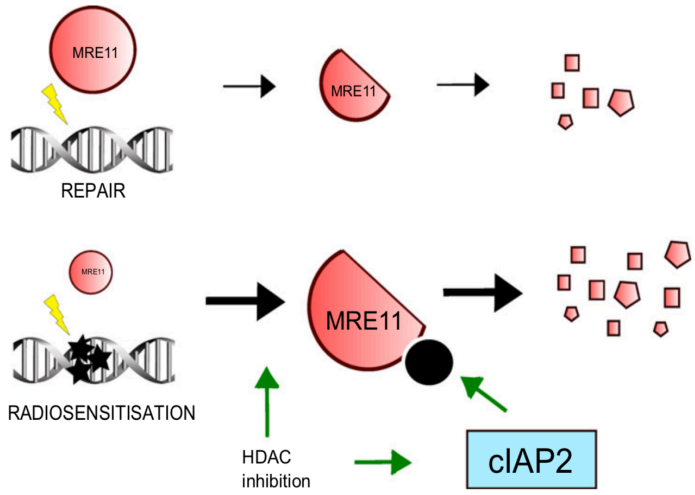

Figure 1-8. Model mechanism for PAN-mediated radiosensitisation in bladder cancer through the action of cellular inhibitor of apoptosis protein 2 (cIAP2). HDAC inhibition results in increased truncated form of MRE11 and cIAP2 transcription. High cIAP2 levels lead to the ubiquitination and downregulation of MRE11 via proteosomal degradation, hence contribute to decreased DSB repair by homologous recombination. The figure is taken from Nicholson et al., 2017.

Together with the prediction of acetylation sites in 31 known MRN-interacting proteins using Phosida (Gnad et al., 2011) and Biogrid (Stark et al., 2006) databases, these suggest the possibility of a wider role for non-histone acetylation in the DDR. A recent large-scale screen determined numerous non-histone acetylated proteins which respond to DNA damage (Elia et al., 2015). However, the functional significance of the detected acetylation sites was not properly addressed. Thus, a proteomic mass spectrometry experiment was carried out in the T24 bladder cancer cell line using anti-acetyl lysine antibodies to isolate cellular proteins which are differentially regulated with and without HDAC inhibition. Apart from previously identified acetylation substrates like Ku80 and MRE11, 634 unique acetylation sites were discovered in 228 proteins following an acetyl enrichment experiment. One of these, suppressor of MEK1 (sMEK1), the regulatory subunit of serine/threonine-protein phosphatase PP4 complex was selected as the primary subject of this thesis since it has a known role in DNA repair and is associated with chromatin (Chowdhury et al., 2008).

1.6 Suppressor of MEK1 (sMEK1)

The suppressor of MEK1 (sMEK1), also defined as protein phosphatase 4 regulatory subunit 3 (PP4R3) (Gavin et al., 2002; Gingras et al., 2005) belongs to the PP2A family which act as highly conserved serine/threonine phosphatases (Huang et al., 1997; Andreeva and Kutuzov, 2001). Of the seven alternatively-spliced isoforms described on available databases (UniProtKB/Swiss-Prot, GeneCards®), the most highly abundant is the largest endogenous variant of 833 amino acid residues with a molecular weight of 95.368 kDa. During interphase, sMEK1 can be found in both the nucleus and cytoplasm, albeit with a higher nuclear level, but at metaphase it is concentrated in the pericentriolar regions of the centrosome and microtubule organising centre due to its role in regulation of the cytoskeleton.

Being an evolutionarily conserved gene and protein in *C. elegans*, Drosophila, Dictyostelium cells and *Homo sapiens*, sMEK1 is vital in modulating a diverse range of essential biological and physiological functions. These include apoptotic cell death (Byun et al., 2012), cell proliferation (Zhang et al., 2005), cell cycle arrest (Nakada et al., 2008), mutation rate (Mourtada-Maarabouni and Williams, 2008), microtubule organisation (Cohen et al., 2005), DNA repair and damage checkpoints (Chowdhury et al., 2008) and tumour necrosis factor (TNF) signalling (Zhou et al., 2002) in human cells. sMEK1 is also known to functionally bind to various intracellular proteins including those displayed in Figure 1-9 and also adenosine triphosphate (ATP)-dependent chaperonin (Gingras et al., 2005), HDAC3 (Zhang et al., 2005; Chowdhury et al., 2008), target of rapamycin (TOR) (Bertram et al., 2000) and insulin receptor substrate 4 (IRS-4) (Mihindukulasuriya et al., 2004).

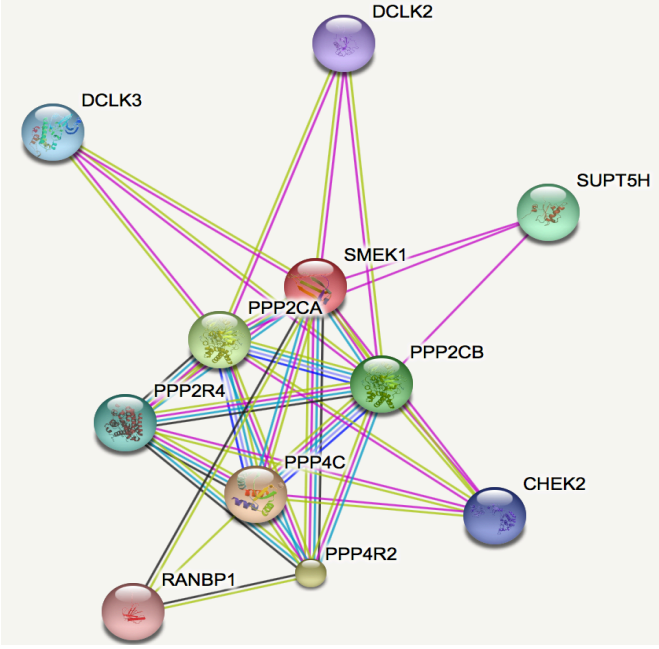

Figure 1-9. Mapping of the protein-protein interactions with sMEK1. sMEK1 mostly interacts with components of the PP4 phosphatase complex (PPP4C and PPP4R2) as well as others in the PP2 family (PPP2CA, PPP2CB and PPP2R4). RAN binding protein 1 (RANBP1) controls the nuclear import of proteins and nucleic acids for cell cycle regulation. Doublecortin-like kinases (DCLKs) regulate microtubule binding and polymerisation through a Ca^{2+}/calmodulin-dependent kinase domain, while checkpoint kinase 2 (CHEK2) is a tumour suppressor with known roles in DNA damage such as DNA repair, cell cycle arrest and apoptosis. sMEK1 can also interact with SUPT5H, which is a transcription elongation factor. The figure is adapted from the STRING database version 10.5.

Furthermore, sMEK1 protein is a pivotal regulator of hepatic gluconeogenesis (Yoon et al., 2010), with prior studies showing that its ectopic expression upregulates hepatic gluconeogenesis. sMEK1 knockdown decreases blood glucose levels by enhancing

hepatic CREB-regulated transcription coactivator 2 (CRTC2) phosphorylation. This highlights the importance of maintaining the phosphorylation-dephosphorylation equilibrium in the vast majority of cellular processes involved in diseases such as cardiovascular disease, diabetes, hypertension and stroke. A recent discovery has also shed some light on the role of sMEK1 in tumorigenesis, where its downregulation is observed in ovarian and cervical tumour tissues as well as carcinoma cell lines with hypermethylated CpG islands for gene silencing (Dong et al., 2012). Being a novel pro-apoptotic tumour suppressor protein, reduced sMEK1 expression promotes the pro-proliferative effect observed in cancer cells by evading cell death. sMEK1 also suppresses the VEGFR-2-mediated PI3K/Akt/eNOS signalling pathway in ovarian tumours, thence inhibits endothelial cell proliferation and angiogenesis (Kim et al., 2015).

1.6.1 Protein phosphatase 4 (PP4) complex

The removal of γH2AX from chromatin in the late phase of the DNA damage response (DDR) is poorly understood despite being a process tightly coordinated by the extent of DNA repair. It most likely requires protein phosphatases which 'erase' the γH2AX histone marker and nucleosome remodelling activities to facilitate its removal from DNA lesion sites via histone exchange (Linger and Tyler, 2007). In Figure 1-10, Pph3, an orthologue of the mammalian PP4 phosphatase catalytic subunit (PP4C) in budding yeast, is the sole γH2AX phosphatase that couples double-strand break (DSB) repair with the termination of checkpoint signalling independently of a role in DNA repair (Ronne et al., 1991; Brewis et al., 1993). By expressing a non-phosphorylatable H2A mutant, the delay in checkpoint recovery manifested by *pph3*Δ cell is greatly alleviated (Keogh et al., 2006). Therefore, the formation of the γH2AX chromatin domain and its subsequent dissolution are crucial to control checkpoint signalling.

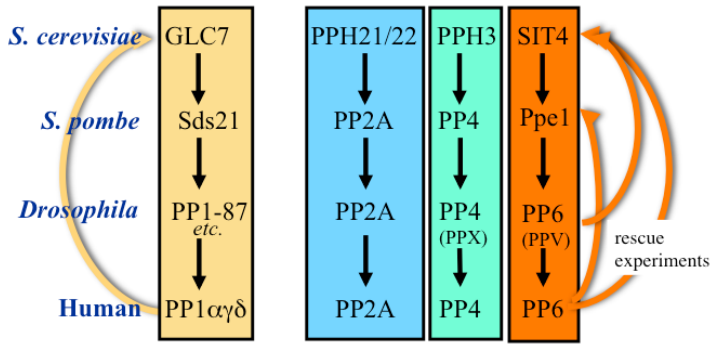

Figure 1-10. Conservation of PPP phosphatases through evolution with segregation into different types. Each phosphatase enzyme has individual regulatory subunits that support separate functions. The figure is adapted from Brautigan Research Group, University of Virginia School of Medicine, Centre for Cell Signalling (https://research.med.virginia.edu/cell-signaling/brautigan-research-group).

In human cells, this phosphatase activity is attributed to PP2A (Chowdhury et al., 2005) and PP4 (Nakada et al., 2008), both acting non-redundantly, possibly in response to different DNA damage types. PP4 can dephosphorylate γH2AX at the sites of IR-induced DSB as well as in intact undamaged chromatin, whereas PP2A has minimal function at those sites. Depletion of PP4C not only increases the steady-state levels of γH2AX by slowing down its turnover, but also results in defective checkpoint recovery with late entry into mitosis after the initial arrest (Nakada et al., 2008). This is potentially mediated by the persistent binding of mediator of DNA damage checkpoint 1 (MDC1) to γH2AX at DNA lesion sites through an interaction between MDC1 tandem BRCT domains and an H2AX epitope encompassing phosphoserine 139 and its free carboxyl terminus (Stucki et al., 2005). This then promotes recruitment of DNA repair and checkpoint signalling proteins such as 53BP1, NBS1, RNF8 and BRCA1 (Harper and Elledge, 2007). Unlike PP2A acquisition during eukaryotic evolution or loss by budding yeast, PP4 is an evolutionarily conserved γH2AX phosphatase with an important role in the spatio-temporal regulation of DDR to promote recovery from G2/M checkpoint arrest following irradiation treatment.

1.7 Bromodomain (BRD)-containing effector proteins

Bromodomains (BRDs), the 'readers' of acetyl-lysine, are ubiquitously-expressed structurally diverse complex multidomain subunit proteins that contain one or more evolutionarily conserved effector modules for context-specific interaction with acetylated histones and/or transcription factors. To date, 61 diverse BRDs have been found to be encoded by the human genome, present mainly in a total of 46 nuclear proteins. Despite variations in the structural mechanism of acetyl-lysine recognition and sequence requirement for BRD substrates (Filippakopoulos and Knapp, 2014), the binding modes are roughly similar across different BRD structural classes as shown in Figure 1-11 (Picaud et al., 2016). BRDs dominantly act as scaffolding proteins that link chromatin organisation and transcriptional regulation to cell cycle progression for further signal propagation after acetylated peptide binding. They may also contain catalytic functions, for instance ATP-dependent helicase, histone methyl- or acetyl-transferase activities (Filippakopoulos et al., 2012). Due to the critical roles involved in chromatin biology and gene expression control, perturbated cellular BRD levels are implicated in a wide diversity of diseases particularly cancer (Belkina and Denis, 2012).

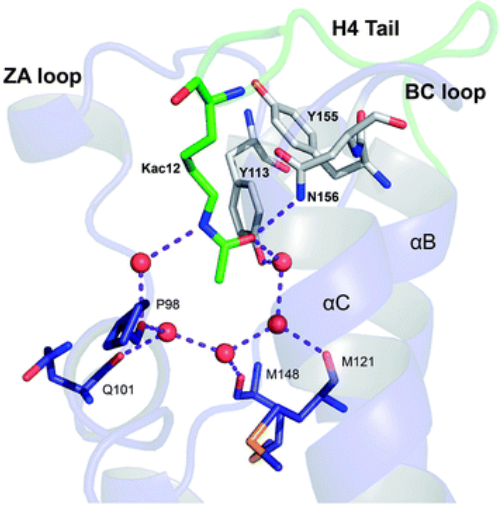

Figure 1-11. Structure of acetyl-lysine binding site in bromodomain 4 (BRD4). The recognition of an acetylated peptide is mediated by the formation of a hydrophobic binding cleft consisting of four canonical helices (αZ, αA, αB, αC) made up of 120 amino acid residues and two connecting loop regions (ZA and BC loops). It was identified as an evolutionarily conserved motif in the Drosophila *brahma* in the early 1990s (Tamkun et al., 1992). The figure is obtained from Furdas et al., 2012.

A high prevalence of mutated or deregulated chromatin regulator proteins such as SWI/SNF chromatin remodelling and trithorax-like histone-modifying complexes in

invasive urothelial carcinoma (Cancer Genome Atlas Research Network, 2014) has prompted the development of small-molecule epigenetic inhibitors as an alternative approach to target DNA or these modifying enzymes with limited off-target effects. As the most extensively researched member of the bromodomain and extraterminal (BET) protein family, bromodomain containing 4 (BRD4) is frequently amplified in urothelial carcinoma tissues (Wu et al., 2016) with positive correlations to tumour grade, metastatic progression and poor prognosis (Yan et al., 2014). When acting alone, the class I HDACi romidepsin indiscriminately kills both cancer and benign cells but achieves synergistic anti-neoplastic effects in combination with the BRD4 inhibitor JQ1 (Hölscher et al., 2018). Mapping of the changes in gene expression profiles across multiple cancer cell types after the combined treatment revealed hundreds of differentially-regulated genes, resulting in cell cycle arrest and caspase-dependent apoptosis (Borbely et al., 2015; Shahbazi et al., 2016). This can be rationalised by BRD4 enrichment on HDACi-activated genes contributing to the maintenance of oncogenic transcription (Mishra et al., 2017). Histone H3K27 hyperacetylation within a 5 kb region around their transcriptional start sites promotes direct recruitment of the transcriptional machinery, as well as indirect BRD4 binding to the enhancer regulatory elements. By selectively targeting the highly druggable interaction site of BRD4, abolished acetyl-lysine binding leads to transcriptional repression of growth-promoting and anti-apoptotic oncogenic factors. These include c-Myc in multiple myeloma (Delmore et al., 2011), the androgen receptor in prostate cancer (Asangani et al., 2014), EZH2, Survivin and Bcl-2 (Zuber et al., 2011; Venkataraman et al., 2014; Fu et al., 2015). Therefore, there is growing interest to design novel dual HDAC/BRD inhibitors (Shao et al., 2017), highlighting the potential for acetylation modification as an anti-cancer radiosensitising strategy.

1.8 Objectives of the thesis

The objectives of this thesis are:

(1) To identify if there are acetylation site(s) in the DNA repair-related protein sMEK1 which potentially regulates the DDR,

(2) To validate sMEK1, as one of the robust acetylated targets from our previous mass spectrometry study,

(3) To use a co-immunoprecipitation approach, using antibody-conjugated beads, to probe the interactions of acetylated substrates with bromodomain-containing effector proteins,

(4) To study specific acetylation site(s) of sMEK1 involved in radiosensitisation, i.e. downregulation of the DDR, through site-directed mutagenesis and RNA interference-mediated protein depletion in terms of cell survival and the extent of DNA damage induction and repair.

These acetylated proteins potentially represent therapeutic targets or predictive biomarkers which can be carried forward into future work.

2. MATERIALS AND METHODS

2.1 Antibodies

Table 2-1. The list of antibodies used in co-immunoprecipitation and western blots.

Antibody type	*Manufacturer*	*Working dilution*
Acetylated-Lysine		
- Mouse mAb (Ac-K-103)	Cell Signaling *#9681*	1:1000
- Rabbit mAb mix (Ac-K^2-100)	Cell Signaling MultiMab™ *#9814*	1:1000
- Rabbit pAb	Chemicon® *#AB3879*	1:1000
Beta actin		
- Mouse mAb [AC-15]	abcam *#ab6276*	1:5000
- Rabbit pAb	abcam *#ab8227*	1:1000
Bromodomains (BRD)		
- BRD4: Rabbit mAb [EPR5150(2)]	abcam *#ab128874*	1:200
- BRD2: Rabbit mAb [EPR7642]	abcam *#ab139690*	1:1000
- BRD3: Rabbit pAb	*GeneTex #GTX115058*	1:1000
- BRDT [C3]: Rabbit pAb	GeneTex *#GTX100201*	1:500
Cyclophilin A -Rabbit pAb	abcam *#ab41684*	1:1000
GADPH -Mouse mAb [1E6D9]	Proteintech *#60004-1-Ig*	1:5000
γH2A.X Histone (pSer139)		
- Mouse mAb [9F3]	abcam *#ab26350*	1:1000
- Mouse mAb [JBW301]	Merck Millipore *#05-636*	1:2000
- Rabbit pAb	Merck Millipore *#07-627*	1:500
HA tag		
- Rabbit pAb	abcam *#ab9110*	1:4000
- Mouse mAb [HA.C5]	abcam *#ab18181*	1:1000
Histone H3		
- Mouse mAb [1B1B2]	Cell Signaling *#14269*	1:1000
- Rabbit mAb [D1H2]	Cell Signaling XP® *#4499*	1:2000

Antibody type	*Manufacturer*	*Working dilution*
Normal IgG -Rabbit	Cell Signaling *#2729*	1-5 μg
Nucleolin -Rabbit pAb	abcam *#ab70493*	1:2000
Phospho-ATM (pSer1981) - Mouse mAb [10H11.E12] - Mouse mAb [10H11.E12]	 Calbiochem® *#DR1002* Cell Signaling *#4526*	 1:1000 1:1000
PARP1 -Rabbit mAb [E102]	abcam *#ab32138*	1:1000
p115 -Rabbit pAb	abcam *#102470*	1:5000
sMEK1 -Rabbit pAb	abcam *#ab70635*	1:2000
Anti-Rabbit Secondary IgG	LI-COR IRDye® 680RD	1:15000
Anti-Mouse Secondary IgG	LI-COR IRDye® 800CW	1:15000

2.2 Buffers

2.2.1 Phosphate-Buffered Saline (PBS)

One tablet of PBS (Thermo Fisher Scientific Invitrogen™ Gibco® Cat. *#18912014*, UK) was dissolved in 500 mL distilled water (dH_2O), followed by heat-sterilisation using autoclave (high pressure 100 kPa, 121°C).

2.2.2 Lysis buffer

Fifty millimolar HEPES ($C_8H_{18}N_2O_4S$ ≥99.5%, Sigma-Aldrich Cat. *#H3375*, USA), 100 mM sodium chloride (ReagentPlus® NaCl ≥99%, Sigma-Aldrich Cat. *#S9625*, Germany), 10 mM ethylenediamine tetraacetate acid (0.5 M EDTA pH 8.0, Thermo Fisher Scientific Invitrogen™ Cat. *#AM9260G*, USA), 1% Triton X-100 (BioXtra $(C_2H_4O)_nC_{14}H_{22}O$, Sigma-Aldrich Cat. *#T9284*, USA) and phosphatase inhibitor

mixture of 4 mM sodium pyrophosphate, 2 mM sodium orthovanadate, 10 nM sodium fluoride, 50 mM B-glycerophosphate.

2.2.3 SDS-PAGE Running buffer (10x)

One hundred and twenty-one grams Tris base (Trizma® $C_4H_{11}NO_3$ ≥99.9%, Sigma-Aldrich Cat. *#T1503*, USA), 238 g HEPES, 10 g sodium dodecyl sulfate (SDS C_{12}, Thermo Fisher Scientific Cat. *#28312*, USA) made up to 1 L with dH_2O.

2.2.4 Western Blot Transfer buffer (10x)

One hundred and forty-four grams glycine (UltraPure™ $C_2H_5NO_2$, Thermo Fisher Scientific Invitrogen™ Cat. *#15527013*, UK), 30.3 g Tris base made up to 1 L with dH_2O.

2.2.5 Phosphate Buffered Saline-Tween® 20 (PBS-T)

One tablet of PBS per 500 mL dH_2O and 0.05% v/v of Tween (Sigma-Aldrich Cat. *#P7949*, USA).

2.2.6 Blocking buffer

Odyssey® blocking buffer (PBS) (LI-COR Cat. *#P/N 927*, USA) diluted in a 1:1 ratio with PBS-T.

2.2.7 Fractionation buffers

2.2.7.1 Buffer A (2x) pH 7.45 for cytosolic fraction

Twenty millimolar HEPES (953 mg), 20 mM potassium chloride (298 mg) (BioXtra KCl ≥99.0%, Sigma-Aldrich Cat. *#P9333*, UK), 680 mM sucrose (46.5 g) (≥99.5%,

Sigma-Aldrich Cat. *#S0389*, UK), 20% v/v glycerol (40 mL) (Thermo Fisher Scientific Cat. *#17904*, UK) made up to a total volume of 200 mL with dH_2O.

Complete 1x Buffer A was freshly prepared before use, using 12.5 mL of 2x stock buffer, 1x Mini Complete protease inhibitor (2.5 tablets), 1x Phosphatase inhibitor cocktail I containing 25 μM (-)-p-bromotetramisole oxalate, 5 μM cantharidin and 5 nM microcystin-LR (250 μL of 100x stock vial, Thermo Fisher Scientific Cat. *#12821650*, UK), 10 mM N-ethylmaleimide (250 μL of 1 M NEM ≥98%, Sigma-Aldrich BioXtra Cat. *#E1271*, USA) and 2 mM EDTA (100 μL of 0.5 M), made up to 25 mL with dH_2O and vortexed to mix.

2.2.7.2 Buffer B (2x) pH 7.9 for nuclear fraction

Six millimolar EDTA (2.4 mL of 0.5 M), 0.4 mM EGTA (200 μL of 400 mM) (UltraPure™ $C_{14}H_{24}N_2O_{10}$, Amresco® Cat. *#0732-10G*, USA), 10 mM HEPES (476.5 mg) made up to a total volume of 200 mL with dH_2O.

Complete 1x Buffer B was freshly prepared before use with 7.5 mL of 2x stock buffer, 1x Mini Complete protease inhibitor (1.5 tablets), 150 μL of 100x Phosphatase inhibitor cocktail I and 10 mM NEM (150 μL of 1 M), made up to 15 mL with dH_2O and vortexed to mix.

2.2.7.3 Benzonase buffer pH 7.9 for chromatin fraction

Fifty millimolar Tris (UltraPure™ Tris-HCl 1 M pH 7.5, Thermo Fisher Scientific Invitrogen™ Cat. *#15567027*, USA), 50 mM NaCl, 5 mM KCl and 3 mM $MgCl_2$.

2.2.8 Crystal violet stain

Five grams crystal violet powder (Sigma-Aldrich Cat. *#C0775*, China) were dissolved in 200 mL methanol (CH_4O ≥99.8%, Sigma-Aldrich Cat. *#32213*, France), and made up to 1 L with dH_2O.

2.3 Cell Culture

2.3.1 Cell lines and nutrient media

Human T24 urinary bladder transitional cell carcinoma cells (DSMZ Collection of Microorganisms Cat. *#ACC-376*, Germany) and 293T human embryonic kidney cells (DSMZ Collection of Microorganisms Cat. *#ACC-635*, Germany) were used in *in vitro* experiments. These cell lines had previously been validated by the short tandem repeat (STR) analysis service supplied by DNA Diagnostics Centre (Ohio, USA) and also tested negative for *Mycoplasma* contamination within the last year.

The complete medium for each cell line was:

T24 - sterile-filtered, liquid RPMI-1640 Medium with L-glutamine and sodium bicarbonate (Sigma-Aldrich Cat. *#R8758*, UK) supplemented with 10% heat-inactivated Fetal Bovine Serum (FBS, Thermo Fisher Scientific Invitrogen™ Gibco® Cat. *#10270106*, South America).

293T - Dulbecco's Modified Eagle's Medium (DMEM) 1x with high glucose, GlutaMAX™ supplement and pyruvate (Thermo Fisher Scientific Invitrogen™ Gibco® Cat. *#31966021*, UK) supplemented with 10% heat-inactivated FBS.

Cells were grown in a 37°C incubator with a constant level of 5% carbon dioxide (CO_2).

2.3.2 Cell passaging

Bottles of medium were first pre-warmed in a 37°C water bath. At approximately 70-90% confluency, medium was removed from the cells and 2.5% Trypsin (10x) (Thermo Fisher Scientific Invitrogen™ Gibco® Cat. *#15090046*, USA) was added proportional to the flask size (T25: 1 mL; T75: 2 mL; T125: 5 mL), then incubated at 37°C for 1-5 minutes. Once all cells had detached from the surface, trypsin was neutralised by twice the volume of medium containing FBS and transferred to a 15 or 50 mL Falcon tube. The cells were centrifuged at 1,300 rpm for 3 minutes, and then resuspended in 2-10 mL fresh medium after aspirating the supernatant. To seed new plates, cells were counted using a haemocytometer if required, or split in a 1:10 ratio by adding one tenth of the suspension to a new flask containing fresh medium (T25: 5 mL; T75: 12 mL; T125: 30 mL).

2.3.3 Freezing down of cells

The medium was aspirated and cells trypsinised with 2 mL of 2.5% Trypsin (10x) at 37°C for approximately 5 minutes. Four millilitres of medium were added to neutralise the trypsin and the suspended cells were transferred to a 15 mL Falcon tube. Following centrifugation at 1,300 rpm for 3 minutes, supernatant was carefully removed without disturbing the pellet at the bottom. The pellet was resuspended in 5 mL freeze mix consisting of 10% Dimethyl Sulfoxide DMSO (sterile-filtered C_2H_6OS ≥99.7%, Sigma-Aldrich Cat. *#D2650*, UK), 50% FBS and 40% medium, and 1 mL of the mixture was later pipetted into a 2 mL cryovial labelled with date, passage number and cell line. Filled cryovials were placed in an isopropanol bath and stored overnight at -80°C before transferring to liquid nitrogen for long-term storage. In order to revive the cells, a cryovial was moved from liquid nitrogen to dry ice, defrosted quickly in a 37°C water bath and transferred to a tube containing 5 mL medium. After centrifugation at 1,300

rpm for 3 minutes to remove the DMSO-containing freeze mix, the pellet was resuspended and transferred to fresh medium in a flask.

2.3.4 Harvesting cells

Medium was discarded, and the plate was washed twice with 3-5 mL of 1x PBS. Cells were then harvested using a plastic scraper into residual PBS solution and transferred to Eppendorf tubes pre-chilled on ice. After spinning down the cells at 3,000 rpm for 3 minutes in a 4°C centrifuge and removing supernatant, the cell pellets were either frozen on dry ice and stored at -20°C or used immediately for downstream applications.

2.3.5 Overexpression of sMEK1 protein

Cells were transfected when 50-70% confluent. For 10 cm dishes, 10 μg of human sMEK1 gene ORF cDNA clone expression plasmid with C-HA tag (Sino Biological Cat. #HG15037-CY, China) was added to 500 μL Opti-MEM® 1x reduced-serum medium (Thermo Fisher Scientific Invitrogen™ Gibco® Cat. #11058021, UK) in a sterile tube to make up a final concentration of 2 μg DNA/100 μL Opti-MEM. The mixture was vortexed and incubated for 1-2 minutes before adding a suitable transfection reagent:

(i) Polyethylenimine (PEI) at pH 7.4 (50% w/v in H_2O, Sigma-Aldrich Cat. *#P3143*, UK) for 293T cells - 20 μL added in a 2:1 ratio to 10 μg of DNA;

(ii) FuGENE® HD Transfection reagent (Promega Cat. *#E2311*, USA) for T24 cells - 30 μL added in a 3:1 ratio to 10 μg of DNA.

After 10-15 minutes incubation at room temperature in a sterile hood, the mixture was added dropwise to the cells and incubated at 37°C for 24-48 hours.

2.3.6 CRISPR gene knockout of sMEK1

T24 cells were transfected with sMEK1 Double Nickase plasmid (h2) (Santa Cruz Biotechnology Cat. *#sc-412572-NIC-2*, USA) in 6 cm dishes with a 4:1 ratio of FuGENE to DNA in order to improve transfection efficiency. A control plate was also included in the set-up by transfection with non-resistant plasmids or no plasmid. Following 24-48 hours' incubation, 2 μg/mL puromycin (Merck Millipore Calbiochem® Cat. *#540411*, UK) was added for selection and enrichment of cells that had stably taken up the plasmid. The concentration of puromycin used was pre-determined by a kill curve with a range of doses to investigate how much antibiotic was necessary to kill all untransfected cells within 3-7 days.

Cells were monitored on a daily basis and selection medium frequently changed until all the control cells were dead. If those remaining on the pSilencer plate were growing as overlapping colonies, the procedure was repeated with fewer cells seeded pre-transfection. Upon formation of large colonies (~200 cells), they were transferred to a 96- or 48-well plate with one colony per well and then further expanded by transferring to larger flasks. At the 6-well stage for early passage numbers, one clone was split into two wells, of which one was frozen down when confluent, while another was transferred into a T75 flask and a sample taken to analyse the extent of sMEK1 protein knockout by western blot.

2.3.7 siRNA gene knockdown of sMEK1

Individual ON-TARGETplus siRNA (Dharmacon™ Horizon Cat. *#J-019093-05*, USA) which targets the open reading frame (ORF) and non-coding regions of the human *sMEK1* gene, was dissolved in sterile RNase-free water to make up a 20 μM stock. The transfection procedure was conducted using Oligofectamine™ reagent (Thermo Fisher

Scientific Invitrogen™ Cat. *#12252011*, USA) on adherent T24 cells at 30-50% confluency in a 6-well plate. Cells were plated in 1 mL of RPMI growth medium without antibiotics prior to transfection. For optimisation to obtain the highest transfection efficiency and lowest off-target effects, complexes of varying concentrations were prepared as below followed by gentle mixing:

Well	Complex 1	Complex 2
1	5 µL of a 20 µM stock oligonucleotide + 180 µL of Opti-MEM® I reduced serum medium without serum	2 µL of Oligofectamine™ reagent + 13 µL of Opti-MEM® I medium without serum
2	5 µL of a 20 µM stock oligonucleotide + 180 µL of Opti-MEM® I reduced serum medium without serum	4 µL of Oligofectamine™ reagent + 11 µL of Opti-MEM® I medium without serum
3	10 µL of a 20 µM stock oligonucleotide + 175 µL of Opti-MEM® I reduced serum medium without serum	2 µL of Oligofectamine™ reagent + 13 µL of Opti-MEM® I medium without serum
4	10 µL of a 20 µM stock oligonucleotide + 175 µL of Opti-MEM® I reduced serum medium without serum	4 µL of Oligofectamine™ reagent + 11 µL of Opti-MEM® I medium without serum
Total	**185 µL**	**15 µL**

An additional 5-10 minutes incubation of Complex 2 at room temperature was done before combining the diluted oligonucleotide with diluted Oligofectamine ™ reagent to give a total volume of 200 µL. After gently mixing, the mixture was incubated at room temperature for 15-20 minutes. While waiting for complex formation, the growth medium was removed from the cells and the cells washed once with medium without serum. A volume of 800 µL of medium without serum was later added to each well

containing cells followed by the dropwise addition of 200 µL complexes from the previous step. A negative control was also set up using non-targeting siRNA (unmodified 20 nmol, Qiagen AllStars Cat. *#1027281*, Germany) with no known sequence homology to any mammalian genes. The cells were subsequently incubated at 37°C in a CO_2 incubator for 4 hours, after which 500 µL of growth medium containing 3x normal serum concentration (30% FBS) was added to the wells without removing the transfection mixture. Finally, sMEK1 protein levels were assayed at 48-96 hours' post-transfection by western blot. The extent of sMEK1 knockdown was determined by ImageJ quantification of each band size and intensity, with reference to actin as the loading control as well as being normalised to the negative control.

2.4 Site-directed mutagenesis (SDM)

2.4.1 Primer design

Mutagenic oligonucleotide primers for acetyl-dead (K416R) and acetyl-mimic (K416Q) variants of sMEK1 were designed using the Agilent web-based QuikChange primer design programme available online at www.agilent.com/genomics/qcpd. Two complementary oligonucleotides, containing the desired mutation flanked by unmodified nucleotide sequence, were synthesised.

(I) Acetyl-dead (A1247G)

Forward	5'-cgcatactgtcaagtctgggattatcttgcctttctctttg-3'	T_m = 78.9°C
Reverse	5'-caaagagaaaggcaagataatcccagacttgacagtatgcg-3'	T_m = 78.9°C

(II) Acetyl-mimic (A1246C and A1248G)

Forward	5'-atggaacgcatactgtcaagctggggattatcttgcctttctc-3'	T_m = 82.0°C
Reverse	5'-gagaaaggcaagataatccccagcttgacagtatgcgttccat-3'	T_m = 82.0°C

2.4.2 Thermal cycling

A QuikChange Lightning site-directed mutagenesis (SDM) kit (Agilent Technologies Cat. *#210518*, USA) was utilised in the mutant strand synthesis reaction. For each sample, the reaction mixture was prepared in a thin-walled tube of 200 μL in size:

10x QuikChange Lightning buffer	5 μL
dsDNA template	100 ng
Forward & reverse primers	125 ng each
dNTP mix	1 μL
QuikSolution reagent	1.5 μL
ddH_2O	Up to 50 μL

A control reaction was also set up:

10x QuikChange Lightning buffer	5 μL
pWhitescript 4.5kb control plasmid (5 ng/μL)	5 μL
Forward & reverse control primers (100 ng/μL)	1.25 μL
dNTP mix	1 μL
QuikSolution reagent	1.5 μL
dH_2O	34 μL

Finally, 1 μL of QuikChange Lightning enzyme was added to each tube and subjected to the cycling parameters outlined below:

	Step	Temperature	Time	No. of cycles
1.	*Initial denaturation*	95°C	2 min	1
2.	*Denaturation*	95°C	20 s	18
	Annealing	60°C	10 s	
	Extension	68°C	6 min	
3.	*Final Extension*	68°C	5 min	1
4.	*Hold*	4°C	∞	-

2.4.3 DpnI digestion

A volume of 2 μL of the provided *Dpn*I restriction enzyme was added directly to each amplification reaction. After gently and thoroughly mixing by pipetting the solution up and down several times, the reaction mixture was briefly centrifuged and then immediately incubated at 37°C for 5 minutes to digest the parental non-mutated methylated and hemi-methylated supercoiled dsDNA.

2.4.4 Bacterial transformation - heat shock method

XL10-Gold ultracompetent cells were gently thawed on ice. For the transformation of each control and sample reaction, 45 μL of ultracompetent cells were aliquoted into a pre-chilled 14 mL BD Falcon polypropylene round-bottom tube, followed by the addition of 2 μL β-ME mix provided with the kit. The contents of the tube were swirled gently and then incubated on ice for 2 minutes. Subsequently, 2 μL of the *Dpn*I-treated DNA from each control and sample reaction were transferred to separate aliquots of the ultracompetent cells. A negative control was also set up by mixing dH_2O with competent cells. The transformation reactions were swirled gently to mix and incubated on ice for 10-30 minutes, before heat-pulse treatment in a 42°C water bath for 30

seconds without shaking. Immediately, the tubes were replaced on ice for 2 minutes and 250 μL of room temperature S.O.C Medium (Thermo Fisher Scientific Invitrogen™ Cat. *#15544034*, UK) was added. The tubes were later capped tightly and shaken horizontally at 225-250 rpm in a 37°C shaking incubator for an hour. Depending on the transformation efficiency, 10-150 μL from each tube was spread onto a pre-warmed LB agar plate containing appropriate antibiotic concentration for the plasmid vector (e.g. kanamycin 50 μg/mL; ampicillin 100 μg/mL) and incubated overnight at 37°C. Two different volumes were plated to ensure that at least one gave well-spaced distinguishable colonies which were non-overlapping.

2.5 Plasmid Purification

2.5.1 Plasmid isolation via Mini-prep

Individual colonies picked from the selective plate were inoculated into a 3-5 mL LB culture medium containing suitable antibiotic and grown overnight in a 37°C shaking incubator at 225 rpm. The bacterial cells were harvested by centrifugation at >8,000 rpm in a conventional table-top microcentrifuge for 3 minutes at room temperature. Using a QIAprep® Spin Miniprep kit (Qiagen Cat. *#27104*, Germany), up to 20 μg of plasmid DNA could be purified for sequencing or cloning. This was achieved by alkaline cell lysis and subsequent adsorption of DNA onto a silica membrane under high salt conditions.

Firstly, pelleted bacterial cells were resuspended completely in 250 μL Buffer P1 (resuspension buffer: 50 mM Tris-Cl, pH 8.0; 10 mM EDTA; 100 µg/mL RNase A; optional LyseBlue reagent) by vortexing, and transferred to a new microcentrifuge tube. A volume of 250 μL Buffer P2 (lysis buffer: 200 mM NaOH, 1% SDS w/v) was later

added and thoroughly mixed by 4-6 times inversion until the solution appeared clear. The lysis reaction was not allowed to proceed beyond 5 minutes. In the presence of optional LyseBlue reagent, the suspension would turn blue. Then, 350 μL Buffer N3 (neutralisation buffer containing guanidine hydrochloride: Qiagen Cat. *#19064*) was added followed by immediate and thorough mixing by inverting the tube 4-6 times until the solution became homogenously colourless with a cloudy appearance, indicating effective precipitation of SDS. After 10-minutes' centrifugation at 13,000 rpm in a table-top microcentrifuge, the supernatants were applied to QIAprep spin columns and subjected to centrifugation for 30-60 seconds and the flow-through was discarded. Addition of 0.5 mL Buffer PB (wash buffer with high concentration of guanidine hydrochloride and isopropanol: Qiagen Cat. *#19066*) with 30-60 seconds centrifugation to discard flow-through, was essential to wash the column as well as to remove trace nuclease activity. The column was also repeatedly washed by adding 0.75 mL Buffer PE (concentrated wash buffer containing absolute ethanol: Qiagen Cat. *#19065*), then centrifuged for 30-60 seconds and flow-through discarded before full-speed centrifugation for an additional 1 minute. This ensured the removal of residual wash buffer, since ethanol from Buffer PE might inhibit downstream enzymatic reactions. By placing the washed column in a fresh 1.5 mL microcentrifuge tube, DNA elution was performed with 50 μL Buffer EB (10 mM Tris-Cl, pH 8.5) added to the membrane centre, left standing for 1 minute and finally spun down at full-speed for 1 minute.

2.5.2 Plasmid isolation via Maxi-prep

A single colony was picked from a freshly streaked selective plate and inoculated directly into a culture of 200 mL LB medium (Luria Bertani Broth, Sigma-Aldrich Lennox Cat. *#L3022*, U.K.) containing the appropriate selective antibiotic. The medium was incubated overnight at 37°C with vigorous shaking (~225 rpm). An EndoFree®

Plasmid Maxi kit (Qiagen Cat. *#12362*, Germany) was used to purify up to 10 mg endotoxin-free plasmid DNA from bacterial cells. The basic principle involved modified alkaline cell lysis to release plasmid DNA, after which binding to the QIAGEN resin occurred under suitable low-salt and pH conditions. Using a stringent medium-salt wash, RNA, proteins, dyes and impurities of low-molecular-weight were selectively removed. Elution of the purified plasmid DNA was done in high-salt buffer, followed by a concentration and desalting step by isopropanol precipitation.

Bacterial cells were harvested by centrifugation at 6,000 *g* for 15 minutes at 4°C. The pellets obtained could be frozen down at -20°C for long-term storage, or used directly in the purification protocol by resuspending in 10 mL Buffer P1 (resuspension buffer: 50 mM Tris-Cl, pH 8.0; 10 mM EDTA; 100 µg/mL RNase A; optional LyseBlue reagent) until no cell clumps remained. Then, 10 mL Buffer P2 (lysis buffer: 200 mM NaOH, 1% SDS w/v) was added, mixed thoroughly by vigorously inverting the sealed tube 4-6 times and incubated at room temperature (15-25°C) for 5 minutes. If LyseBlue was present, the cell suspension turned blue upon Buffer P2 addition. Pre-chilled Buffer P3 (neutralisation buffer: 3.0 M potassium acetate, pH 5.5) of 10 mL was added to the lysate, mixed thoroughly by 4-6 times vigorous inversion followed by immediate pouring into the barrel of a QIAfilter Maxi Cartridge. After 10 minutes' incubation at room temperature, the cap was removed from the cartridge outlet nozzle and a plunger gently inserted to filter cell lysate into a fresh 50 mL tube. Subsequently, 2.5 mL Buffer ER (QIAfilter wash buffer: 1 M potassium acetate, pH 5.0) was added to the filtered lysate, mixed by inverting the tube ~10 times and incubated on ice for 30 minutes. A QIAGEN-tip 500 was equilibrated with 10 mL Buffer QBT (equilibration buffer: 750 mM NaCl; 50 mM MOPS, pH 7.0; 15% isopropanol v/v; 0.15% Triton® X-100 v/v) and left to drain completely by gravity flow, after which filtered lysate was applied to the

same column to enter the resin. A volume of 30 mL Buffer QC (wash buffer: 1.0 M NaCl; 50 mM MOPS, pH 7.0; 15% isopropanol v/v) was used twice to wash the column, and DNA was later eluted with 15 mL Buffer QN (elution buffer: 1.6 M NaCl; 50 mM MOPS, pH 7.0; 15% isopropanol v/v) into a 30 mL endotoxin-free tube. The eluted DNA was precipitated by adding 10.5 mL (0.7 volumes) room-temperature isopropanol, mixed and centrifuged promptly at ≥15,000 *g* for 30 minutes at 4°C, then the supernatant carefully decanted. The remaining DNA pellet was washed with 5 mL endotoxin-free room temperature 70% ethanol, and centrifuged at ≥15,000 *g* for 10 minutes. After carefully decanting the supernatant, the pellet was air-dried for 5-10 minutes and the DNA re-dissolved in 0.5-1 mL of endotoxin-free Buffer TE (10 mM Tris-Cl, pH 8.0; 1 mM EDTA). The final yield of DNA concentration was measured using a NanoDrop™ One Microvolume UV-Vis spectrophotometer (Thermo Fisher Scientific Cat. *#ND-ONE-W*, Version 1.4.0).

2.6 Sanger Sequencing

Plasmid DNA was analysed by Sanger sequencing. Forward primers were designed for every 300 base pairs spanning the entire protein-coding region of *sMEK1* gene to ensure full sequence coverage with minimal overlapping.

Primer	**Sequence**	**Melting point, Tm**
1F	5’- GCACGATGACCGACACCCG -3’	72.6°C
2F	5’- ATGTCAGGTTCAAGGAAAGGACCC -3’	69.0°C
3F	5’- AAAGGCATCTTTCTCTTGAATCGAACTG -3’	69.6°C
4F	5’- TAAGGTAGAGATTGTTGGCATGTTGCA -3’	69.7°C
5F	5’- GAGAGTTTGTCATGCAGGAGGC -3’	63.8°C
6F	5’- CAAACCTAGTAAAGATGATTTTCAGACTGC -3’	66.4°C

7F	5’- TGATGAACTCTGCCATAATAGAGATGTTTG -3’	68.3°C
8F	5’- TAGTGTCTCCATCTGACAAAACTAAAAATGAT -3’	66.9°C
9F	5’- TACTACAAAGGGAGGCCTCGTG -3’	66.2°C

Five microlitres each of the primer and DNA were prepared per reaction at the concentrations specified below: -

Plasmid DNA - 100 ng/μL

Primers - 3.2 pmol/μL

The tubes were analysed by the sequencing service provided by Source BioScience (Nottingham, UK). Relevant sequencing data was inspected using Chromas Lite software (Version 2.6.5). The FASTA sequence was copied and pasted into BLAST@NCBI (https://blast.ncbi.nlm.nih.gov/Blast.cgi) to translate nucleotides into peptides. Top protein hits were ranked based on the percentage similarity after aligning and comparing the region covered by each primer.

2.7 DNA damage induction and drug treatment

2.7.1 Chemical treatment

Panobinostat (PAN) is a histone deacetylase (HDAC) inhibitor. Two millimolar PAN was prepared from the stock solution (LBH589, Selleck Chemicals Cat. *#S1030*, USA) and dispensed as aliquots of 1 mL. Five different PAN concentrations i.e. 0, 5, 10, 15 and 25 μM were prepared by serial dilution using DMSO as the solvent. A volume of 10 μL was added to 10 cm plates to observe the changes in sMEK1 protein expression with PAN in the nanomolar range. The cells were then grown for 24-48 hours’ post-treatment in a 37°C incubator in 5% CO_2.

2.7.2 Irradiation

Cells were pre-treated with DMSO (control) or 25 nM PAN, and incubated for 24 hours before treatment with ionising radiation (IR) (Gamma-Service Medical GmbH GSR-D1 Caesium-137, Serial *#A0108*) dose of 5 Gy. Following irradiation, the cells were transported on ice and either harvested immediately at t=0 hour to study the immediate cellular response to radiation-induced DNA damage, or replaced in a 37°C incubator with 5% CO_2 until t=4 hours to probe the extent of recovery or repair after the initiation of DNA damage.

2.8 Protein Analysis

2.8.1 Cell lysis

One tablet of Mini Complete™ protease inhibitor cocktail (Sigma-Aldrich Roche Cat. *#11836153001*, Germany) was dissolved fully in 10 mL lysis buffer by vortexing. Approximately twice the pellet volume of freshly-made lysis buffer was added to resuspend cell pellets on ice and the solution was incubated for a minimal duration of 5 minutes. The lysates were briefly probe-sonicated with five pulses (BioLogics Inc. Model 300 V/T ultrasonic homogenizer, pulser set at 30), followed by the addition of 0.5 µL benzonase (Nuclease 27.7 U/μL, Novagen® EMD Millipore Cat. *#707464*, Germany) to digest nucleic acids and release nuclear proteins associated with DNA. After 30 minutes' incubation on ice, the tubes were centrifuged at full-speed (14,000 rpm) for 8 minutes at 4°C, then the lysates were transferred to fresh Eppendorf tubes without disturbing the pellets at the bottom of the tubes.

2.8.2 BCA quantification

Total protein concentration in individual tubes was determined using a Pierce™ BCA Protein Assay kit (Thermo Fisher Scientific Cat. *#23227*, USA) by comparison to known protein standards. Bovine serum albumin (BSA) standards of 0, 100, 200, 300, 400, 500, 600, 700, 800, 900, 1000 and 2000 ng/μL, were prepared from 2 mg/mL stock in 0.9% saline and 0.05% sodium azide (Thermo Fisher Scientific Cat. *#23209*, USA). In preparing the BCA working reagent (WR), 20 μL Reagent B (4% cupric sulfate) was added per 1 mL of Reagent A (sodium carbonate, sodium bicarbonate, bicinchoninic acid and sodium tartrate in 0.1 M sodium hydroxide) at a 1:50 ratio. With reference to the protocol, quantification of 10 µL of each standard and 1 µL of unknown lysate was performed in duplicate on a 96-well plate within the limited working range of 125-2000 µg/mL. Following addition of 200 µL of the WR to each well and thorough mixing by gently pipetting up and down, the plate was covered and placed in a 37°C incubator for 30 minutes. Upon cooling to room temperature, it was read by a plate reader spectrophotometer (BMG Labtech POLARstar Omega) to measure the absorbance value at or near 562 nm. The average absorbance measurements of the blank standard duplicates at 562 nm were subtracted from other measurements of the standards and unknown lysates. A standard curve was fitted with linear regression in the 'calculations' tab of MARS software (BMG) and the protein concentration (ng/µL) of each unknown lysate could be determined.

2.8.3 Co-immunoprecipitation (co-IP)

Dynabeads™ Protein A (Thermo Fisher Scientific Invitrogen™ Cat. *#10002D*, Norway) were resuspended with vortexing, and 10 µL aliquoted per sample into new Eppendorf tubes with the pipette tip end clipped off to avoid clumping. The Dynabeads were

washed 3x with 100 µL cold lysis buffer, vortexed and captured using a magnetic rack while removing washes. Then, 300-500 µg of cell lysate in a volume of 200 µL was pre-cleared by adding to the washed beads for 30-60 minutes with rotation at 4°C, to remove off-target or non-specific binding to the beaded support before assembly of binding complexes. Cleared lysate was then transferred to a fresh tube and 5% of the total volume saved as the load fraction. Then, 1-5 µg of antibody against the protein of interest was added to the lysate, with non-specific IgG of the same species (Rabbit/Mouse) used as a control. After an overnight incubation at 4°C on rotating wheels, the lysate-antibody mixture was added to washed beads and incubated for an hour at 4°C with rotation. The beads were finally washed 6x with 100 µL PBS-T using a magnetic rack while discarding flow-through and washes.

To isolate recombinant HA-tagged sMEK1 expressed in the cells after transfection and their interacting proteins, Pierce™ Anti-HA magnetic beads (Thermo Fisher Scientific Cat. *#88836*, USA) were used. Ten microlitres of beads were washed per sample, as described above with suitable buffer, and the lysate added following a pre-clearance step with 10 µL Dynabeads™ Protein A. A control was set up using lysate from untransfected cells, or overnight incubation of transfected sample with non-specific IgG and subsequently Dynabeads for 1 hour.

For acetylated protein immunoprecipitations and co-immunoprecipitation of the associated binding complexes, 5 µL of Anti-acetyl lysine agarose beads (ImmuneChem Cat. *#ICP0388*, Canada) were used. Pre-clearance was carried out using 5 µL Pierce™ Control agarose resin (Thermo Fisher Scientific Cat. *#26150*, UK). After washing with

suitable buffer, these beads were subjected to centrifugation at 3,000 *g* for 1 minute and the washes discarded without disturbing the beads at the bottom of the tube.

2.8.4 SDS-PAGE

Bound complexes were eluted from the beads by boiling with 15 µL 2x Laemmli sample buffer (Sigma-Aldrich Cat. *#S3401-10VL*, MO, USA) or 7.5*µ*L 4x (BioRad Cat. *#1610747*, USA) on a heat block (Labnet AccuBlock™ Digital Dry Bath) at 95°C for ≥ 5 minutes. Load fractions were simultaneously subjected to boiling after adding Laemmli buffer (2x: same volume; 4x: 1/3 volume) to make up a final concentration of 1x. The samples were then briefly centrifuged prior to loading. However, in the acetyl-lysine pull down assay, it was necessary to spin down the agarose beads at full speed 17,000 *g* using a bench-top centrifuge (Thermo Fisher Scientific accuSpin Micro 17) for 3 minutes, to minimise loading of beads that could adversely affect the speed of samples running on a gel. A protein concentration of 30 µg was sufficient for a total lysate western blot, and samples were made up to the same final volume with lysis buffer.

An electrophoresis tank was set up with a short gel plate facing inwards and the middle reservoir filled with 1x running buffer (10-fold dilution from 10x stock). Full-range Rainbow™ molecular weight markers (GE Healthcare RPN800E Cat. *#45-001-591*, USA) of 2 µL, 10 µL load and 15 µL eluted fractions from immunoprecipitations were loaded into separate wells respectively on a precast gel (BioRad Mini-PROTEAN® TGX™ Gels gradient 4-20% precast, 15-well: Cat. *#4561096*; 10-well: Cat. *#4561094*, UK). Care was taken not to exceed the maximum volume of each gel loading well. The gel was run at 100 V for 1 hour 10 minutes (BioRad PowerPac™ HC 250V, 3.0A,

300W or Labnet Enduro™ 300V); upon completion the blue marker dye reached the bottom of the gel, with well-separated markers.

2.8.5 Western Blot

Cold transfer buffer 1x (10-fold dilution from 10x stock and 20% methanol) was prepared for western blot. The setup from bottom to top was: the red/clear side of the cassette, sponge, filter paper, Immobilon P membrane (Thermo Fisher Scientific Cat. *#88518*, UK), gel, filter paper, sponge and finally the black side of the cassette. Materials such as sponges, filter paper, gel and membrane were soaked in transfer buffer on a tray until completely wet. The membrane was held by the edges to avoid blotches as a result of touching the centre. During the stacking process, membrane and gel were checked for bubbles, smoothed out with a roller and continuously kept wet by topping up with transfer buffer. Western blots were run at 40 V for 2 hours with an ice pack placed in the tank.

2.8.6 Immunoblotting with antibodies

Upon completion, the membrane was transferred into a black box and incubated with 1x blocking buffer for 30-60 minutes in order to block non-specific binding on the membrane. Specific primary antibodies, diluted in blocking buffer to desirable concentrations, were incubated with the blot overnight at 4°C on a rocker. After 3x washing with PBS-T at 10-minutes intervals, secondary antibodies labelled with infrared dye (goat anti-rabbit: 680 red channel, goat anti-mouse: 800 green channel, LI-COR) were diluted 1:10000 in LiCor block: PBS-T mixture, then added to the membrane for 45-60 minutes at room temperature. The membrane was finally washed 3x at 10-minute intervals using PBS-T then stored in PBS-T until read on an Odyssey

scanner (LI-COR Infrared Imager, software version 3.0.30), and analysed with LI-COR Image Studio Lite program (Version 5.2).

2.9 Subcellular Fractionation

A total of four 15 cm confluent plates were used per condition for subcellular fractionation. Cells were washed twice with PBS, then lifted with 5 mL of PBS + 3 mM EDTA at 37°C after 10-15 minutes incubation. Following sample collection of each plate in 4x 1.5 mL centrifuge tubes, the cells were spun down at 500 *g* for 3 minutes at 4°C. Supernatant was discarded and the cells were resuspended in 1 mL of cold PBS, later centrifuged at 500 *g* for 3 minutes at 4°C and supernatant discarded while keeping the pellets intact. Subsequently, cells were resuspended in twice the pellet volume (~250 μL) of 1x Buffer A plus inhibitors. A volume of 3.5 μL 10% Triton X100 (final concentration: 0.1%) was added and mixed by gentle tapping, after which the tubes were incubated for 5-30 minutes on ice. Upon complete incubation, the tubes were centrifuged at 500 *g* for 3 minutes, supernatant collected and then centrifuged again at 500 *g* for 3 minutes before pooling them into one tube. The cytoplasmic fraction was obtained after the final centrifugation at 5,000 *g* for 10 minutes.

The remaining nuclear pellet was washed twice with Buffer A plus inhibitors, centrifuged at 500 *g* for 3 minutes and supernatants discarded. Subsequently pellets were resuspended in 150 μL of 1x Buffer B plus inhibitors and mixed by tapping. Tubes were centrifuged at 1,700 *g* for 3 minutes after a minimum of 5 minutes incubation on ice, and the supernatants were pooled. Following a final spin at 5,000 *g* for 5 minutes, the nuclear fraction was collected in a new tube.

Pellets remaining in each tube were resuspended in 350 μL Buffer B and 35 μL 10% Triton X100 before spinning down at 5,000 *g* for 5 minutes. Supernatant was discarded and the pellet resuspended in benzonase buffer with 2.5 mM $MgCl_2$. After centrifugation at 5,000 *g* for 5 minutes, the supernatant was again discarded and the pellet resuspended in 150 μL benzonase buffer in addition to 1 μL each of benzonase and RNase (10 mg/mL, Thermo Fisher Scientific Cat. *#EN0531*) enzymes. The tubes were incubated overnight at 4°C on a rotating wheel, centrifuged at 15,000 *g* for 5 minutes, and supernatants later pooled together as the chromatin-bound fraction.

2.10 Functional assays

2.10.1 Clonogenic assay

Following 24-48 hours' treatment with PAN or siRNA transfection as appropriate, T24 cells were trypsinised and counted using a haemocytometer before re-seeding the required number of cells per 10 cm dish. For each condition, three independent biological replicates were performed to improve reliability. An additional 10-15 minutes were given for the cells to partially adhere, after which the plates were subjected to irradiation of 2, 4, 6 or 8 Gy and no IR in controls. Upon completion, all plates were kept in a 37°C incubator with 5% CO_2 for 7-10 days. The optimal timeframe for T24 cells was determined to be 8 days when visible colonies were seen growing on those plates treated with the highest irradiation dose of 8 Gy.

Variation in the seeding density is shown following optimisation in Table 2-2.

Table 2-2. The required seeding densities of T24 cells for clonogenic assays after different treatments as listed below.

Condition	0 Gy	2 Gy	4 Gy	6 Gy	8 Gy
T24 control untreated	500	600	800	800	1200
25 μM PAN (24 hours)	1000	1200	1500	1500	2400
DMSO (24 hours)	500	600	750	750	1200
Non-targeting/ siRNA	500	600	800	800	1200
Rescue transfection WT/ K416R/ K416Q	800	900	1100	1100	1500
Combined siRNA + PAN	1000	1200	1500	1500	2400

Medium was then aspirated and the plates washed with 5 mL of PBS, after which the wash-through was discarded. Excess PBS was drained off by keeping the plates face-down on clean paper towels. For colony staining, 5-6 mL of prepared crystal violet solution was added to each plate, and incubated for 5 minutes at room temperature before washing with tap water. Then, the plates were dried overnight and colonies quantified using a GelCount™ instrument (Oxford Optronix) with optimised standard parameters.

2.10.2 Immunocytochemistry (ICC) of γH2AX foci

T24 cells were treated with either PAN, sMEK1 plasmid overexpression or siRNA and the rescue transfection of wild type (WT), acetyl-dead (K416R) or acetyl-mimic (K416Q) variant of sMEK1, for an appropriate time duration of 24-48 hours. A fixed number of 10^5 cells was subsequently re-seeded into individual wells of an 8-well chamber slide (Thermo Fisher Scientific Nunc™ Lab-Tek™ Cat. *#154534*, Germany) and allowed to grow overnight in 400 μL RPMI culture medium. Following 5 Gy IR,

the cells were incubated at 37°C for 10, 30 minutes, 2, 4, or 24 hours, after which the cells were rinsed briefly with PBS. Control was also set up for each of the conditions without irradiation treatment at t=0.

The cells were fixed using 4% paraformaldehyde (Merck Millipore Cat. *#100496*, UK) in PBS adjusted to pH 7.4 for 10 minutes at room temperature, and washed three times with ice-cold PBS for 5-minute intervals. Since sMEK1 protein is found intracellularly, it was crucial to permeabilise the cells with PBS containing 0.25%Triton X-100 detergent. After 10 minutes' incubation at room temperature, the cells were washed in PBS three times for 5 minutes. PBST (PBS + 0.1% Tween 20) containing 1% bovine serum albumin (BSA) (Europa Bioproducts Cat. *#EQBAH62-1000*, UK) and 22.52 mg/mL glycine was prepared to block non-specific binding of the antibodies, with an incubation period of 30 minutes at room temperature. The cells were later incubated with 200 μL anti-phospho-Histone H2A.X (Ser139) antibody (Merck Millipore mouse mAb clone JBW301 Cat. *#05-636*, USA) diluted to 1:500 ratio in 1% BSA in PBST in a humidified chamber at 4°C overnight. After decanting the primary antibody solution, the cells were washed three times in PBS for 5 minutes. Alexa Fluor™ 568 (red fluorescence) donkey anti-mouse IgG (H+L) secondary antibody (Thermo Fisher Scientific Invitrogen™ Cat. *#A10037*, USA) was diluted 1:500 in 1% BSA in PBST and 200 μL was added per well for an hour's incubation at room temperature in the dark. The washing step with PBS for 5 minutes each in the dark was repeated three times before proceeding to immunostaining with the second primary antibody anti-sMEK1 (abcam rabbit pAb Cat. *#ab221392*, UK) at a 1:100 dilution and its corresponding secondary antibody Alexa Fluor™ 488 (green fluorescence) goat anti-rabbit IgG (H+L) (Thermo Fisher Scientific Invitrogen™ Cat. *#A11034*, USA) at a 1:500 dilution using the same procedure described previously. For mounting and positive staining of the

nuclei, ProLong™ Diamond Antifade Mountant with DAPI (Thermo Fisher Scientific Invitrogen™ Cat. *#P36962*, USA) was used with a glass slide placed over the specimen. Extra care was taken to minimise trapped air bubbles which would affect the image quality. Finally, scanning of the slides was performed using a Zeiss 710 confocal laser scanning microscope, analysed with ZEISS ZEN lite (Version black 2.3 SP1/ blue 2.5) and FIJI software (FIJI Is Just ImageJ). The nuclear outline as indicated by DAPI (blue staining) was traced on FIJI to allow the number of gamma H2A.X (γH2AX) foci, as well as the changes in nuclear sMEK1 expression level, to be quantified across time after the action of IR. This relied on the assumption that the fluorescence intensity is directly proportional to the protein abundance.

Target	**Fluorophore**	**Excitation wavelength/ nm**	**Emission wavelength/ nm**
DAPI	Blue	358	461
sMEK1	Green	490	525
γH2AX	Red	578	603

2.11 Statistical analysis

All the statistical analyses were carried out using GraphPad software (Prism version 6.0), and an unpaired Student's *t* test performed to indicate the statistical comparison of independent samples treated under different conditions. Data were plotted as mean ± standard error of the mean (SEM), with *P* values shown in the figures. A *P* value of <0.05 was considered a statistically significant difference.

3. RESULTS

3.1 Increased global acetylation and delayed DNA damage response with panobinostat

To investigate the changes in global protein acetylation after exposure to ionising radiation (IR) over the course of DNA repair, human embryonic kidney (HEK) 293T cells were treated with 5 Gy radiation dose and harvested immediately post-IR or after 4-hour recovery time (Figure 3-1A), in the presence or absence of the HDAC inhibitor panobinostat (PAN) at the IC_{50} drug concentration of 25 nM. This cell line was chosen due to the cancer stem cell-like phenotype seen in HEK293T cells lacking normal pRb and p53 functions after immortalisation by adenovirus type 5 E1a and E1b, enabling them to be readily cultured and passaged for various cancer experiments. In control dishes, an equal volume of dimethyl sulfoxide (DMSO) was added to compensate for the undesirable effect of dissolving PAN in a polar solvent and to account for any effects DMSO might have on the cells that could appear like a drug effect. Using acetyl-lysine (AcK) antibodies with different epitopes to detect acetylated proteins on a western blot, a band corresponding to the molecular weight of histones at ~17 kDa was clearly increased as expected in PAN-treated cells (Figure 3-1B). Altered patterns of higher molecular weight bands were also observed with PAN treatment immediately after and 4-hour post-IR relative to non-irradiated cells, suggesting non-histone proteins may be differentially acetylated in the DNA damage response (DDR) after HDAC inhibition. Here, a combination of PAN with IR treatment at either time point resulted in increased overall amount of acetylated proteins compared to that of DMSO and IR, with the detection of many higher molecular weight species than histones. This indicates dynamic acetylation of proteins during the DDR, and this process can be disrupted by inhibiting HDAC enzymes.

Next, I aimed to validate the *in vitro* radiosensitising potential of PAN in the HEK293T cell line, by immunoblotting for phospho-ATM (P-ATM) and gamma H2A.X (γH2AX) using the same timeline as before at t=0 (immediate DDR) and 4 hours (later DDR) after irradiation. These levels were measured on a western blot to mark the progress of DNA damage/repair with time, then quantified using ImageJ software. The reliability of P-ATM and γH2AX as biomarkers of IR-induced DNA damage is demonstrated by the significantly increased levels immediately after 5 Gy IR in both the DMSO- and PAN-treated cells (Figure 3-2). At 4-hour post-IR however, P-ATM and γH2AX in the DMSO-control dropped back to the basal levels comparable to that of non-irradiated cells, but with PAN treatment, a significantly higher γH2AX level was attained together with a small non-significant decrease of P-ATM. With normalisation to actin as the loading control, PAN administration was found to be associated with a significant delay in the DDR, as shown by the persistence of DNA damage markers in comparison to DMSO (*P= 0.0061 for γH2AX; 0.011 for P-ATM*). These results led to the hypothesis that the radiosensitising mechanism of action of PAN potentially occurs through acetylation of non-histone target proteins with a role in DNA repair.

A

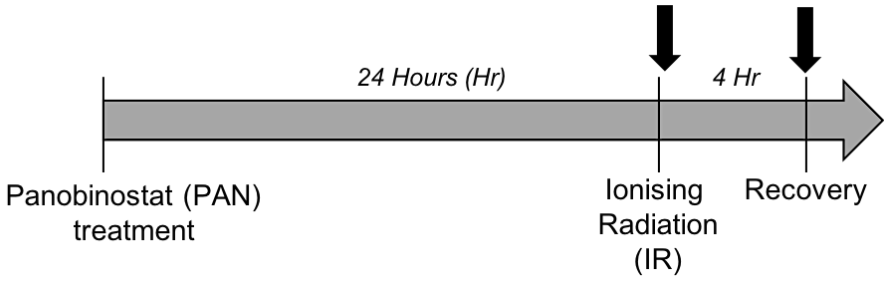

B

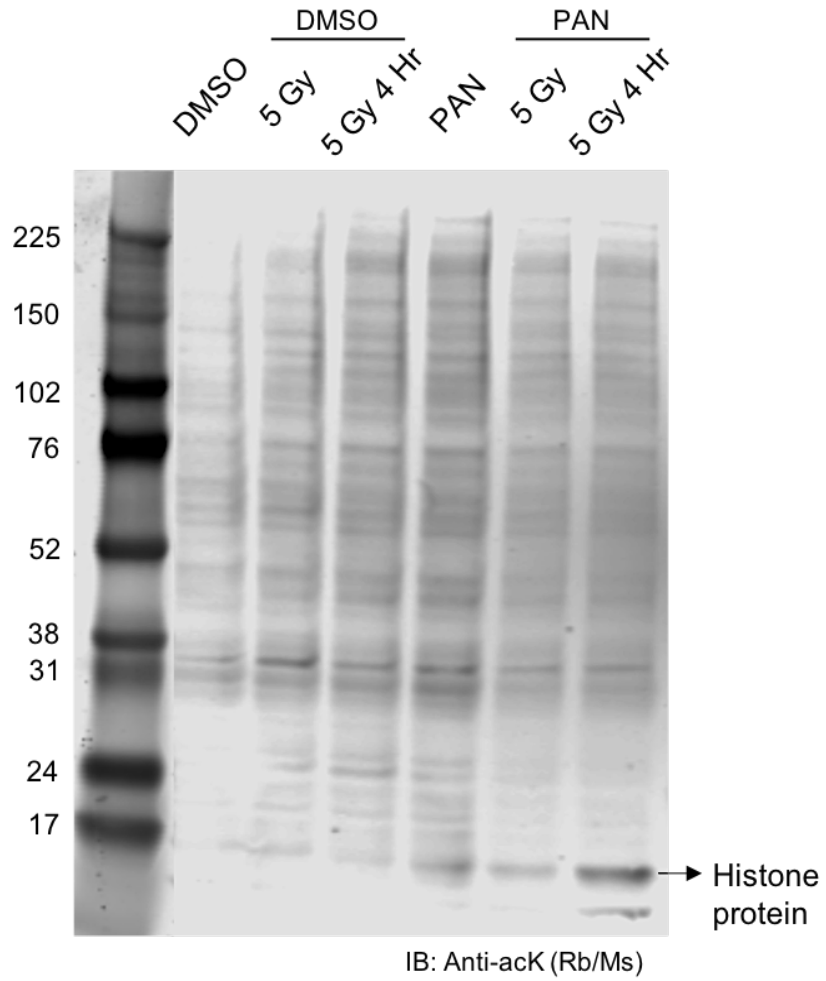

Figure 3-1. Increasing global acetylation pattern of the histone and non-histone proteins in PAN-treated cells with or without irradiation. (A) Timeline of 24-hour PAN treatment followed by IR and 0 or 4-hour recovery time before harvesting the cells. For control samples, an equal volume of DMSO was used. (B) Changes in the global acetylation pattern in DMSO- or PAN-treated HEK293T cells before and after irradiation. Acetyl peptides were immunoblotted using antibodies targeting different epitopes with anti-acetyl lysine antibodies of both mouse and rabbit origins. Most of the acetylated proteins are detected at higher molecular weights above 17 kDa, thus indicating the acetylation of non-histone proteins as well as histones after HDAC inhibition by PAN.

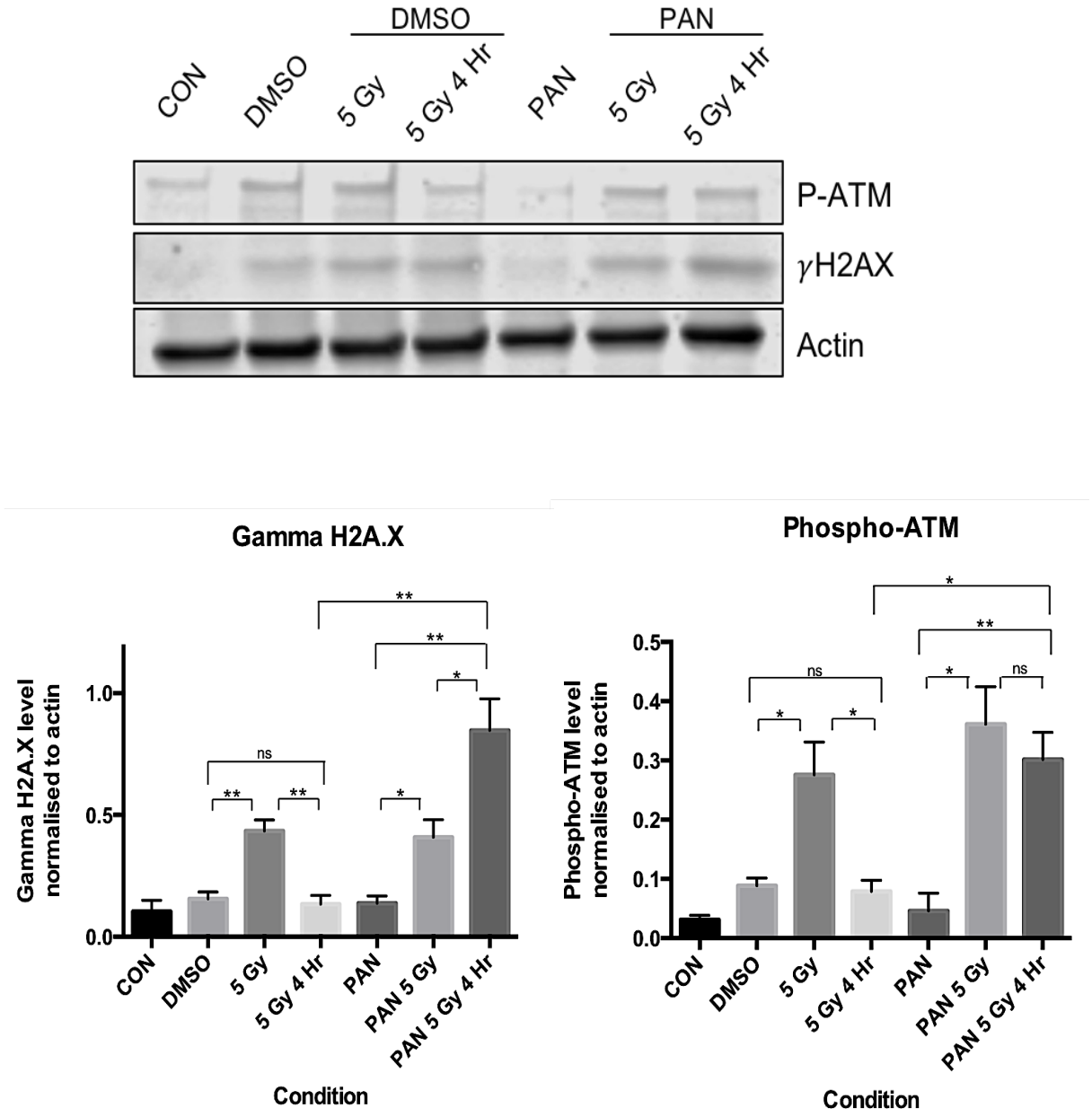

Figure 3-2. Panobinostat induces a delayed DNA damage response after ionising radiation. Western blot illustrating the level of DNA damage markers including phospho-ATM (P-ATM) and gamma H2A.X (γH2AX) before, immediately after or 4 hours after 5 Gy radiation in HEK293T cells. Actin acts as the loading control for quantification. The basal level of these markers is obtained from their respective control lanes labelled as DMSO or PAN alone without IR. P-ATM and γH2AX levels are quantified after normalising to the actin abundance over n=3 independent replicates. Data are represented as mean $\pm$ standard error of the mean (SEM). ** $p < 0.01$; * $p < 0.05$; ns $p > 0.05$.

3.2 Downregulation of sMEK1 protein expression independent of panobinostat concentration

From a recent acetylome screen by mass spectrometry conducted in the lab after PAN treatment, 169 novel acetylation sites on non-histone proteins have been discovered, some of which have previously identified roles in the DDR, such as UCHL5 deubiquitinase and THRAP3 RNA processing factor (Nicholson et al., submitted). Suppressor of MEK1 (sMEK1), the regulatory subunit of serine/threonine-protein phosphatase PP4 complex, was also identified and chosen for investigation, since it has a known role in DNA repair and is associated with chromatin (Chowdhury et al., 2008) but has not been extensively studied to date. It is hypothesised that increasing histone acetylation via HDAC inhibition alters chromatin compaction and accessibility of the promoter to transcription factors, so it was decided to examine the effects of PAN treatment and/or IR on endogenous sMEK1 expression, and any correlation to downregulation of the DDR.

The urinary bladder transitional carcinoma cell line T24 which is representative of invasive bladder tumour with a metastatic profile (Zhao et al., 2017), was treated with an equal volume of either DMSO (control) or 25 nM PAN for 24 hours before being subjected to 5 Gy IR. A significant downregulation ($P= 0.0024$) of endogenous sMEK1 protein levels was observed with PAN treatment alone without IR (Figure 3-3). To better understand if the protein downregulation occurs in a PAN concentration-dependent manner, T24 cells were treated with 10, 25 and 50 nM PAN for 24 hours before harvesting the cells to run a western blot using total lysate fractions of 30 μg. In comparison to DMSO control, the average expression of endogenous sMEK1 protein was reduced by 20% after 24 hours independently of the PAN concentration (Figure 3-

4). Shorter time intervals of 1-, 2-, 4- and 8-hour post-treatment were also studied to establish whether the changes occurred at the level of messenger RNA (mRNA) expression or protein degradation. Using the computational method of protein expression control analysis (PECA) which dissected global mRNA- and protein-level regulation with substantial temporal differences, Teo et al. (2014) found that significant downregulation of RNA expression was mostly observed at 16 hours with an average 1.5-fold change, whereas the protein level underwent rapid transient changes in its corresponding degradation coefficient with a pronounced magnitude and much less fluctuation towards the late phase (Cheng et al., 2016). Since no significant changes in total endogenous sMEK1 level were visualised (Figure 3-5), this implies that the downregulation took place at a later time-point than 8 hours after PAN treatment, possibly through mRNA regulation.

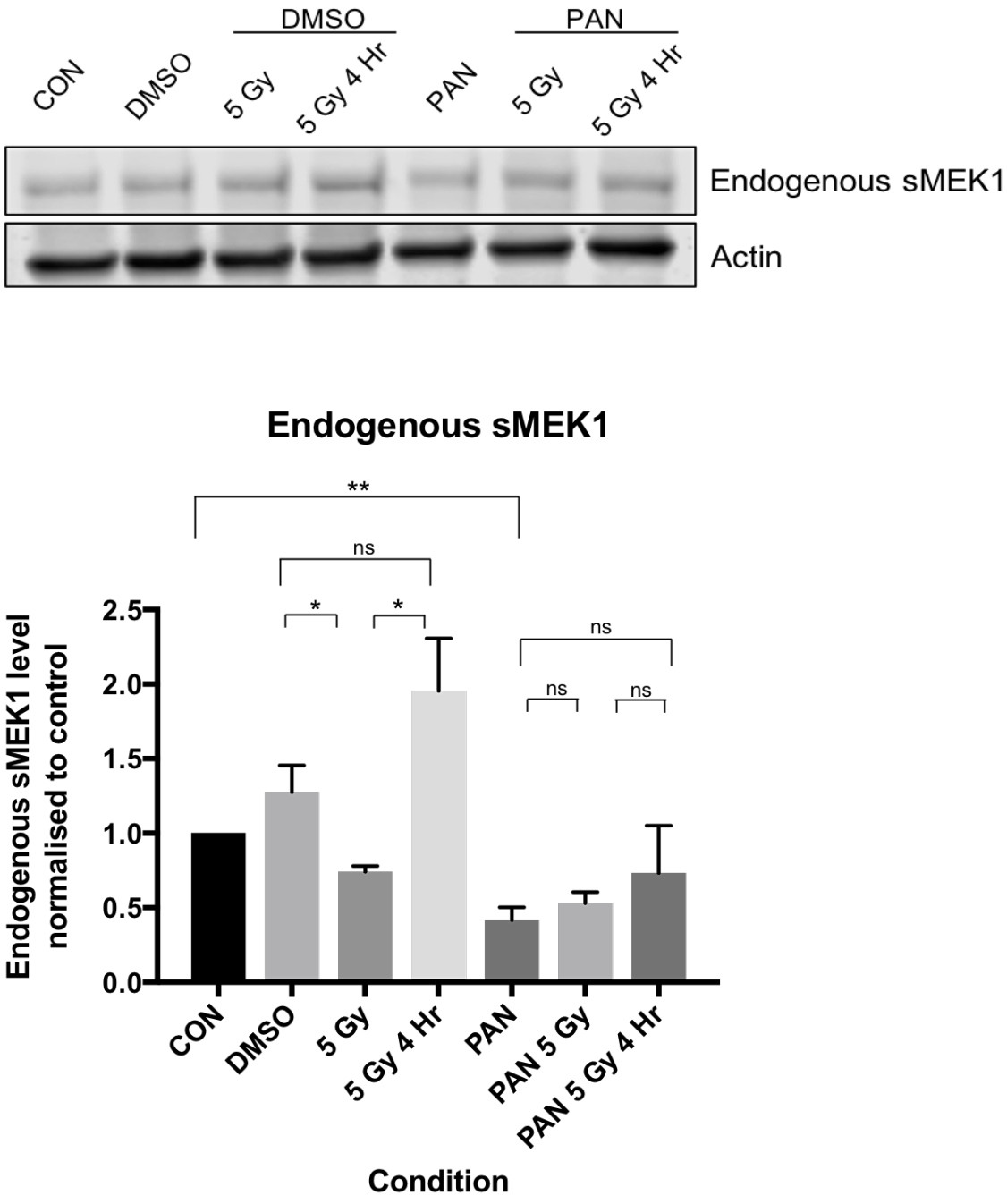

Figure 3-3. **Downregulation of endogenous sMEK1 protein by panobinostat treatment alone.** Changes in the endogenous sMEK1 expression level with DMSO (control) or PAN before and after irradiation in T24 cells. Actin acts as the loading control for quantification. Average level of sMEK1 under each condition is calculated from n=3 independent experiments and data are plotted as mean ± SEM after normalising to the untreated control. ** $p < 0.01$; * $p < 0.05$; ns $p > 0.05$.

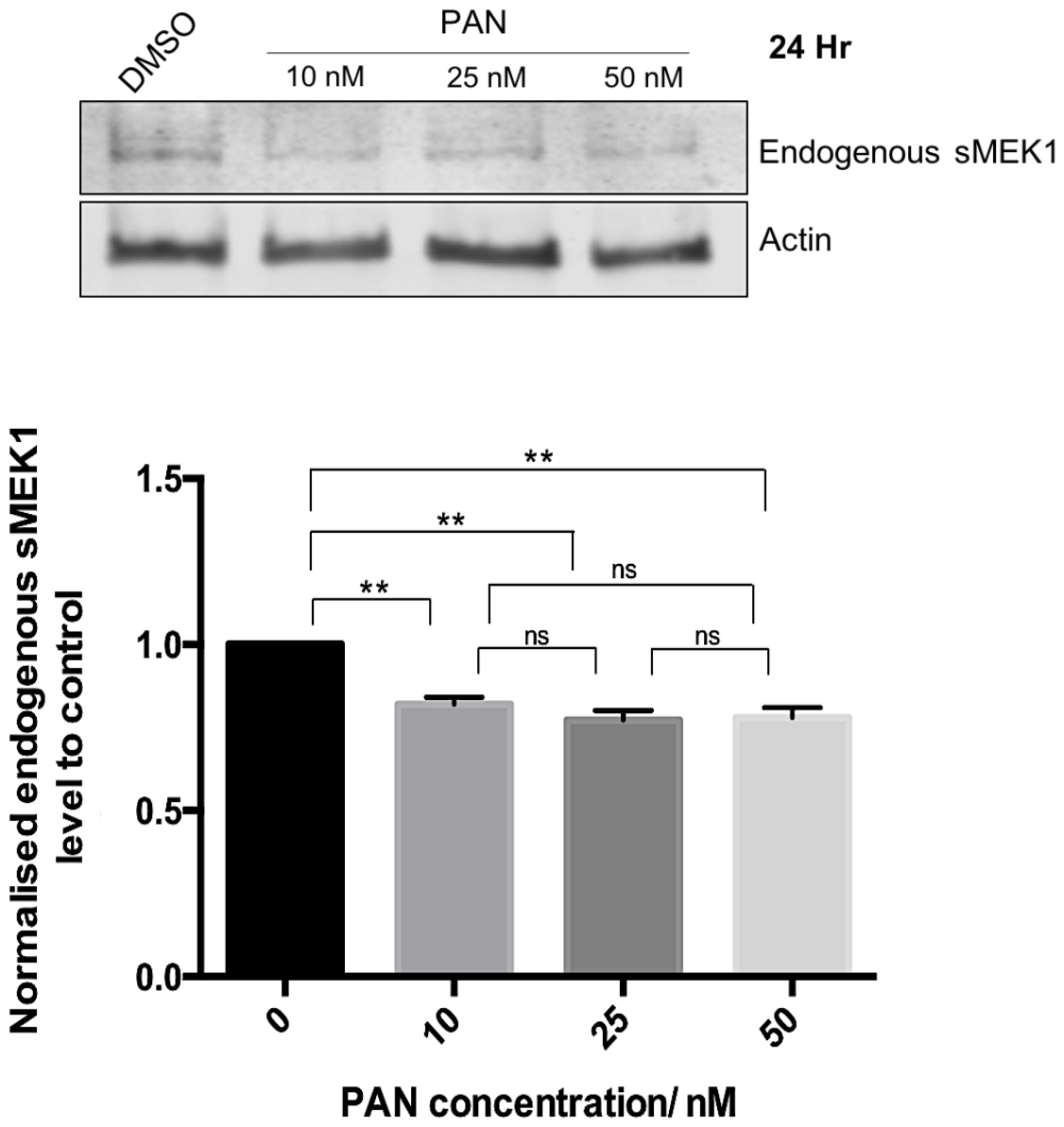

Figure 3-4. **Downregulation of endogenous sMEK1 protein in a concentration-independent manner of panobinostat after 24-hour interval.** The endogenous sMEK1 protein expression level is downregulated 24 hours after PAN treatment of 10, 25 or 50 nM in T24 cells. Actin as the loading control for subsequent quantification. Data are displayed as mean ± SEM for n=3 independent replicates with normalisation to the sMEK1 to actin ratio in DMSO control, in order to facilitate the calculation of the percentage reduction in sMEK1 protein expression. ** $p < 0.01$; ns $p > 0.05$.

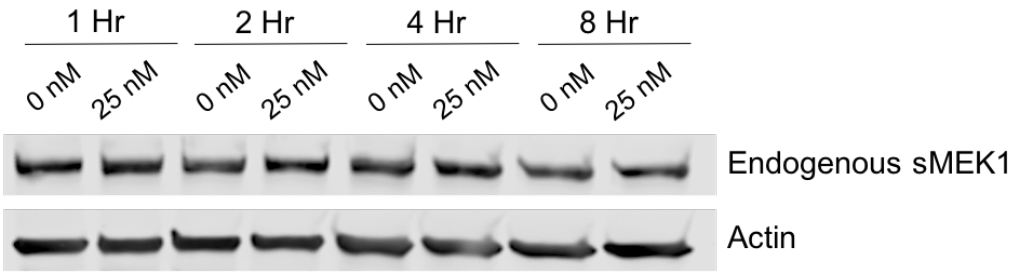

Figure 3-5. **PAN-mediated downregulation of endogenous sMEK1 protein occurs beyond 8-hour duration.** Fluctuations in endogenous sMEK1 level at shorter time intervals of 1, 2, 4 and 8 hours after DMSO or 25 nM PAN treatment in T24 cells. No visually significant change is observed up to 8 hours, suggesting the regulation likely occurs at the level of messenger RNA at a later time-point between 8-24 hours.

To amplify the minor changes observed at low endogenous protein levels, HEK293T cells were transiently transfected with sMEK1 cDNA plasmid obtained from Sino Biological Inc. using polyethylenimine (PEI) reagent for 24-48 hours on three separate dishes. Overexpressed sMEK1 tagged with hemagglutinin (HA) at the C-terminal was immunoprecipitated by anti-HA magnetic beads and analysed by immunoblotting for sMEK1 (Figure 3-6A). Unexpectedly, this plasmid encoded for a smaller sMEK1 protein variant of ~70 kDa with a ~25 kDa molecular weight difference from the most abundant endogenous isoform of 95 kDa. Sequencing of the plasmid was subsequently performed using forward primers designed for the full length endogenous sMEK1 at a frequency of every 300 base pairs, and ~239 amino acids were found to be missing near the N-terminal domain (Appendix 1).

As per the UniProtKB and PhosphoSite Plus databases on the annotated domain structure of sMEK1 (Figure 3-6B), the overexpressed variant lacked the SMK-1 domain, a component of the insulin/insulin-like growth factor (IGF)-1 signalling (IIS) longevity pathway as well as the Armadillo-type fold, but still retained the acetylation site of Lysine K655 previously identified in the mass spectrometry acetylome screen.

Transfected HEK293T cells were treated with 0, 10 or 25 nM PAN diluted with DMSO, and harvested to check for sMEK1 expression levels after 4, 8 and 24 hours by western blot. Changes in endogenous and transfected sMEK1 levels occurring after 4-8 hours of PAN treatment (Figure 3-7) were not statistically significant ($P > 0.05$). Only at 24-hour post-exposure of PAN was endogenous, but not transfected sMEK1 significantly downregulated to a similar extent in a concentration-independent manner compared to DMSO-treated cells ($P= 0.0090$ *for 10 nM;* 0.0056 *for 25 nM*). Despite insignificant changes in the expression of transfected sMEK1-HA after PAN treatment, the trend of regulation is comparable to its endogenous counterpart. Altogether, these results suggest that the expression of endogenous sMEK1 is likely regulated by PAN at the level of mRNA transcripts during an 8-24 hours' time interval.

A

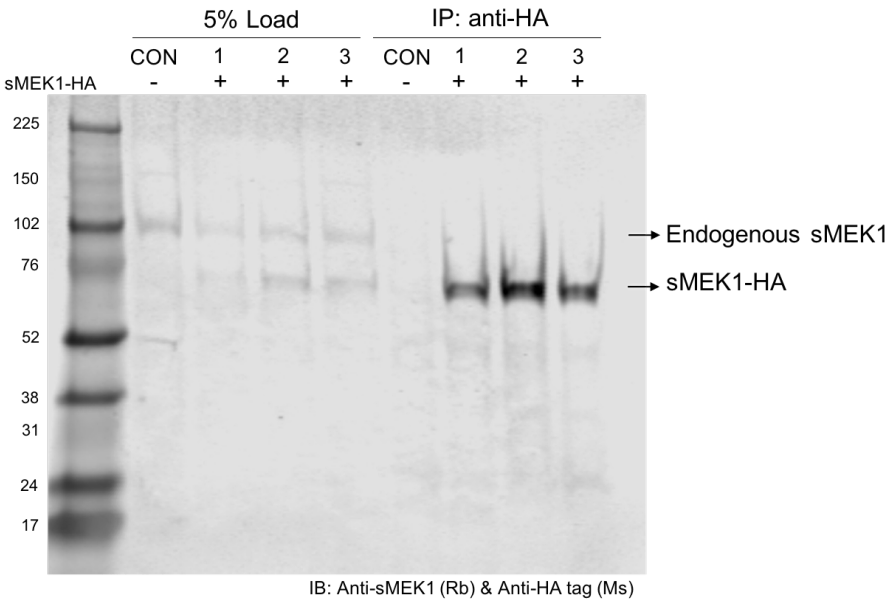

B

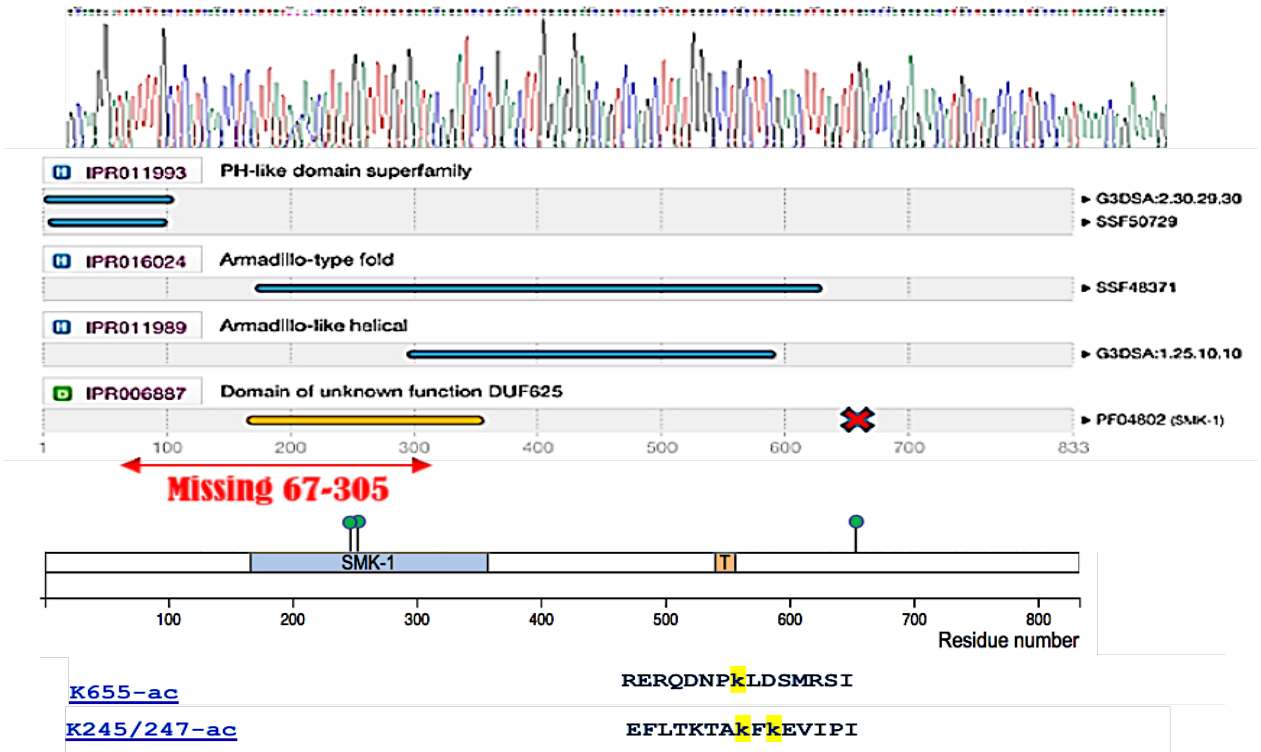

Figure 3-6. Smaller transfected sMEK1-HA lacks 239 residues in the N-terminal domain in comparison to the endogenous isoform. (A) Transfection of HEK293T cells with sMEK1 cDNA plasmid for 24-48 hours on three separate dishes. Overexpressed sMEK1-HA is detected at a lower molecular weight of 70 kDa after co-immunoprecipitation using anti-HA magnetic beads. (B) The known domain structure of sMEK1 protein of 833 amino acids from available online databases including UniProtKB and PhosphoSite Plus. When compared to the sequencing results obtained (Appendix 1), amino acid residues 67-305 are found to be missing from the N-terminal domain, which resulted in a ~25 kDa molecular weight difference, while still retains the acetylated Lysine residue K655 (marked as a red cross).

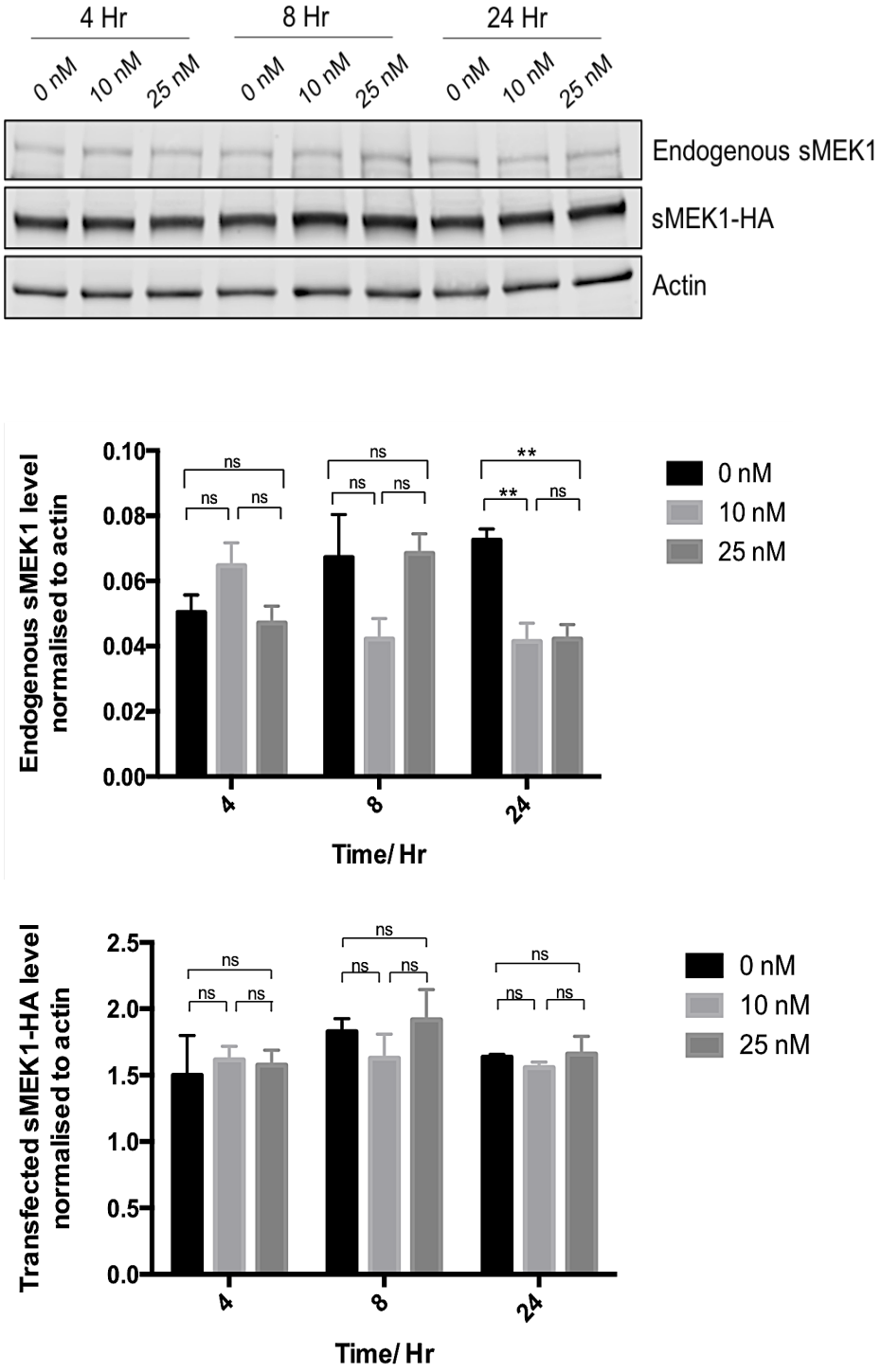

Figure 3-7. Downregulation of endogenous but not transfected sMEK1 between 8-24 hours after panobinostat treatment in a concentration-independent manner. Changes in both the endogenous and transfected sMEK1 levels in HEK293T cells with PAN concentrations of 0, 10 or 25 nM at varying time intervals of 4, 8 and 24 hours within 24-48 hours of transfection. Downregulation of endogenous sMEK1 occurs between 8-24 hours' post-treatment independently of PAN concentration without any significant changes in transfected sMEK1-HA expression. Data from n=3 independent replicates are represented as mean ± SEM. ** $p < 0.01$; ns $p > 0.05$.

3.3 Increased acetylation status of sMEK1 protein following panobinostat treatment

sMEK1 protein not only appeared as one of the top robust hits with three independent biological repeats in the mass spectrometry acetylome study after PAN treatment in the T24 cell line (Nicholson et al., submitted), but it was also recently identified as a nuclear chaperone and cofactor of cleaved Wnt receptor Receptor-like tyrosine kinase (Ryk) in the regulation of cortical neurogenesis (Chang et al., 2017), which is a possible non-histone substrate for histone acetyltransferases (HATs) and HDACs (Glozak et al., 2005). Given that PAN has been demonstrated to increase the global acetylation pattern of histone and non-histone proteins in cells by disrupting the dynamic acetylation-deacetylation equilibrium, it is also predicted to increase sMEK1 acetylation.

To confirm the acetylation status of sMEK1 after 25 nM PAN treatment in transfected HEK293T cells, overexpressed sMEK1-HA was pulled down with anti-HA magnetic beads after 24-hour PAN or DMSO treatment and/or IR and immunoblotted with anti-sMEK1 and anti-acetyl lysine polyclonal antibodies. A band corresponding to acetylated sMEK1-HA was detected at ~70 kDa in all the lanes of PAN-treated cells before and after irradiation (Figure 3-8A). In the DMSO control with or without IR, faint bands of acetylated sMEK1-HA were also observed, suggesting the presence of a low level of acetylation under untreated conditions. Reciprocal co-immunoprecipitation using anti-acetyl lysine agarose beads was then performed to capture acetylated proteins as well as its interacting partners in the eluted fraction. Higher overall levels of acetylated sMEK1 protein, both endogenous and transfected, were found after PAN treatment than DMSO (Figure 3-8B). With reference to total histone H3 level as the loading control and changes in acetylated sMEK1 abundance across different conditions, it can be inferred that loss of sMEK1 acetylation takes place immediately

upon exposure to IR in DMSO-treated cells but is strongly acetylated after 4-hour recovery time. In the presence of PAN however, the acetylation-deacetylation equilibrium was shifted and sMEK1 was less or not deacetylated immediately after irradiation. More sMEK1 acetylation was also detected in PAN-treated cells when allowed to recover from IR over a duration of 4 hours.

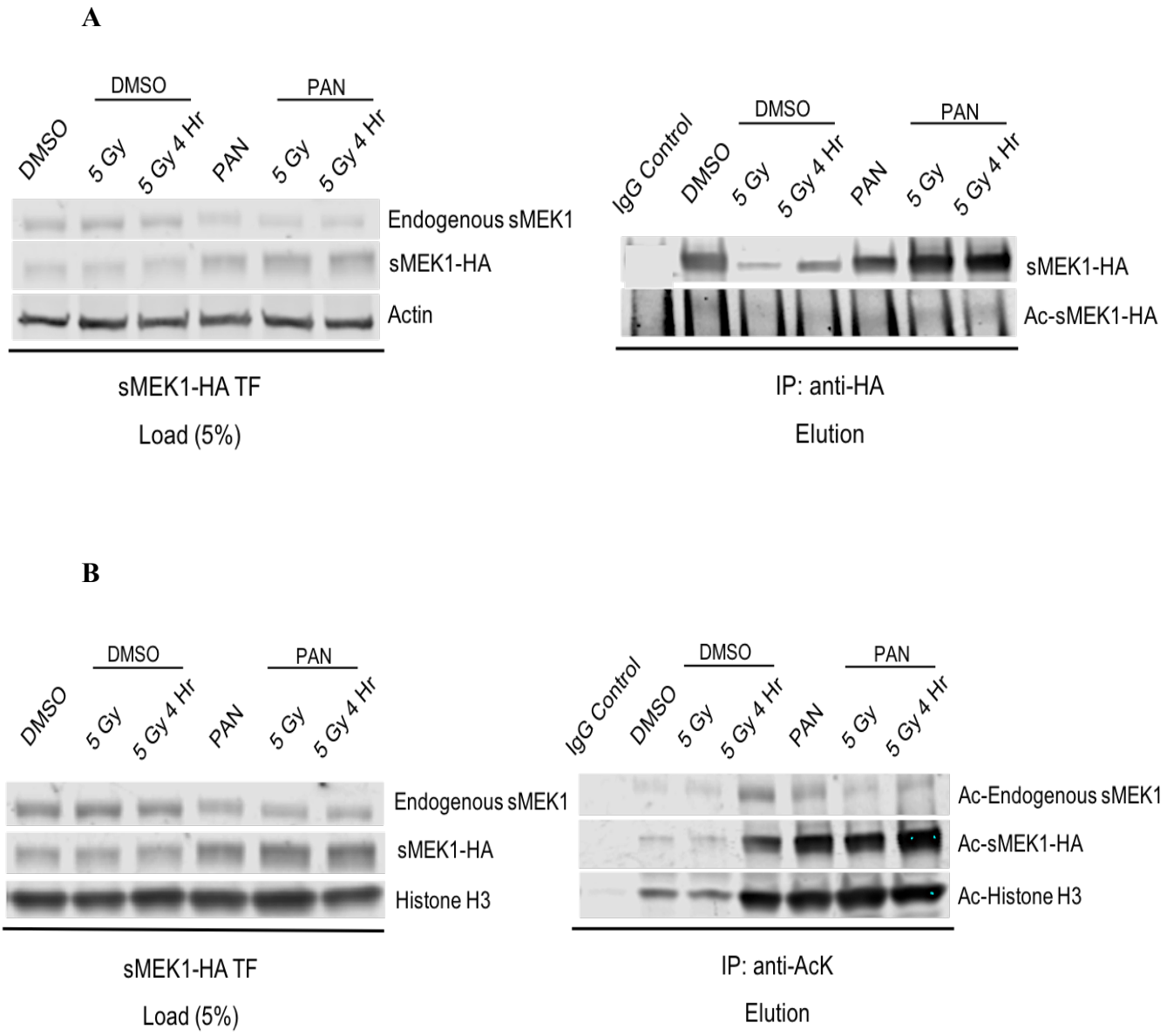

Figure 3-8. Increasing acetylation of sMEK1 protein after 24-hour panobinostat treatment. (A) Confirmation of sMEK1 acetylation status in PAN-treated HEK293T cells as previously identified in the mass spectrometry acetylome screen. Co-immunoprecipitation of overexpressed sMEK1-HA was performed using magnetic beads conjugated to anti-HA antibody, and later immunoblotted with anti-sMEK1 and anti-acetyl lysine polyclonal antibodies that recognise different epitopes of acetyl-lysine to detect the presence of acetylated sMEK1-HA. Actin is used as a loading control in the 5% load fractions. Low level of sMEK1 acetylation is also detected in DMSO control lanes before and after irradiation as demonstrated by faint bands corresponding to sMEK1-HA's molecular weight. (B) Western blot showing the reciprocal co-immunoprecipitation by anti-acetyl lysine agarose beads followed by anti-sMEK1 immunoblotting. Using histone H3 level as the loading control, a higher abundance of the endogenous and transfected sMEK1 acetylation is observed after PAN treatment in comparison to DMSO.
Abbreviations: TF, transfected; IP, immunoprecipitation.

3.4 Changes in the subcellular localisation and relative abundance of sMEK1 with panobinostat and/or ionising radiation

Depending on the level of involvement in the early (0-hour) or later phase (4-hour) of DDR, the repair proteins are recruited and assemble at the sites of DNA double strand breaks (DSBs) at various time-points after IR. Both the endogenous and transfected sMEK1 showed a significant decrease in their expression levels immediately after a radiation dose of 5 Gy in DMSO-control cells (*P= 0.0403 for endogenous; 0.0018 for transfected*), then increased significantly and was restored back to its basal level by 4-hour post-IR (*P= 0.0258 for endogenous; 0.046 for transfected*) (Figures 3-3 and 3-9). This implies the potential of sMEK1 to inhibit early stages of the DDR and/or to play a crucial role in the later stages of DNA damage signalling, consistent with its known function of dephosphorylating γH2AX upon repair to promote recovery from G2/M checkpoint arrest (Nakada et al., 2008). In contrast, PAN-treated cells mostly demonstrated a higher overall expression level of transfected sMEK1-HA, possibly compensating for the loss-of-function as a result of increased acetylation by PAN.

To test the hypothesis that sMEK1 localised to the nucleus and chromatin after IR-induced DNA damage, subcellular fractionation was performed. This enabled the changes in relative abundance of the sMEK1 protein in each subcellular compartment of HEK293T cells to be studied in more detail before and after IR with DMSO or PAN treatment. Cyclophilin A was used as a purity control for the cytoplasm, while histone H3 was used for the nucleus and chromatin to ensure minimal cross-contamination between different compartments. By loading an equal amount of total protein fraction onto each gel for western blot, the relative abundance between different subcellular compartments could be compared. In control untreated cells, sMEK1 was found more

abundantly in the nucleus compared to cytoplasm, with the lowest level detected on chromatin (Figures 3-10 to 3-14). Low levels of cyclophilin A in the nuclear and chromatin fractions as well as low levels of histone H3 in the cytoplasm, indicates an intact extraction of the appropriate subcellular compartment without disturbing the proteins enclosed by a separate inner membrane.

Immediately after irradiation in DMSO-treated cells, sMEK1 migrated from the cytoplasm and/or chromatin to the nucleus. This is evident by decreased levels of cytoplasmic sMEK1 in Figure 3-11 ($P > 0.05$) and sMEK1 on the chromatin in Figure 3-13 (*P= 0.0242 for transfected; 0.0149 for endogenous*) but significantly increased nuclear sMEK1 in Figure 3-12 (*P= 0.0116 for transfected; 0.0010 for endogenous*). After 4-hour recovery, significantly higher levels of sMEK1 were observed on the chromatin (*P= 0.0005 for transfected; 0.0002 for endogenous*) with a significant decrease in nuclear sMEK1 (*P= 0.0044 for transfected; 0.0175 for endogenous*). The primary differences that distinguished PAN-treated cells from the DMSO control were clearly visible in the nuclear and chromatin fractions at t=0 and 4-hour post-IR. In the presence of PAN, early chromatin localisation of sMEK1 was detected immediately after irradiation (*P= 0.0476 for transfected; 0.0755 for endogenous*) and by 4 hours, a higher abundance of sMEK1 was found in the nucleus instead, possibly due to chromatin dissociation as shown by a significant decrease in sMEK1 at the chromatin level 4 hours after irradiation (*P= 0.0077 for transfected; 0.0010 for endogenous*).

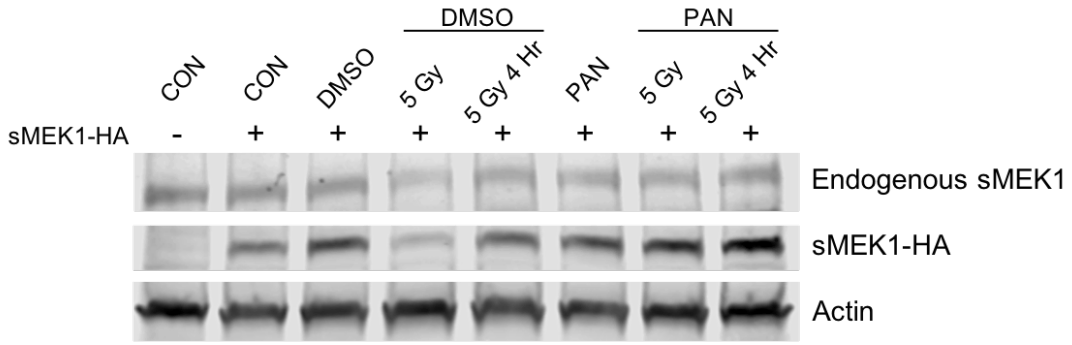

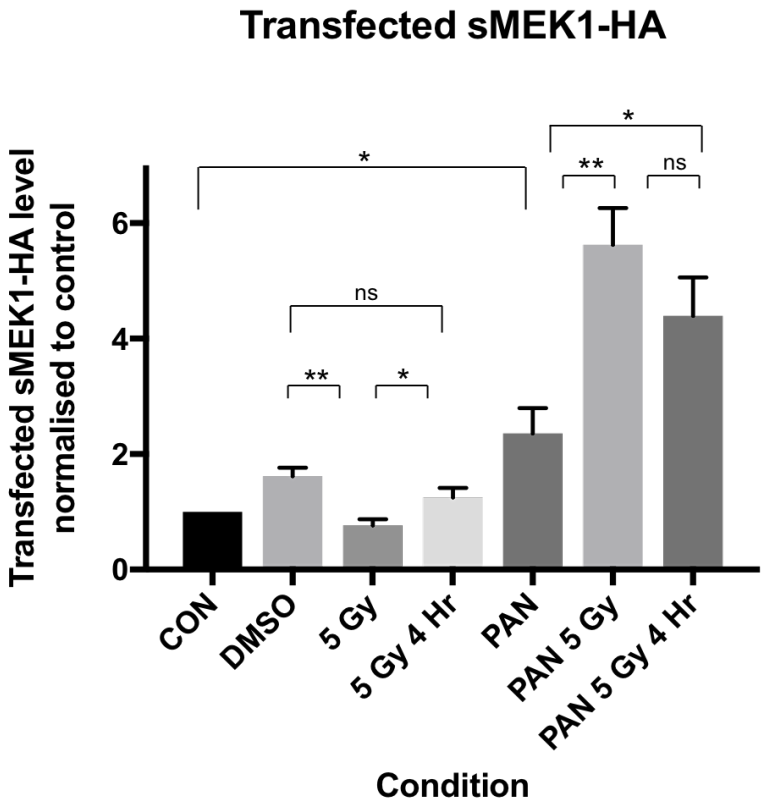

Figure 3-9. Western blot depicting the changes in transfected sMEK1-HA expression level under different conditions. Prior to 5 Gy irradiation, HEK293T cells were subjected to 24-hour treatment with DMSO (control) or PAN. Actin acts as a loading control for the normalisation of sMEK1-HA levels to facilitate comparison with the control untreated cells. A higher overall expression level of sMEK1-HA is seen in PAN-treated cells than in DMSO despite roughly equal transfection efficiency at a similar cell confluency. Data from n=3 independent experiments are shown and plotted as mean ± SEM. ** $p < 0.01$; * $p < 0.05$; ns $p > 0.05$.

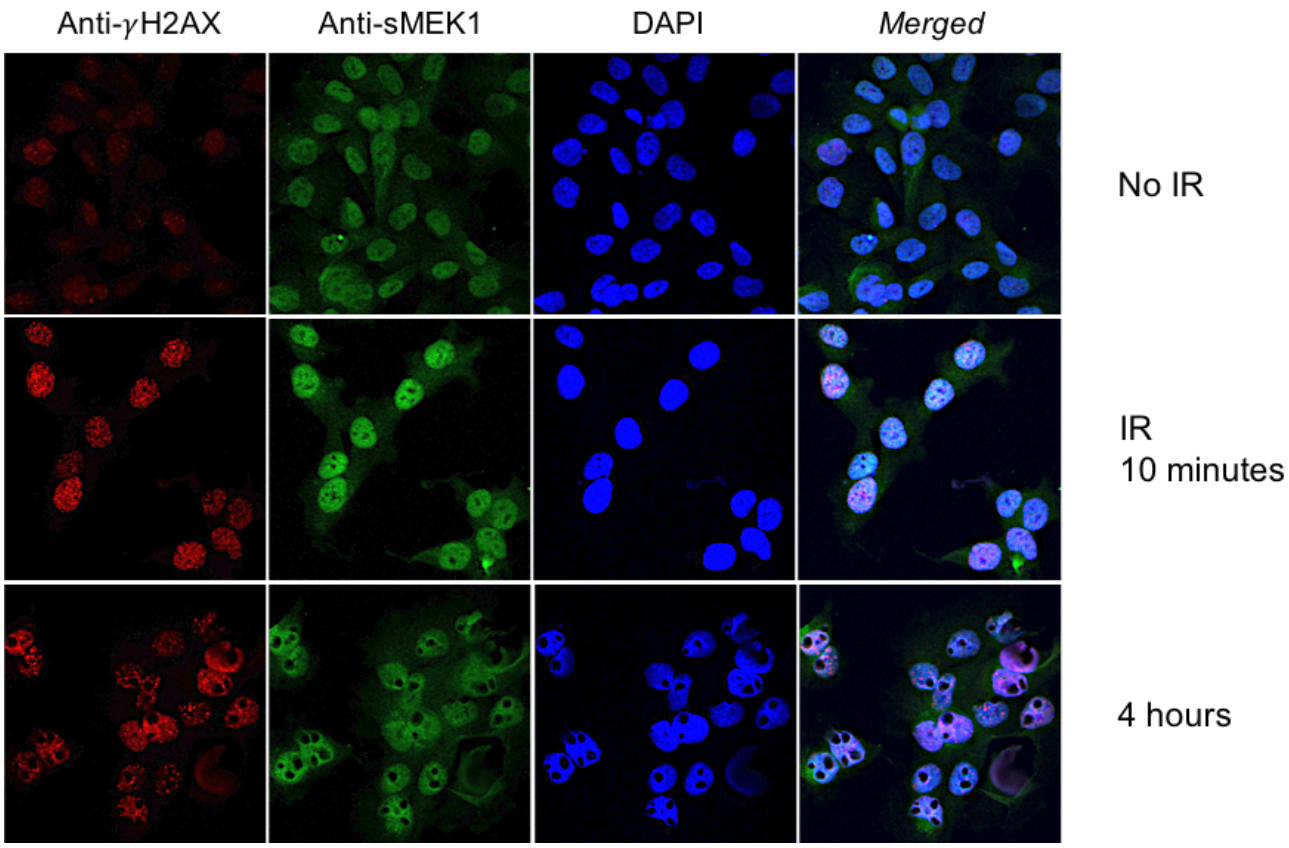

Figure 3-10. Representative images of control untreated cells before and after ionising radiation under immunofluorescence microscopy. T24 cells were co-stained with anti-γH2AX (red), anti-sMEK1 (green) and DAPI (blue) at 10-minutes (early DDR) and 4-hour (later DDR) post-irradiation. The level of γH2AX indicates the progress of DNA damage response (DDR) after IR-induced double strand breaks, whereas DAPI stains the nucleus. Assuming that fluorescence intensity is directly proportional to the protein abundance, stronger green fluorescence in the nucleus indicates a higher level of nuclear sMEK1 when compared to the cytoplasm. On the other hand, low abundance of cytoplasmic sMEK1 is present prior to radiation likely due to its role in the cytoskeleton, but decreases immediately after IR. The nuclear sMEK1 protein level increases in early DDR and at 4-hour post-IR, hence providing additional support for its function in the regulation of DNA damage repair.

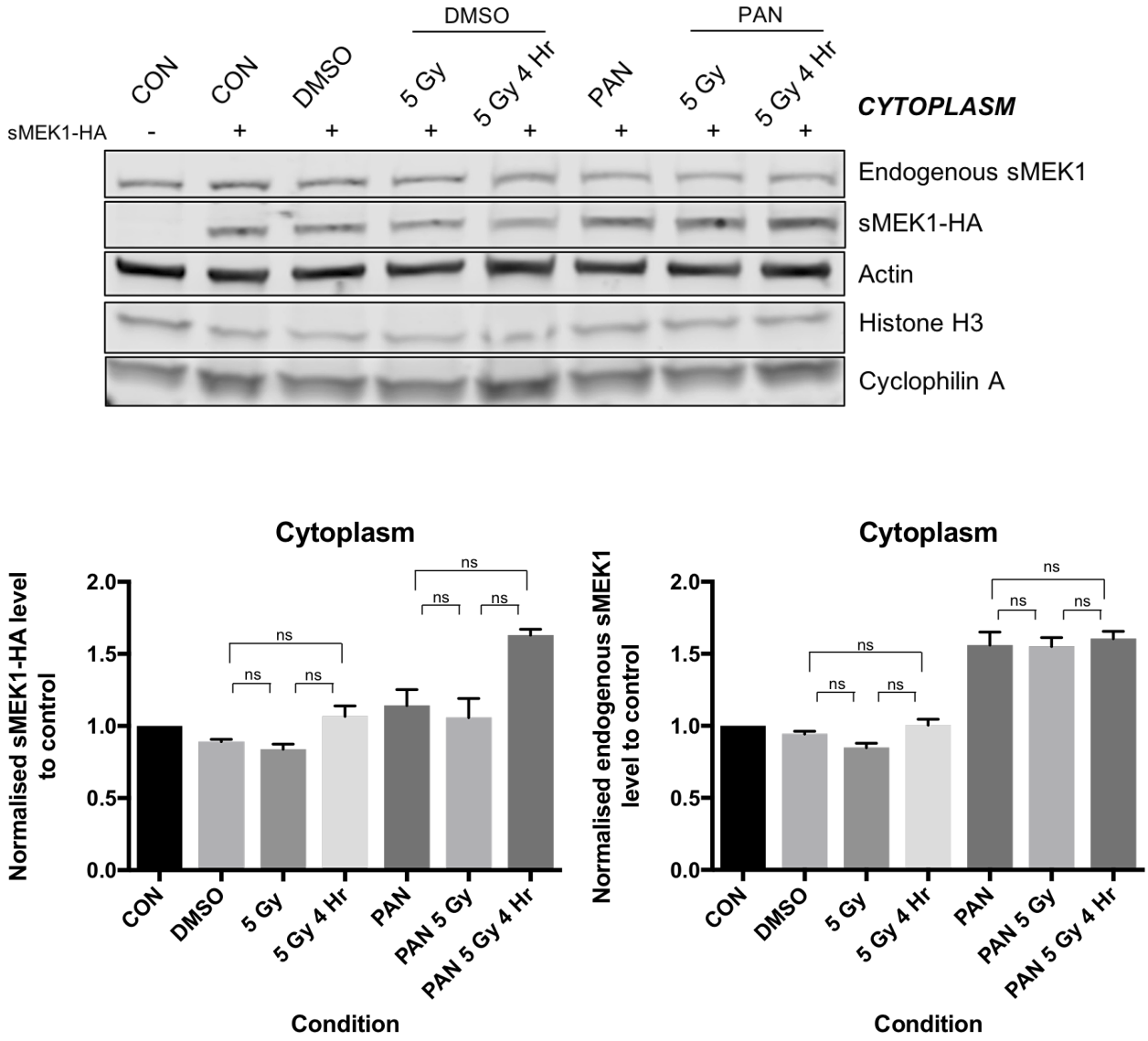

Figure 3-11. Cytoplasmic sMEK1 protein level under different conditions of DMSO or PAN before and after irradiation. Subcellular fractionation was carried out on transiently transfected HEK293T cells. Actin is used as purity and loading controls in the cytoplasm, and histone H3 in the nucleus and chromatin. The ratio of sMEK1 to their respective loading control (actin/histone H3) in each subcellular compartment is calculated before normalising to the untreated controls. Both the transfected and endogenous sMEK1 follow a similar trend in their expression changes. With n=3 independent replicates, data are displayed as mean ± SEM. ns $p > 0.05$.

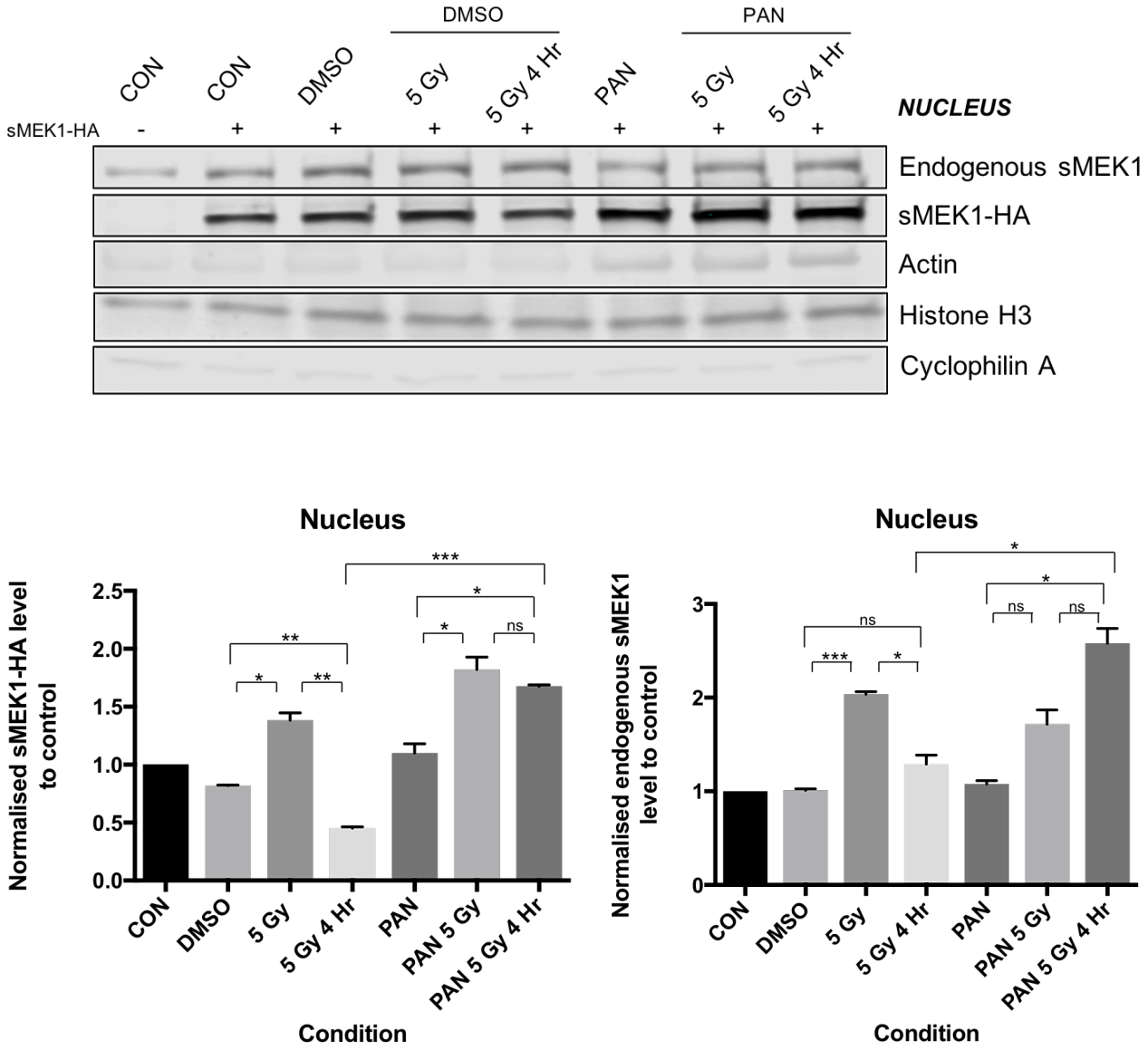

Figure 3-12. Nuclear sMEK1 protein level under different conditions of DMSO or PAN before and after irradiation. Subcellular fractionation was carried out on transiently transfected HEK293T cells. Actin is used as purity and loading controls in the cytoplasm, and histone H3 in the nucleus and chromatin. Low level of cyclophilin A indicates an intact nuclear compartment during fractionation without cross-contamination from the cytoplasmic proteins. The ratio of sMEK1 to their respective loading control (actin/histone H3) in each subcellular compartment is calculated before normalising to the untreated controls. Both the transfected and endogenous sMEK1 follow a similar trend in their expression changes. With n=3 independent replicates, data are displayed as mean ± SEM. *** $p < 0.001$; ** $p < 0.01$; * $p < 0.05$; ns $p > 0.05$.

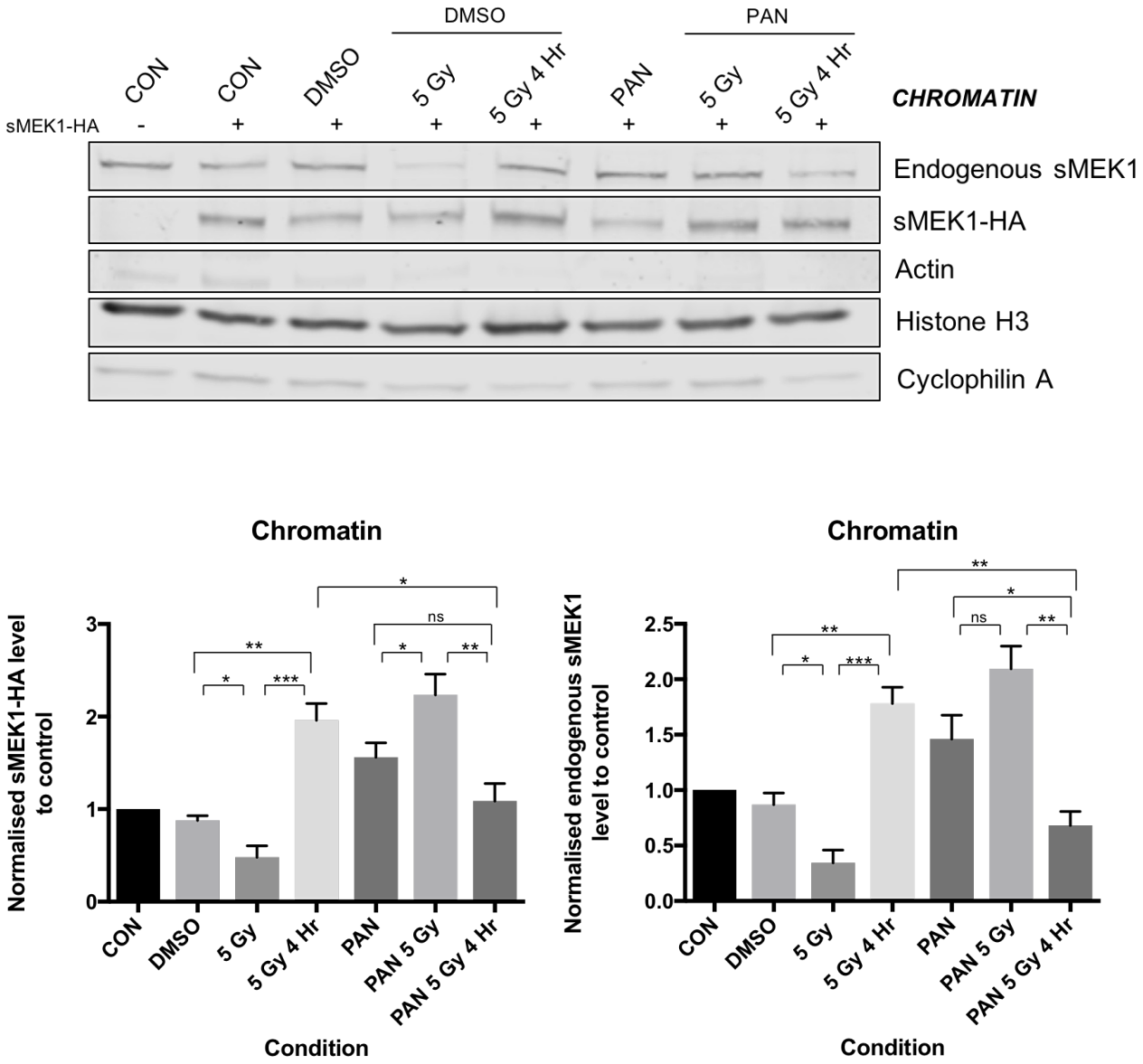

Figure 3-13. sMEK1 protein on the chromatin level under different conditions of DMSO or PAN before and after irradiation. Subcellular fractionation was carried out on transiently transfected HEK293T cells. Actin is used as purity and loading controls in the cytoplasm, and histone H3 in the nucleus and chromatin. Low level of cyclophilin A indicates an intact chromatin fraction without cross-contamination from the cytoplasmic proteins. The ratio of sMEK1 to their respective loading control (actin/histone H3) in each subcellular compartment is calculated before normalising to the untreated controls. Both the transfected and endogenous sMEK1 follow a similar trend in their expression changes. With n=3 independent replicates, data are displayed as mean ± SEM. *** $p < 0.001$; ** $p < 0.01$; * $p < 0.05$; ns $p > 0.05$.

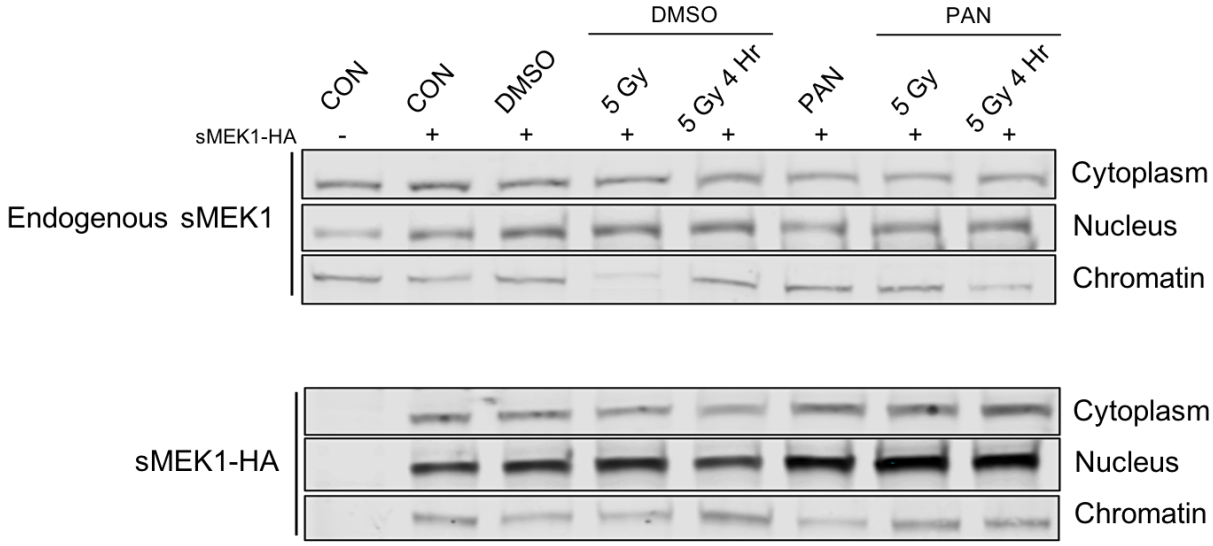

Figure 3-14. An overview of changes in endogenous and transfected sMEK1 levels under different conditions in each subcellular compartment, taken from the previous western blots in Figures 3-11 to 3-13. Since an equal amount of total lysate was loaded for all the samples on western blots, this allows a direct comparison of sMEK1 protein levels between the cytoplasm, nucleus and chromatin. The highest abundance is found in the nucleus, followed by cytoplasm and the lowest abundance on the chromatin.

3.5 Interactions between acetylated sMEK1 and bromodomain 4 at the level of chromatin

Bromodomain containing 4 (BRD4) is the most highly abundant BRD in cells (Devaiah et al., 2016). Its interaction with acetylated sMEK1 (Ac-sMEK1) was therefore studied using anti-BRD4 antibody to co-immunoprecipitate BRD4 and its associated binding partners. This proved challenging due to its large molecular weight of >150 kDa, therefore a high concentration of BRD4 protein was required for effective pull-down. Using 30 μg total protein lysate obtained from fractionation, only the nuclear and chromatin compartments contained sufficiently detectable levels of BRD4 to warrant further investigation (Figure 3-15). In spite of failed co-immunoprecipitation in the nuclear fraction probably due to inadequate BRD4 levels (Figure 3-16A), valuable insights were found regarding the interactions on chromatin between Ac-sMEK1 and

BRD4 under the different treatment conditions. Since the abundance of acetylated sMEK1 in the chromatin fraction was not independently assessed after subcellular fractionation, it is assumed that the acetylation level follows a similar ratio as in the total lysate fraction (Figure 3-8B). In Figure 3-16B, low level Ac-sMEK1-BRD4 interactions existed in DMSO control cells. However, these interactions appeared decreased in cells which were harvested immediately after IR. At 4 hours after radiation when sMEK1 was strongly acetylated, a thicker band intensity of Ac-sMEK1 in the elution fraction indicates a stronger interaction with BRD4 was detected.

In the presence of PAN, increased acetylation as a result of HDAC inhibition sustained Ac-sMEK1-BRD4 interactions which were lost after 4-hour post-IR, possibly due to low levels of sMEK1 present on chromatin and/or competition with other acetylated targets for binding to the BRD4. The interaction of BRD4 was observed solely with the acetylated form of endogenous sMEK1 but not transfected sMEK1-HA. This can be accounted for by the missing N-terminal ARM repeats in the smaller transfected variant which might play a crucial role in mediating protein-protein interactions, in this instance with BRD4.

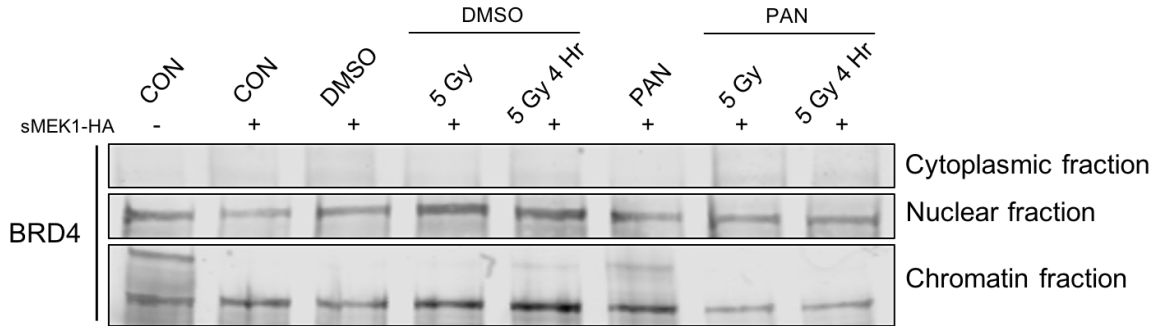

Figure 3-15. Differential abundance of the BRD4 effector proteins in each subcellular compartment. Western blot showing the BRD4 level in 30 μg lysate fractions from the cytoplasm, nucleus and chromatin. High levels of BRD4 are needed to ensure successful co-immunoprecipitation of BRD4 as well as the bound acetylated substrate protein(s). With n=3 independent replicates, only the nuclear and chromatin compartments were studied further.

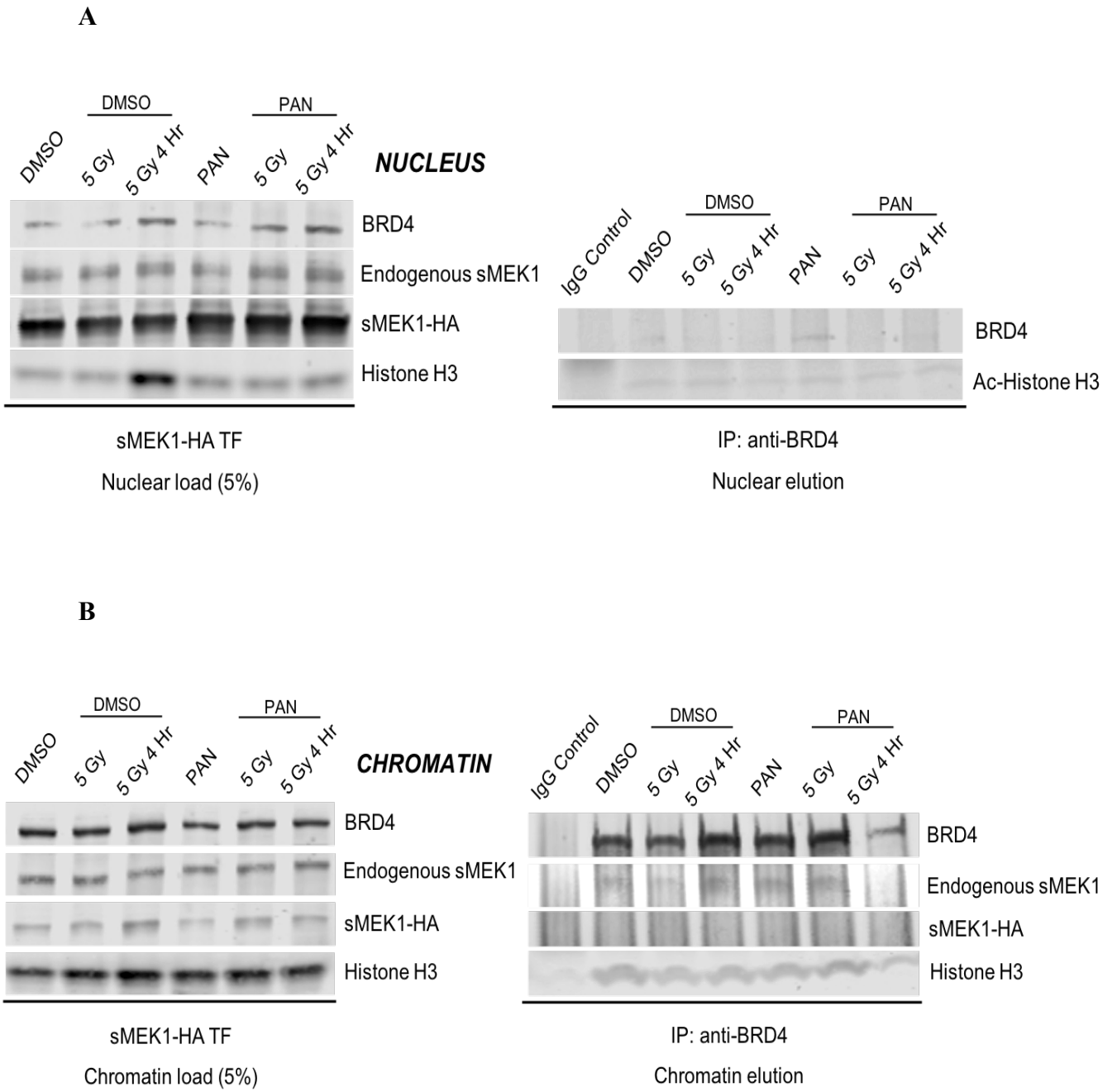

Figure 3-16. Transient interactions between acetylated sMEK1 and bromodomain 4 on chromatin. (A) Co-immunoprecipitation of BRD4 in the nucleus for 150 μg total protein. This failed with low levels of BRD4 detected in the elution fractions, therefore it was not useful to visualise the potential interaction with Ac-sMEK1. (B) Co-immunoprecipitation performed on the chromatin fraction of 200 μg total lysate. Histone H3 is not only used as a loading control, but also an indication of the pull-down efficiency by anti-BRD4 antibody because its acetylated form is known to bind BRD4 proteins. A thick band corresponding to BRD4 at ~150 kDa indicates an effective pull-down, and the level of interaction with Ac-sMEK1 varies between DMSO- and PAN-treated cells before and after IR. The data are obtained from n=3 independent experiments.

3.6 Functional characterisation of acetyl-lysine K655 residue

To investigate the functional significance of the previously identified PAN-mediated sMEK1 acetylation on the Lysine K655 residue, site-directed mutagenesis (SDM) was used to introduce single amino acid substitutions. Arginine (R) was selected as an acetyl-dead residue that retains the positive charges on its amino side chain but is unable to be acetylated, while the glutamine (Q) residue which possesses a similar structure and acetamide functional group (CH_3CONH-) to the acetyl-lysine acts as an acetyl-mimic. Sanger sequencing was performed following cloning, using specifically-designed mutagenic oligonucleotide primers, to confirm the successful point mutations with minimal errors outside the region of interest.

A comparable total abundance of acetylated mutant sMEK1 was detected in the elution fractions of both DMSO- and PAN-treated cells after performing co-immunoprecipitation by anti-AcK agarose beads, and a similar trend in the acetylation levels before, immediately after and 4-hour post-IR (Figure 3-17). This suggests PAN treatment has no or only a minimal effect on altering the acetylation status of mutant sMEK1 (K416R and K416Q) in comparison to DMSO, unlike its ability to increase wild-type sMEK1 acetylation (Figure 3-8).

The expression level of mutant sMEK1 was checked following transfection in HEK293T cells, and then compared to that of the wild-type transfection (Figure 3-9) after 24 hours of DMSO or PAN treatment with or without irradiation. Despite variations in the acetyl-dead or acetyl-mimic sMEK1 levels, no statistically-significant difference ($P > 0.05$) was generally detected under different conditions after performing unpaired student t-tests (Figures 3-18 and 3-19). Some similarities with the wild-type transfection in term of the overall expression changes were however, only observed in

sMEK1-K416Q transfection (Figure 3-19). The overexpression of acetyl-mimic K416Q variant was able to reverse the downregulation of wild-type sMEK1 expression seen immediately after irradiation in DMSO-treated cells. Significantly upregulated expression of acetyl-mimic K416Q mutant was also detected at 4-hour post-IR under DMSO control condition (*P= 0.0324*) similar to that of the wild-type, thus implies that post-translational modifications such as acetylation may have a role in regulating the protein expression levels.

Transfection of sMEK1 Double Nickase plasmid (h2) obtained from Santa Cruz Biotechnology was attempted to establish a CRISPR stable sMEK1-knockout T24 cell line for functional studies. However during the antibiotic selection stage, all of the surviving cells failed to grow into distinct colonies of ~200 cells. This is likely because sMEK1 plays a role in the cytoskeleton, chemotaxis and polarity which are essential for cell division and survival (Cohen et al., 2005). As an alternative, to transiently and selectively knockdown sMEK1 gene at the mRNA expression level, specific individual ON-TARGETplus siRNA was used. Different ratios of sisMEK1 to the transfection reagent oligofectamine were tested to determine the optimised concentration of each component for subsequent functional assays. In Figure 3-20, 5 μL of 20 μM stock sisMEK1 oligonucleotide in 2 μL oligofectamine yielded the most effective (84%) reduction in endogenous sMEK1 protein level after normalising to the non-targeting (NT) control treatment under similar conditions. Therefore this condition was chosen to represent transient sMEK1-knockdown in T24 cells.

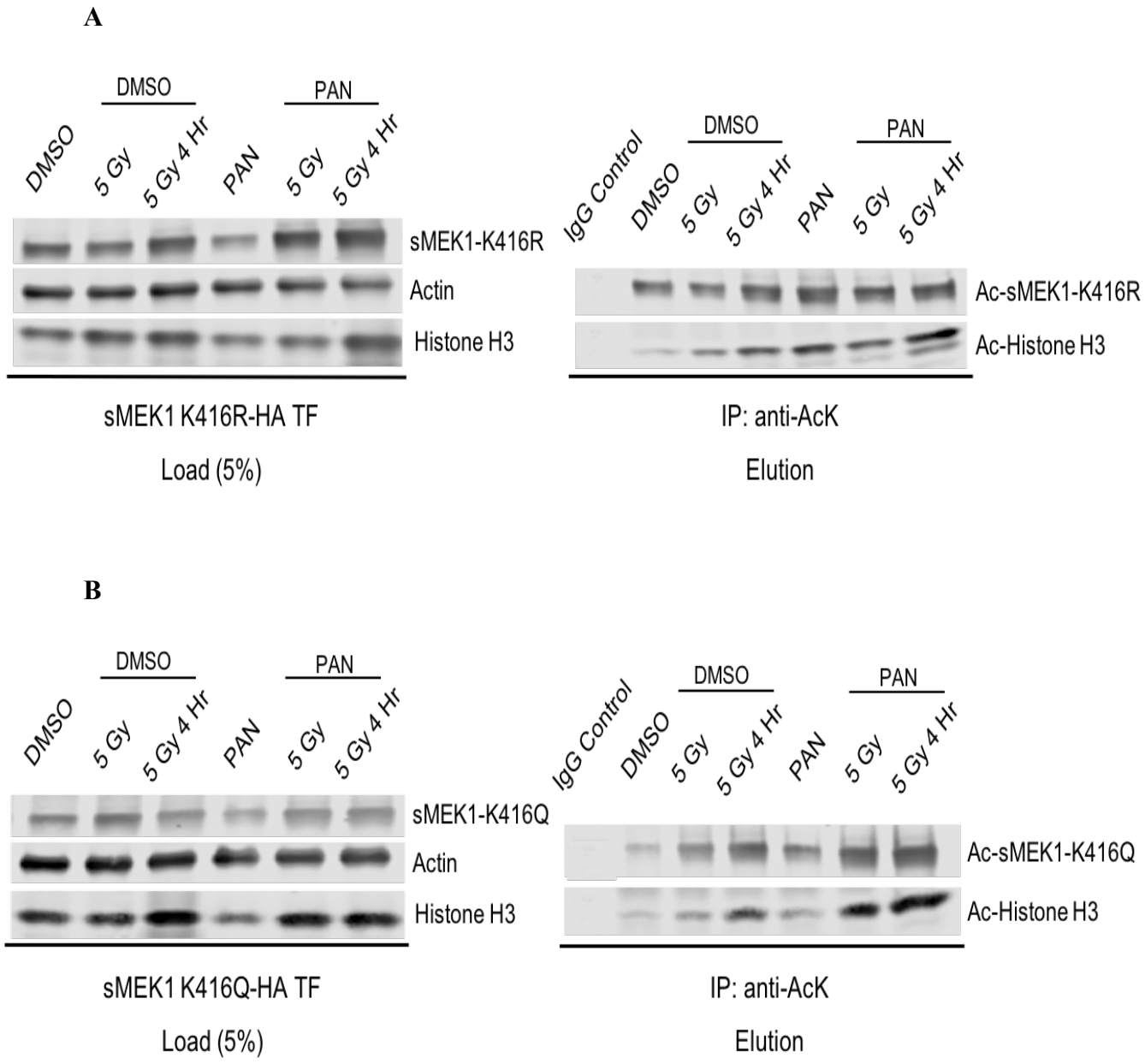

Figure 3-17. **Site-directed mutagenesis of transfected sMEK1-HA plasmid at the lysine residue of K416.** Co-immunoprecipitation of acetylated sMEK1-HA by anti-AcK beads in HEK293T cells after 24-48 hours' transfection of (A) acetyl-dead (K416R) or (B) acetyl-mimic (K416Q) mutant. The desirable point substitutions are confirmed by Sanger sequencing (Appendix 2) after cloning using specifically-designed mutant oligonucleotide primers.

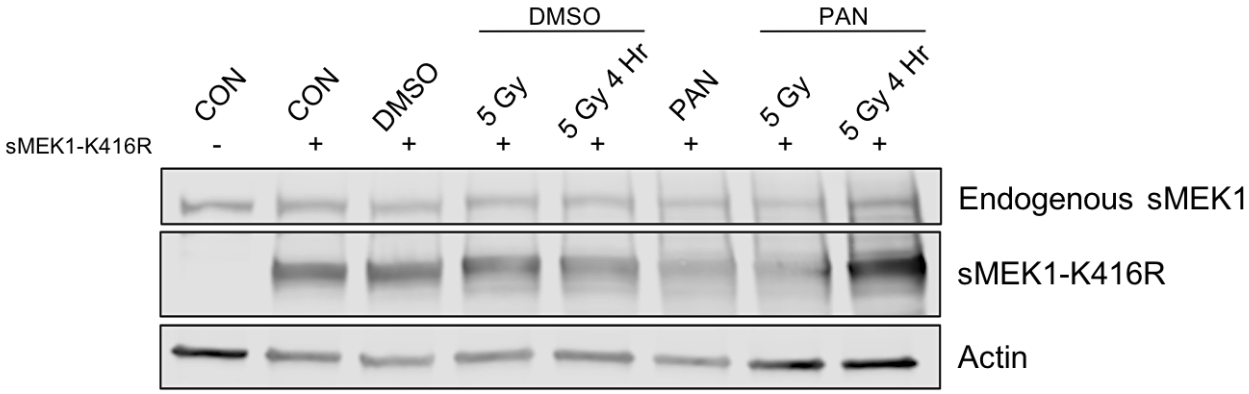

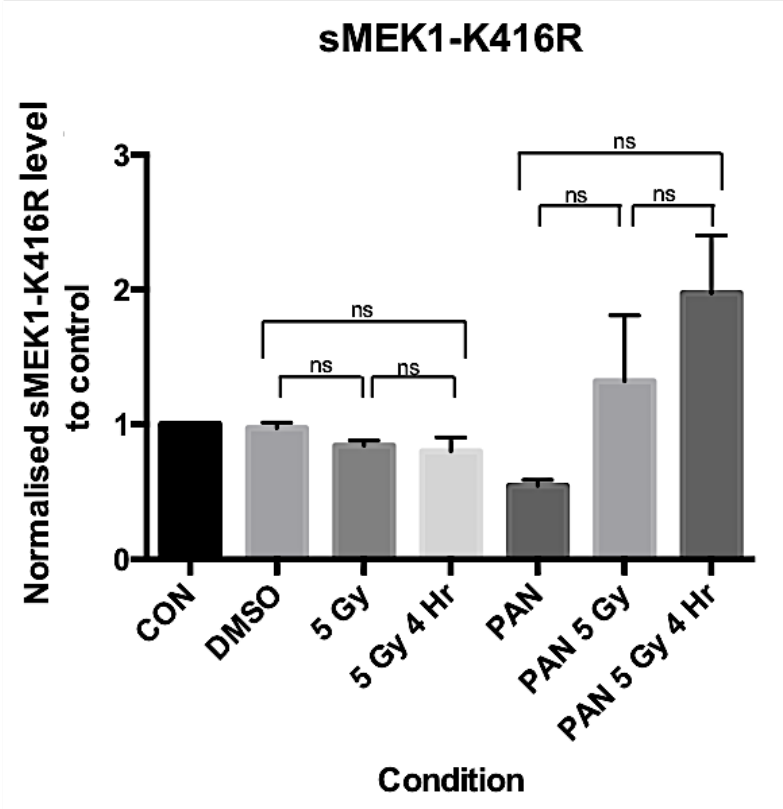

Figure 3-18. Changes in the expression level of acetyl-dead K416R mutant sMEK1 protein with DMSO or PAN treatment before and after IR. Graphic representation of the data from n=3 independent experiments as mean ± SEM. ns $p > 0.05$.

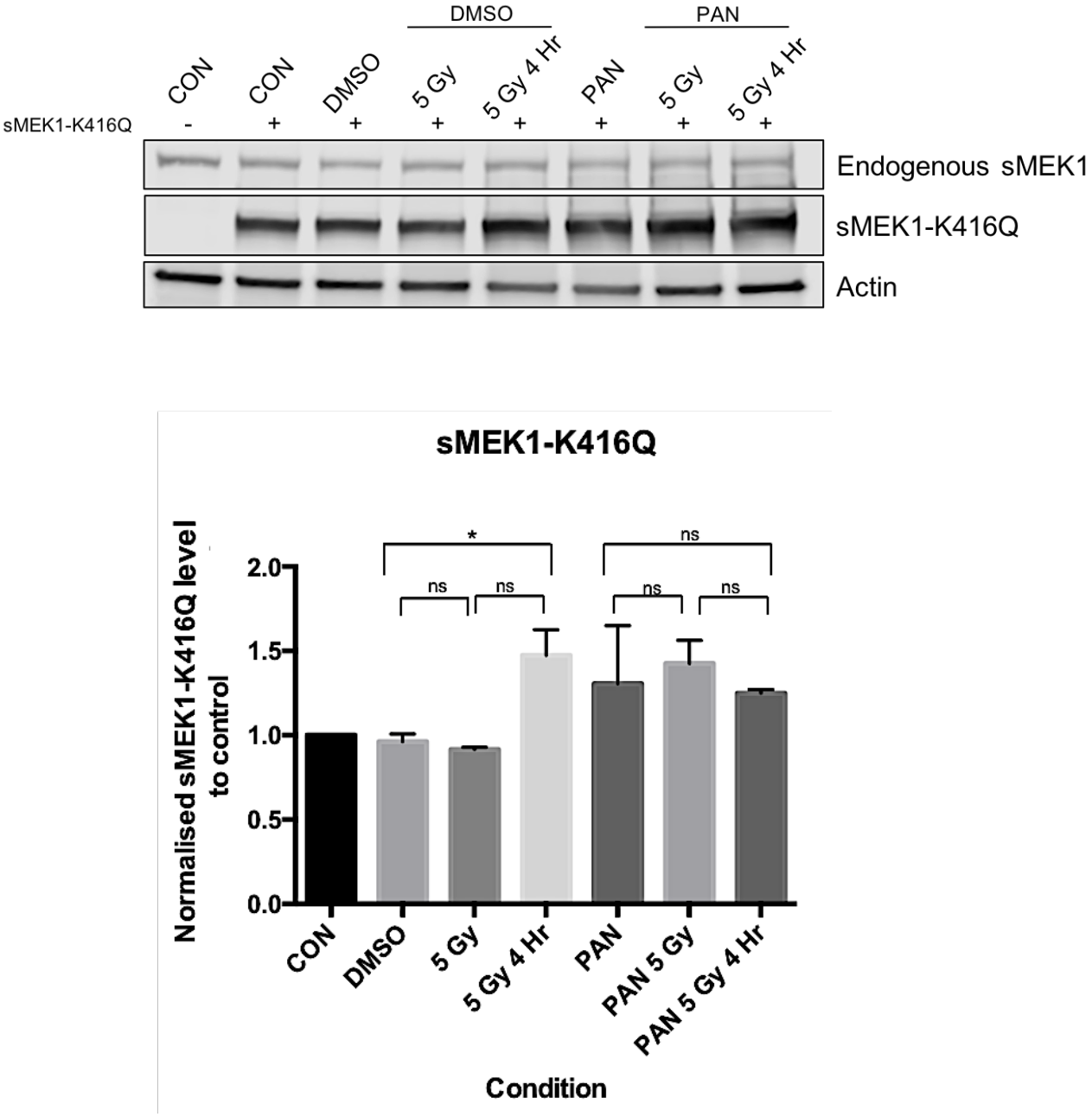

Figure 3-19. Changes in the expression level of acetyl-mimic K416Q mutant sMEK1 protein with DMSO or PAN treatment before and after IR. Graphic representation of the data from n=3 independent experiments as mean ± SEM. * $p < 0.05$; ns $p > 0.05$.

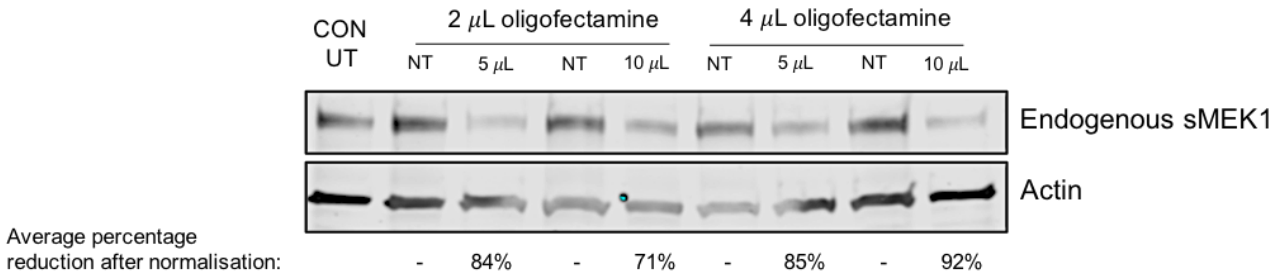

Figure 3-20. **siRNA-mediated protein depletion of endogenous sMEK1.** sisMEK1 was transfected into T24 cells of low passage number using oligofectamine reagent. Different ratios of sisMEK1 to oligofectamine were tested to optimise the extent of sMEK1 knockdown. The percentage reduction in sMEK1 protein expression level was normalised to the non-targeting oligonucleotide treatment under similar conditions, after which the average was calculated for n=3 independent replicates. Five microlitres sisMEK1 in 2 μL oligofectamine were chosen to establish transient sMEK1-knockdown in T24 cells for all subsequent functional experiments.
Abbreviations: CON UT, control untreated; NT, non-targeting.

3.7 Radiosensitisation of bladder cancer cells by sMEK1 knockdown

To verify the hypothesis that sMEK1 loss-of-function is a result of increased acetylation, and to test its radiosensitisation effect observed with PAN treatment, clonogenic cell survival assays were performed. This method measures the cell's reproducibility to form a colony of >50 cells following irradiation, indicating an indefinite proliferative potential (Munshi et al., 2005). T24 cells were subjected to IR doses of 0, 2, 4, 6 and 8 Gy, and the number of colonies remaining at the end of a 7-day incubation period was counted. A survival curve was plotted using the linear-quadratic (LQ) model, to describe the relationship between the radiation dose and the fraction of surviving cells.

Firstly, the known role of PAN as a radiosensitiser was confirmed by clonogenic assays in the presence of control untreated T24 as well as DMSO-treated cells, as evidenced by an increase in cell death at IR doses of 4 Gy and above (Figure 3-21A). This enabled

PAN to be used as a positive control for reliable comparisons against sMEK1 knockdown and the acetyl-dead or acetyl-mimic mutant variants. Using non-targeting oligonucleotide as a negative control, siRNA-mediated knockdown of endogenous sMEK1 protein achieved overlapping radiosensitivity similar to PAN (Figures 3-21B and 3-21D). The radiosensitisation effect was rescued by the re-transfection of wild-type (WT) plasmid into sMEK1-depleted T24 cells using FuGENE reagent (Figure 3-21C).

Rescue transfection by acetyl-dead (K416R) mutant plasmid after knocking down endogenous sMEK1 protein restored the relatively radioresistant levels observed in control untreated T24 cells (Figure 3-22A); on the other hand, acetyl-mimic (K416Q) mutant transfection resulted in only partial restoration (Figure 3-22B). The extent of knockdown and re-expression of sMEK1 protein level was also checked by western blot (Figure 3-22D). Less re-expression was seen for K416R than K416Q. To demonstrate a contribution to PAN-mediated radiosensitisation by loss-of-function of sMEK1, 25 nM PAN was given prior to clonogenic assay 24 hours after sisMEK1 oligonucleotide transfection. Only partial radiosensitisation was attained after combining sMEK1 knockdown and PAN treatment (Figure 3-22C), suggesting that sMEK1 might be one of the few target proteins involved in this mechanism.

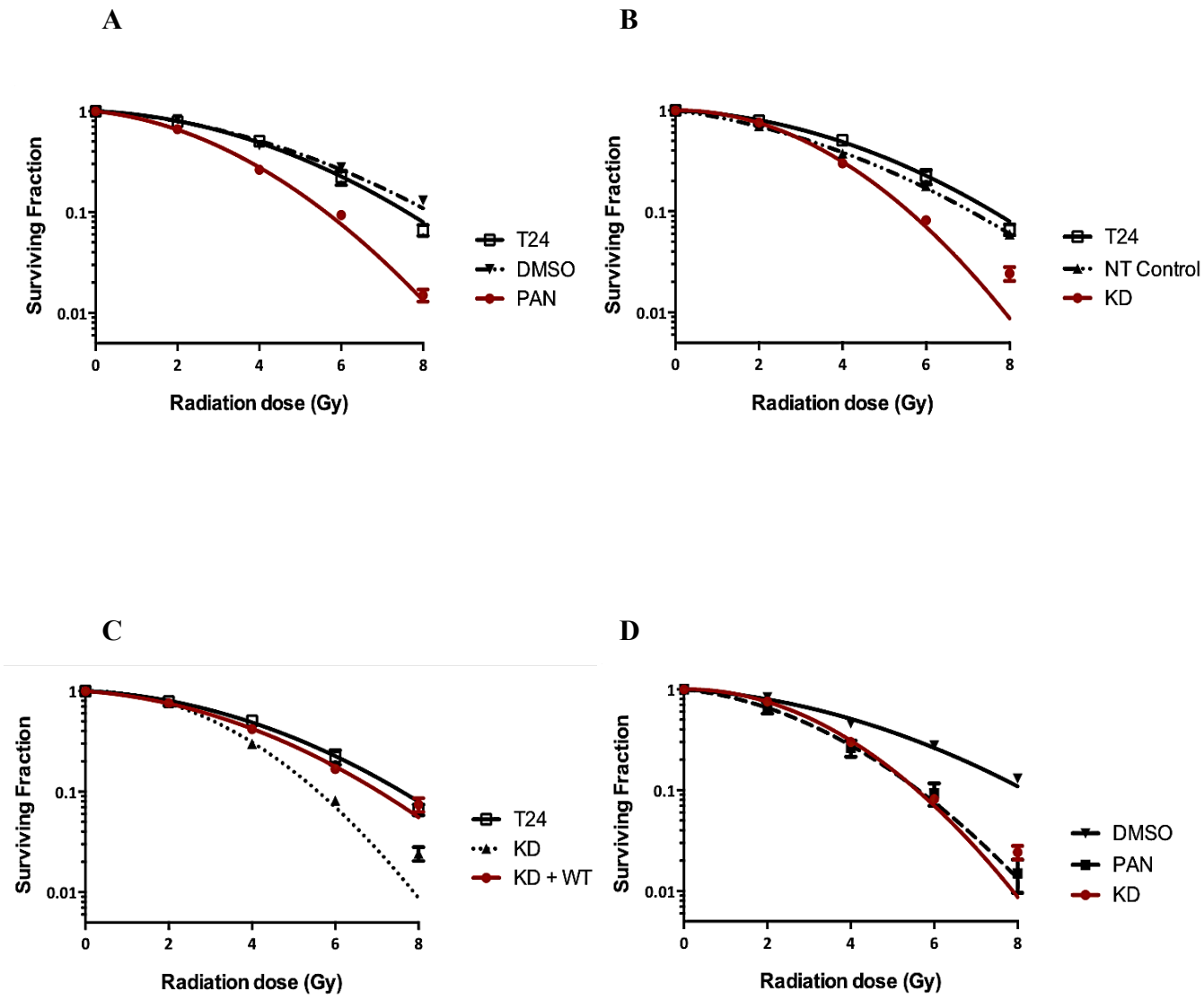

Figure 3-21. Loss of sMEK1 protein results in the radiosensitisation of bladder cancer T24 cells. For the negative control, an appropriate number of untreated T24 cells were re-seeded and irradiated with 2, 4, 6 and 8 Gy or 0 Gy in control, followed by a 7-day incubation period. Clonogenic assays were repeated after (A) 24-hour PAN or DMSO (control) treatment, or (B) 48 hours after the transfection of 5 μL of stock 20 μM sisMEK1 or non-targeting oligonucleotides using 2 μL oligofectamine reagent, or (C) the rescue transfection by wild-type sMEK1 plasmid at 24 hours after siRNA-mediated depletion of the endogenous sMEK1 expression. (D) Comparison of the extent of radiosensitisation effect achieved by sMEK1 knockdown to that of PAN. All survival curves plotted using the linear-quadratic model with appropriate controls. Data from a minimal number of n=3 independent experiments, each with two repeats.
Abbreviations: NT, non-targeting; KD, knockdown; WT, wild-type.

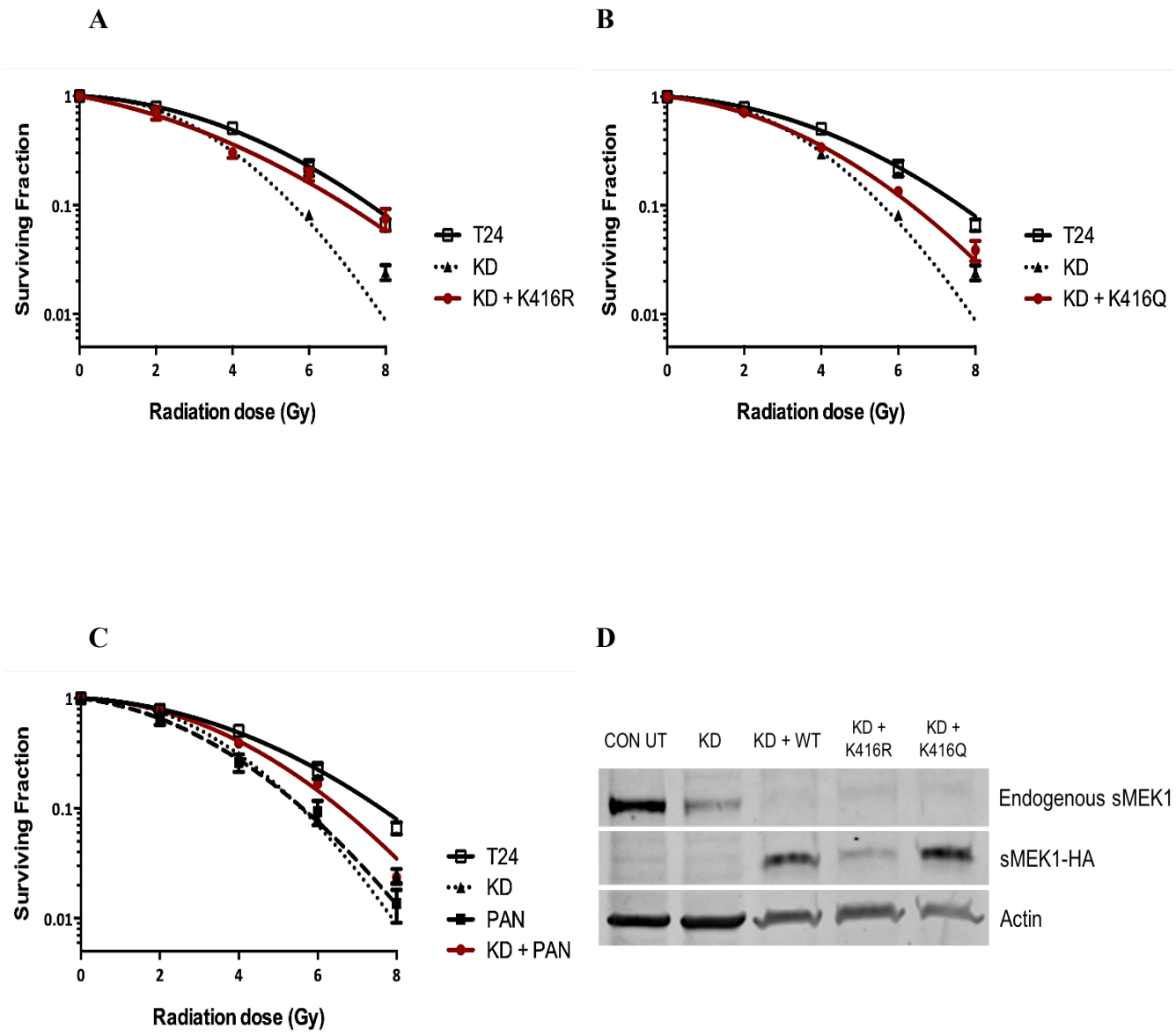

Figure 3-22. Variation in the radioresistant/radiosensitive levels after siRNA-mediated sMEK1 depletion combined with panobinostat treatment, or the rescue transfection of wild-type or site-directed mutagenesis plasmid. For the negative control, an appropriate number of untreated T24 cells were re-seeded and irradiated with 2, 4, 6 and 8 Gy or 0 Gy in control, followed by a 7-day incubation period. Clonogenic assays were repeated in sMEK1-depleted cells after the rescue transfection by (A) acetyl-dead K416R mutant plasmid or (B) acetyl-mimic K416Q mutant plasmid at 24-hour post-sisMEK1 transfection, or (C) the combined treatment of sMEK1 knockdown via siRNA followed by 25 nM PAN addition after 24-hour interval. All survival curves plotted using the linear-quadratic model with appropriate controls. Data from a minimal number of n=3 independent experiments, each with two repeats. (D) Western blot showing the extent of sMEK1 depletion at 24-48 hours after siRNA transfection and the re-expression level of wild-type or mutant sMEK1 protein following rescue transfection by FuGENE reagent. Actin acts as the loading control.
Abbreviations: KD, knockdown; K416R, acetyl-dead; K416Q, acetyl-mimic.

3.8 Correlation between the number of gamma H2A.X foci and the progress of DNA repair after ionising radiation

Detection of γH2AX foci in the cell nuclei using immunofluorescence microscopy together with 4′,6-diamidino-2-phenylindole (DAPI) co-staining is used as a reliable quantitative marker of DSBs. A series of time points up to 24 hours was chosen with reference to the existing literature to demonstrate the kinetic changes in γH2AX level over the course of the DNA damage response after IR-induced double strand breaks (Redon et al., 2009). It was hypothesised that the loss-of-function of sMEK1, through increased acetylation by PAN, would result in a time-delay before reaching a peak in γH2AX foci number with a slower decrease upon recovery.

A total of seven conditions i.e. control T24, PAN treatment, sMEK1 overexpression, sisMEK1-mediated knockdown (KD) and rescue transfection by wild-type (WT), acetyl-dead (K416R) or acetyl-mimic (K416Q) plasmid, were included for immunocytochemistry at t = 0 before irradiation and at t = 10, 30 minutes, 2, 4 and 24 hours after IR, using anti-γH2AX and anti-sMEK1 antibodies. Under untreated conditions, within 10-minutes of a 5 Gy radiation dose, an increased nuclear sMEK1 level was observed (*P= 0.0419*) (Figure 3-24A), while γH2AX foci number per nucleus increased significantly (*P= 0.0064*) (Figure 3-23A). The highest peak γH2AX level was achieved at 30 minutes post-IR, when there was a significant drop in the nuclear sMEK1 abundance (*P= 0.0160*). An increasing trend of nuclear sMEK1 occurred and peaked after 2 hours when γH2AX was rapidly dephosphorylated, thus further corroborating previous observations of sMEK1 involvement in the later stage of DDR. By 4 hours, both the nuclear sMEK1 level and γH2AX foci number had decreased further. A more gradual decrease of γH2AX level was then witnessed between 4-24

hours after IR until it nearly returned to the basal level. On the other hand, the nuclear sMEK1 expression was downregulated potentially due to fewer γH2AX foci being present by 24 hours in the late phase of DNA repair.

With the exceptions of sMEK1 knockdown and the rescue transfection by the acetyl-mimic, all other conditions appeared to follow a similar trend of changes in γH2AX foci number per nucleus as described above (Figures 3-23A and 3-23B), although the absolute values displayed minor deviations. Notably, PAN alone induced DNA damage before irradiation (*P= 0.0181*). Despite insignificant differences in the peak γH2AX foci number achieved by 30-minutes, PAN demonstrated the slowest recovery from DDR, with about two-fold higher residual foci remaining after 24 hours compared to the untreated controls (*P= 0.0102*) (Figure 3-23A). In endogenous sMEK1-depleted T24 cells and those re-transfected with K416Q mutant plasmid, the peak of γH2AX foci number was achieved at a slightly later time-point of 2 hours after irradiation, but it declined to comparable levels to the control untreated cells by 24 hours (Figure 3-23B). In contrast, for the nuclear sMEK1 expression, all conditions showed a general trend similar to that of control, albeit with large variations in their absolute levels. The highest peak of nuclear sMEK1 was uniformly detected within 10 minutes in the early DDR across different treatment groups except sMEK1 knockdown as well as the wild-type re-transfection (Figure 3-24B), and this correlates with the fractionation results observed in sMEK1-overexpressed cells (Figure 3-12). Unlike other conditions that displayed the lowest nuclear sMEK1 level at 24 hours, PAN-treated (Figure 3-24A) and sisMEK1-knockdown cells (Figure 3-24B) achieved the lowest abundance by 30 minutes post-IR.

A

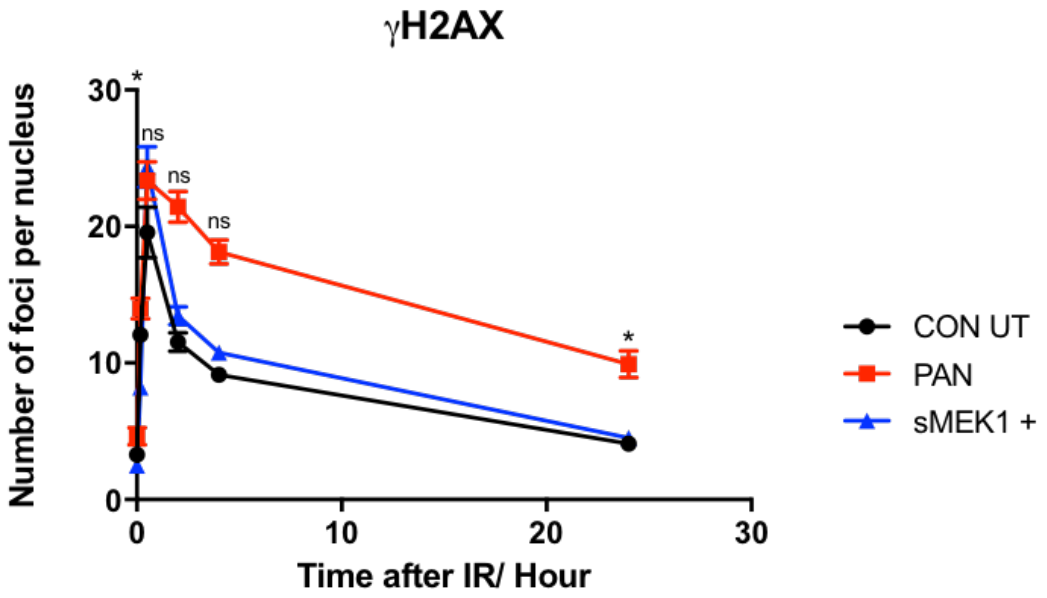

B

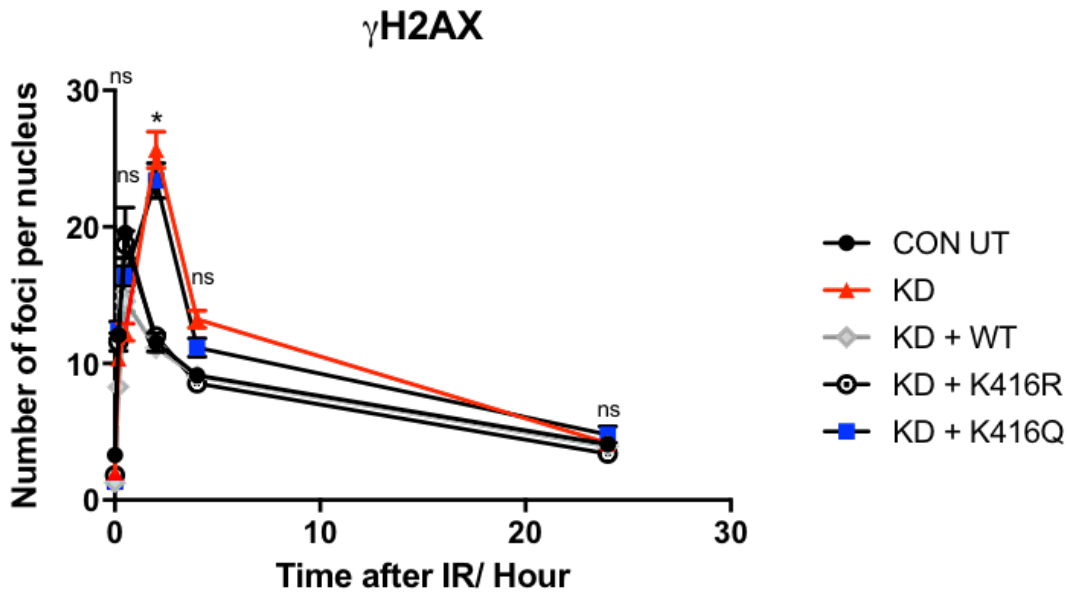

Figure 3-23. Time-delay in reaching the gamma H2A.X foci number peak in sMEK1-depleted T24 cells and the rescue transfection by acetyl-mimic mutant plasmid. Changes in the number of γH2AX foci per nucleus were monitored across time after the exposure to IR for up to 24 hours, using immunofluorescence microscopy of anti-γH2AX (red channel: 568) and DAPI co-staining (blue channel: 358). The average number is calculated based on the quantification of 100 cells under each condition of (A) control untreated T24, PAN treatment, sMEK1 overexpression and (B) sisMEK1 knockdown, rescue transfection by wild-type/ acetyl-dead/ acetyl-mimic mutant sMEK1 plasmid. Data are represented as mean ± SEM over n=2 independent experiments. Unpaired student t-tests are performed on PAN, KD and KD + K416Q in comparison to the CON UT at their respective time-points. * $p < 0.05$; ns $p > 0.05$. **Abbreviations:** CON UT, control untreated; +, overexpression; KD, knockdown; WT, wild-type; K416R, acetyl-dead; K416Q, acetyl-mimic.

A

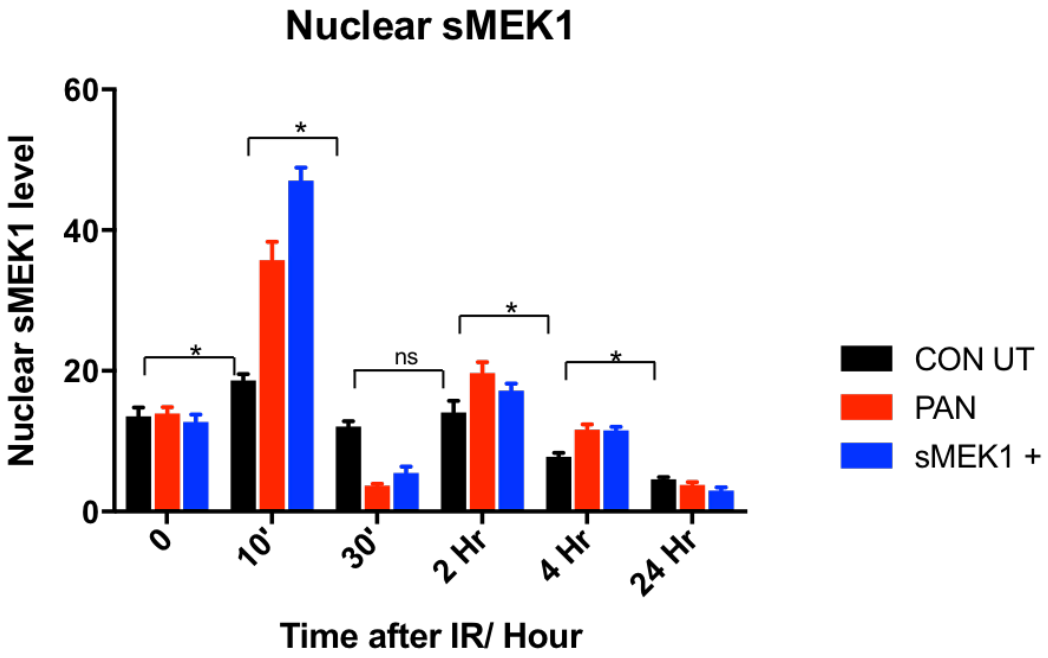

B

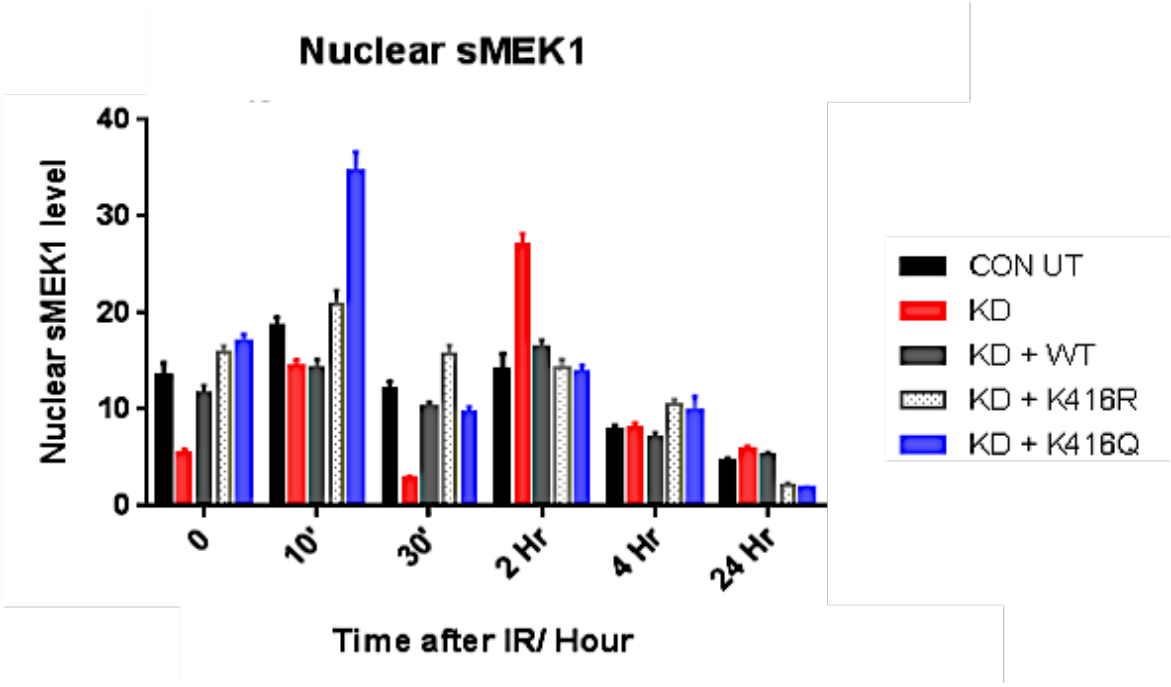

Figure 3-24. **Changes in the nuclear sMEK1 level with ionising radiation across time up to 24 hours under different conditions or treatment.** This was observed using anti-sMEK1 (green channel: 488) with DAPI co-staining (blue channel: 358) under an immunofluorescence microscope. The average level is calculated based on the quantification of 100 cells under each condition of (A) control untreated T24, PAN treatment, sMEK1 overexpression and (B) sisMEK1 knockdown, rescue transfection by wild-type/ acetyl-dead/ acetyl-mimic mutant sMEK1 plasmid. Data are plotted as mean ± SEM for n=2 independent experiments. The CON UT is chosen to represent the overall changes in nuclear sMEK1 levels, after which unpaired student t-tests are performed between consecutive time-points. * $p < 0.05$; ns $p > 0.05$.
Abbreviations: CON UT, control untreated; +, overexpression; KD, knockdown; WT, wild-type; K416R, acetyl-dead; K416Q, acetyl-mimic.

4. DISCUSSION

This study identified and validated the acetylation of suppressor of MEK1 (sMEK1) in the presence of panobinostat (PAN), which was differentially regulated over the course of the DNA damage response (DDR) following ionising radiation (IR). Histone acetyl transferases (HATs) and histone deacetylases (HDACs) are extensively involved in chromatin organisation and dynamics, which is a prerequisite for effective DNA repair (Berger et al., 2017), thus highlighting the functional significance of acetylation in the regulation of the DDR. Although many acetylated proteins have been discovered in response to various DNA repair-related conditions (Bennetzen et al., 2013; Elia et al., 2015), previous mechanistic studies of the action of HDAC inhibitors have primarily focused on the regulation of gene transcription via histones, as well as individual proteins which are already extensively researched, such as p53 and Ku80 (Abraham et al., 2000; Subramanian et al., 2013). A preliminary mass spectrometry acetylome screen after PAN treatment in the T24 bladder cancer cell line identified 169 novel acetylation sites on non-histone proteins (Nicholson et al., submitted), of which some have known roles in the DDR such as UCHL5 deubiquitinase (Nishi et al., 2014) and THRAP3 RNA processing factor (Beli et al., 2012). sMEK1 was selected due to its role as a regulatory subunit of the serine/threonine-protein phosphatase 4 (PP4) complex, that dephosphorylates γH2AX after the repair of IR-induced double-strand breaks (DSBs) for the recovery from G2/M checkpoint arrest (Nakada et al., 2008) as well as its association with chromatin (Chowdhury et al., 2008).

The regulation of acetylation as a post-translational modification is unique to individual proteins. For instance acetylated Ku80 behaves differently from MRE11 and RAD50, which participate in different DSB repair pathways i.e. non-homologous end joining (NHEJ) and homologous recombination (HR) respectively (Shibata et al., 2014). Here,

it was demonstrated that sMEK1 protein levels are modulated by HDAC inhibition and IR (Figures 3-3 and 3-9), potentially because of the increased acetylation resulting in a loss-of-function. A similar compensatory effect mechanism has also been reported in bromo-deficient p300, whereby the expression of mRNA transcripts is upregulated possibly to compensate for the loss of protein function (Chen et al., 2010). In the absence of HDAC inhibition, loss of sMEK1 acetylation was demonstrated immediately upon exposure to IR in DMSO control cells, as shown by reduced levels of acetylated sMEK1, after which it was strongly acetylated again at 4 hours (Figure 3-8). This is likely mediated by various HATs and HDACs enzymes to maintain the dynamic acetylation-deacetylation equilibrium, especially with increasing evidence of new non-histone substrates extending to cytoskeletal proteins, nuclear import factors and molecular chaperones (Glozak et al., 2005) in addition to the canonical histones. The enzyme-catalysed reaction of HATs gives rise to increased global acetylation levels, and this is reversed by HDACs. However by introducing PAN, increased overall sMEK1 acetylation was observed before and after irradiation (Figure 3-8) due to the shifted equilibrium towards acetylation. As a result, the initial decrease in sMEK1 acetylation after radiation was rescued, whereas increasing acetylation 4 hours after was unaffected by the presence of HDAC inhibitor.

The presence of an acetyl group on the lysine residue (endogenous: K655; transfected: K416) of sMEK1 proteins results in a loss of positive charge. It may subsequently alter the protein structure, or its interactions or block other lysine modifications, such as ubiquitylation and methylation (Choi et al., 2018), potentially affecting the protein synthesis, activity, stability as well as localisation. From the PhosphoSite Plus online database, the sMEK1 endogenous isoform of 833 residues is found to be monomethylated on the same Lysine 655 (K655) too. Therefore, the loss of sMEK1

function as a result of PAN administration can be inferred from increased acetylation or loss of monomethylation mark on K655 residue. This is in support of the theory that multiple post-translational modifications, including acetylation and methylation, add a finer tuning level to regulation of DNA repair processes (Gong and Miller, 2013; Chen and Zhu, 2016). Transient interactions with effector protein, bromodomain containing 4 (BRD4) are crucial for chromatin recruitment of the acetylated sMEK1 to perform its role as a part of γH2AX phosphatase towards the late stage of DDR. The highest abundance of sMEK1 was detected in the chromatin fraction of DMSO-treated cells at 4-hour post-irradiation (Figure 3-13), proportionally to the strength and amount of interactions with BRD4 (Figure 3-16B). Nonetheless in the presence of PAN, the interactions between acetylated sMEK1 and BRD4 were observed before and immediately after radiation but lost unexpectedly within 4 hours, despite increased sMEK1 acetylation levels. Although chromatin targeting is a known function of BRD4, the regulation of acetylated protein binding to bromodomains is little understood (Wu et al., 2013). Abnormal accumulation of sMEK1 was instead found in the nuclei of PAN-treated cells by 4 hours (Figure 3-12) possibly due to the loss of these transient interactions. This supports the hypothesis that acetylation sites act as 'switches' to provide a fast control of protein function and response rather than transcription, synthesis or degradation control, as well as suggesting that sMEK1's loss-of-function is likely achieved through defective compartmentalisation by 4 hours after IR.

The effects of sMEK1 protein in the regulation of the PP4 complex activity for γH2AX foci resolution upon DSB repair is in agreement with enhanced radiosensitivity comparable to that of PAN-treated cells after siRNA-mediated depletion of endogenous sMEK1 (Figure 3-21D), and this effect could be rescued by wild type plasmid re-transfection (Figure 3-21C). Loss of sMEK1 increases bladder cancer cell

radiosensitivity, possibly due to the delayed DDR induction (Figure 3-23B) and consequently higher cell death rate. The K655 acetylation site identified in sMEK1 was also important for radiosensitivity, hence implying a role of this post-translational modification in the DDR. In accordance with generally increasing radiosensitivity after HDAC inhibition (Groselj et al., 2013), whereby an increase in sMEK1 acetylation would be radiosensitising, the acetyl-mimic mutant achieved partial radiosensitisation compared to wild type (Figure 3-22B). On the other hand, the radioresistance was restored by acetyl-dead transfection to a similar level as the wild type (Figure 3-22A). Therefore it is likely that the loss of acetylated sMEK1 immediately upon exposure to IR plays a relatively greater role than acetylation, and disrupting this could result in downregulated DNA repair. This can be explained by the need for chromatin dissociation of the PP4 phosphatase complex, which has an antagonistic effect in promoting the induction of γH2AX phosphorylation waves upon DNA damage (Firsanov et al., 2011). Despite successful site-directed mutagenesis of Lysine K655 being confirmed by the sequencing results, co-immunoprecipitation using anti-AcK beads could not prove a loss or decrease in the total acetylation level (Figure 3-17), suggesting the presence of multiple acetylation sites on lysine-rich sMEK1 protein which could be acetylated even in the absence of the HDAC inhibitor PAN. To identify each acetylated lysine residue, samples could be run on western blots before cutting out the corresponding band for mass spectrometry studies. These additional sites may complement the function of the identified K655 residue in DNA damage repair.

Using γH2AX as a quantitative marker of DNA damage under immunofluorescence microscopy, PAN, a potent HDAC inhibitor, upregulated the number of γH2AX foci seen at 24 hours after the initial DNA damage (Figure 3-23A). The significant delay in foci resolution following a given recovery period indicates suppressed repair of DSBs in

PAN-treated cells (Groselj et al., 2013). In sMEK1 knockdown and acetyl-mimic re-transfection, the induction of DDR was significantly delayed as illustrated by γH2AX foci number reaching its peak only after 2 hours instead of 30 minutes (Figure 3-23B), and this may explain the increased radiosensitivity from clonogenic assays. However the foci number had nearly returned to the basal level by 24 hours, implying that loss-of-function of sMEK1 in the PP4 complex could potentially be compensated for by the presence of another regulatory subunit in the same complex (Kloeker and Wadzinski, 1999) or a similar function of PP2A phosphatase in removing the phosphate group from γH2AX foci (Chowdhury et al., 2005). This experimental method nonetheless presents a number of limitations which substantially reduce its reliability as a measurement of the extent of DSB damage/repair after irradiation. For instance, γH2AX foci formation not only occurs at the sites of radiation-induced DSBs, but it can also mark the exposed single-stranded DNA regions during replication stress or intermediate repair processes (Lobrich et al., 2010). Besides, background endogenous 'cryptogenic' foci can limit the ability to detect residual γH2AX (Olive, 2011), particularly at low signal-to-noise ratio upon long recovery timeframe.

Nuclear localisation of sMEK1 protein immediately after exposure to IR appears to be conserved across different conditions with PAN treatment, sisMEK1 knockdown as well as site-directed mutagenesis. This is supported by western blots of subcellular fractionation in the nuclei (Figure 3-12) and increasing nuclear sMEK1 levels detected within 10 minutes after irradiation (Figure 3-24). In a similar manner to the facilitation of nuclear localisation of cleaved Wnt receptor in the regulation of cortical neurogenesis (Chang et al., 2017), sMEK1 may function as a nuclear chaperone and cofactor for important DDR factors required for damage detection and/or further downstream signalling events. Increasing nuclear sMEK1 levels were also generally noted when the

γH2AX foci number started to fall after 2 hours. This can be explained by the high levels of phosphatase complex required for the efficient resolution of γH2AX foci once DSB repair is completed, with its proposed mechanism of assembly depicted in Figure 4-1. However, the measurement of nuclear sMEK1 levels using an immunocytochemistry technique is flawed because it could not distinguish between sMEK1 present in the nucleoplasm or associated with chromatin. As a result, abnormal nuclear accumulation of sMEK1 seen in PAN-treated cells by 4 hours after irradiation using subcellular fractionation, is not recapitulated under immunofluorescence microscopy. Due to extensive chromatin remodelling and nucleosome eviction during DSB repair, it was proposed that cells co-opted the process of recycling γH2AX into chromatin to promote its rapid dissolution (Nakada et al., 2008). Since the PP4 complex primarily dephosphorylates γH2AX in the chromatin rather than nucleoplasm, the level of sMEK1 found in chromatin under different conditions especially towards the late phase of DDR would be of high utmost significance.

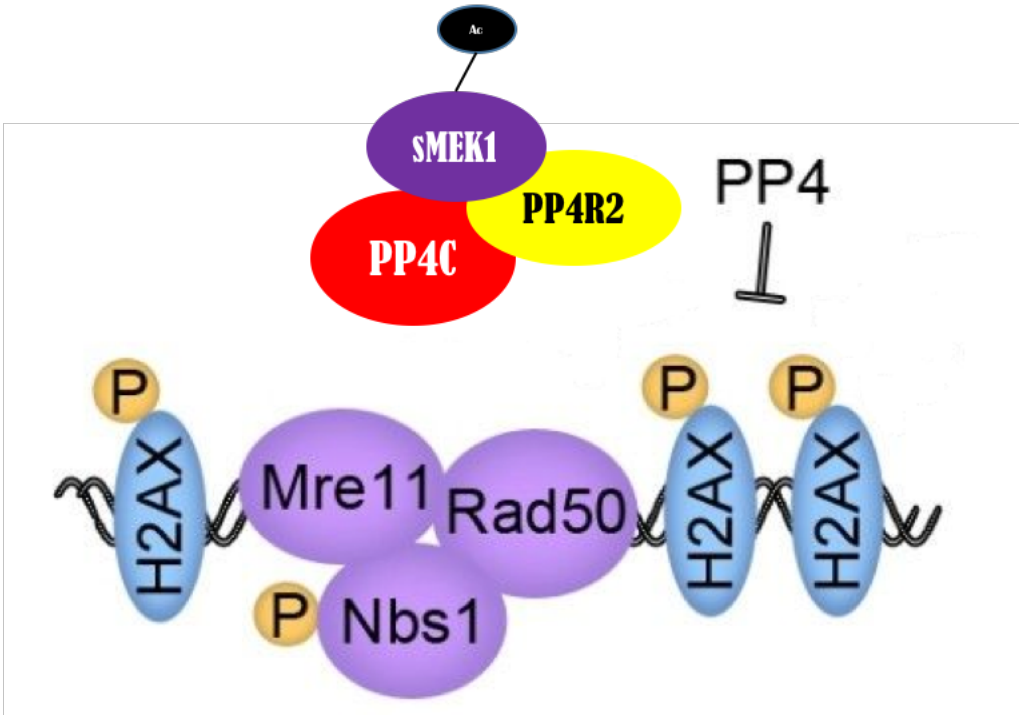

Figure 4-1. Proposed mechanism of the assembly of PP4 phosphatase complex at the sites of double-strand break induced by ionising radiation. Immediately upon DNA insult, phosphorylation waves spread to one or more megabases around the DNA break sites, leading to the formation of γH2AX foci. They are not only involved in the early steps of chromatin decondensation, but also act as major recruitment signals for downstream repair and signalling factors to the nuclear foci. The MRN complex (MRE11-RAD50-NBS1) is recruited to tether the broken DNA ends together. The PP4 complex consists of phosphatase catalytic subunit PP4C and two regulatory subunits, sMEK1 and PP4R2, with a role to resolve γH2AX foci upon complete DNA repair. The black dot represents the acetyl-group(s) added to the sMEK1 protein. This figure is adapted and modified from Freeman and Monteiro, 2010.

Combined treatment of PAN and sMEK1 depletion yielded partial radiosensitivity (Figure 3-22C), therefore sMEK1's loss-of-function due to increased acetylation might be one of the many molecular mechanisms of PAN-mediated radiosensitisation in bladder cancer cell line. This is corroborated by further evidence of the proteosomal degradation of MRE11 by E3 ubiquitin ligase cellular inhibitor of apoptosis protein 2 (cIAP2) in the presence of PAN (Nicholson et al., 2017) which compromises the ability to repair DSB damage via HR and radiosensitises the cells. PAN (LBH589) is a novel hydroxamic acid-based HDAC inhibitor that inhibits a broad spectrum ranging from all classes I, II to IV HDAC enzymes, even at low nanomolar concentrations (Scuto et al., 2008). To date, only two ongoing clinical trials have assessed the combination of HDAC inhibition and radiotherapy: one phase I trial on SAHA and palliative

radiotherapy, as well as one phase II study on the combination of VPA, temozolomide and external beam radiotherapy (www.cancer.org). Other potent *in vitro* radiosensitisers such as TSA and M344 have limited clinical uses because of the drug toxicity and instability. With the radiosensitisation effects mainly operating through deregulated class I HDACs family in bladder cancer, it would be interesting to replicate the current investigation using romidepsin which targets class I HDACs (Hölscher et al., 2018) to determine if this molecular mechanism via sMEK1's loss-of-function is conserved between different radiosensitisers of similar target(s).

sMEK1 is evolutionarily conserved across many species due to its essential cellular functions (Cohen et al., 2005). Apart from acting as a regulatory subunit in the PP4 phosphatase complex for γH2AX resolution, it may also play a major role in cell survival and viability as indicated by no colony formation during the antibiotic selection stage when sMEK1 was completely knocked out. The presence of seven alternatively-spliced transcripts (The Human Protein Atlas) implies that each variant may perform a slightly different function in human cells, and it is supported by the discrepancy observed between the large endogenous and smaller transfected sMEK1 isoforms in terms of their expression and interaction with effector proteins. For instance, both the transfected and endogenous sMEK1 proteins behave differently in the chromatin fraction after PAN treatment (Figures 3-13 and 3-16B). This can be accounted by the lack of N-terminal armadillo (ARM) repeats in the transfected variant of 594 residues, which are frequently involved in mediating protein-protein interactions (Madhurantakam et al., 2012).

Future work should focus on dissecting the precise role of sMEK1 in the PP4 phosphatase complex as well as the functional implications of acetylation on different

pathways of DSB repair. This can be addressed by using an *in vitro* phosphatase assay using pre-labelled [γ-^{32}P]-ATP substrates in the presence or absence of an HDAC inhibitor. With the PP4 family accounting for the majority of serine/threonine dephosphorylation in eukaryotic cells (Andreeva and Kutuzov, 2001), regulatory subunits of these protein phosphatases, sMEK1 in this instance, may localise the PP4 enzyme near specific cellular targets including γH2AX as well as influence the target substrate selection or recognition at these sites (Virshup and Shenolikar, 2009). PAN-mediated acetylation of sMEK1 can also potentially alter the charge complementarity or binding pocket configuration formed by the surface hydrophilic lysine residue(s). Besides, for reliable visualisation of the changes in sMEK1 protein localisation with HDAC inhibition before and after IR, green fluorescence protein (GFP)-tagged fusion protein (Crivat and Taraska, 2012) may be exploited for real-time live imaging of the green fluorescence. To comprehensively examine the main mechanism of DNA repair through NHEJ and HR pathways, immunocytochemistry using various antibodies that specifically recognise different HR factors such as 53BP1, phospho-RPA and RAD51, or NHEJ repair factors like Ku70, Ku80 and DNA-PKcs can be used in addition to γH2AX foci detection in cell nuclei at the sites of DNA damage after IR or laser. Moreover, direct repeat-GFP (DR-GFP) reporter assay based on I-Sce I endonuclease (Nakanishi et al., 2012) would allow the repair efficiency of induced DSB lesion via HR or NHEJ to be probed separately in the context of sMEK1 acetylation.

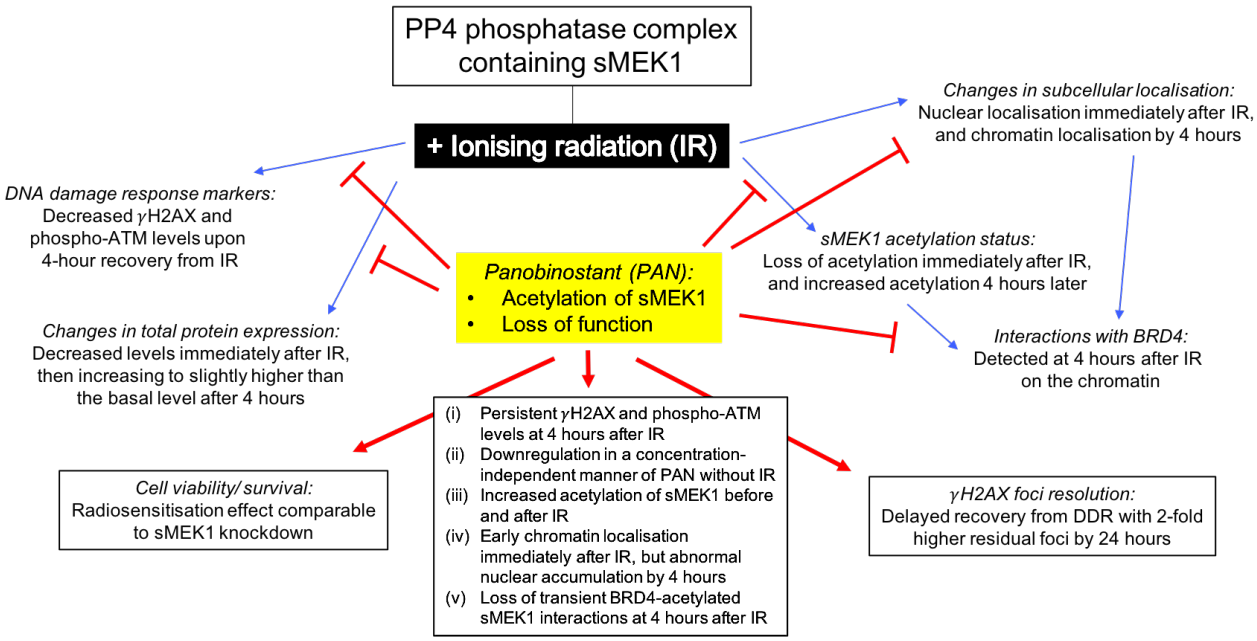

Figure 4-2. Proposed mechanism of action of panobinostat (PAN)-mediated radiosensitisation through increased sMEK1 acetylation.

The proposed mechanism of action of PAN-mediated radiosensitisation through sMEK1 loss-of-function is summarised above in Figure 4-2. In conclusion, suppressor of MEK1 (sMEK1) protein is dynamically (de)acetylated over the time-course of the DNA damage response (DDR) after ionising radiation (IR), and this can be disrupted by the introduction of the HDAC inhibitor panobinostat (PAN). Increased sMEK1 acetylation by PAN results in a loss of transient interactions with bromodomain 4 (BRD4) effector proteins on the chromatin by 4-hour post-IR, and subsequently abnormal nuclear accumulation. Loss-of-function of sMEK1 on the chromatin as a part of the protein phosphatase PP4 complex, contributes to the delayed DDR induction as well as increased radiosensitivity.

Appendix 1

Serine/threonine-protein phosphatase 4 regulatory subunit 3A isoform 3
Species: Homo sapiens
Sequence ID: NP_001271210.1
Length: 594 amino acid residues

1F - Range 1: 28 to 175

Score	Expect	Method	Identities	Positives	Gaps	Frame
145 bits(366)	2e-49	Compositional matrix adjust.	87/149(58%)	95/149(63%)	3/149(2%)	+1

```
Query  55   SXGXSMRXKGRPLLVEDETDGSRLLISKICPXXAEFVXXKMKNF--GPFVCTTKR*RGX*  228
            S G   R KG  LLV  E+DGS LL SKI P  A     + + F    F   T
Sbjct  28   SSGYVERLKGMSLLVRAESDGSLLLESKINPNTAYQKQQEDEKFLTDLFAQLTDEATDEE  87

Query  229  GXKTGXG*LXLQFCAFSPXLRPQNGDAFFFTLSPMSLLPALEVILGMDDTPGRSAATDIF  408
              +     L  +FCAFS  L+PQN DAFF TLS M +LPALEVILGMDDT  RSAATDIF
Sbjct  88   KRQELVNFLK-EFCAFSQTLQPQNRDAFFKTLSNMGILPALEVILGMDDTQVRSAATDIF  146

Query  409  SYLVEYKPSMVREFVMQEAQQNDXVSKKV  495
            SYLVEY PSMVREFVMQEAQQND VSKK+
Sbjct  147  SYLVEYNPSMVREFVMQEAQQNDDVSKKL  175
```

5F - Range 1: 181 to 512

Score	Expect	Method	Identities	Positives	Gaps	Frame
615 bits(1587)	0.0	Compositional matrix adjust.	330/332(99%)	330/332(99%)	0/332(0%)	+2

```
Query  35   TSKDillinlixxHMICDTDPELGGAVQLMGLLRTLVDPENMLATANKTEKTEFLGFFYK  214
            TSKDILLINLI  HMICDTDPELGGAVQLMGLLRTLVDPENMLATANKTEKTEFLGFFYK
Sbjct  181  TSKDILLINLIIEHMICDTDPELGGAVQLMGLLRTLVDPENMLATANKTEKTEFLGFFYK  240

Query  215  HCMHVLTAPLLANTTEDKPSKDDFQTAQllalvlellTFCVEHHTYHIKNYIINKDILRR  394
            HCMHVLTAPLLANTTEDKPSKDDFQTAQLLALVLELLTFCVEHHTYHIKNYIINKDILRR
Sbjct  241  HCMHVLTAPLLANTTEDKPSKDDFQTAQLLALVLELLTFCVEHHTYHIKNYIINKDILRR  300

Query  395  VLVLMASKHAFLALCALRFKRKIIGLKDEFYNRYIMKSFLFEPVVKAFLNNGSRYNLMNS  574
            VLVLMASKHAFLALCALRFKRKIIGLKDEFYNRYIMKSFLFEPVVKAFLNNGSRYNLMNS
Sbjct  301  VLVLMASKHAFLALCALRFKRKIIGLKDEFYNRYIMKSFLFEPVVKAFLNNGSRYNLMNS  360

Query  575  AIIEMFEFIRVEDIKSLTAHVIENYWKALEDVDYVQTFKGLKLRFEQQRERQDNPKLDSM  754
            AIIEMFEFIRVEDIKSLTAHVIENYWKALEDVDYVQTFKGLKLRFEQQRERQDNPKLDSM
Sbjct  361  AIIEMFEFIRVEDIKSLTAHVIENYWKALEDVDYVQTFKGLKLRFEQQRERQDNPKLDSM  420

Query  755  RSILRNHRYRRDARTLEDEEEMWFNTDEDDMEDGEAVVSPSDKTKNDDDIMDPISKFMer  934
            RSILRNHRYRRDARTLEDEEEMWFNTDEDDMEDGEAVVSPSDKTKNDDDIMDPISKFMER
Sbjct  421  RSILRNHRYRRDARTLEDEEEMWFNTDEDDMEDGEAVVSPSDKTKNDDDIMDPISKFMER  480

Query  935  kklkeseekevllkTNLSGRQSPSFKLSLSSG  1030
            KKLKESEEKEVLLKTNLSGRQSPSFKLSLSSG
Sbjct  481  KKLKESEEKEVLLKTNLSGRQSPSFKLSLSSG  512
```

6F - Range 1: 279 to 594

Score	Expect	Method	Identities	Positives	Gaps	Frame
510 bits(1313)	6e-175	Compositional matrix adjust.	316/316(100%)	316/316(100%)	0/316(0%)	+2

```
Query  29   FCVEHHTYHIKNYIINKDILRRVLVLMASKHAFLALCALRFKRKIIGLKDEFYNRYIMKS  208
            FCVEHHTYHIKNYIINKDILRRVLVLMASKHAFLALCALRFKRKIIGLKDEFYNRYIMKS
Sbjct  279  FCVEHHTYHIKNYIINKDILRRVLVLMASKHAFLALCALRFKRKIIGLKDEFYNRYIMKS  338

Query  209  FLFEPVVKAFLNNGSRYNLMNSAIIEMFEFIRVEDIKSLTAHVIENYWKALEDVDYVQTF  388
            FLFEPVVKAFLNNGSRYNLMNSAIIEMFEFIRVEDIKSLTAHVIENYWKALEDVDYVQTF
Sbjct  339  FLFEPVVKAFLNNGSRYNLMNSAIIEMFEFIRVEDIKSLTAHVIENYWKALEDVDYVQTF  398

Query  389  KGLKLRFEQQRERQDNPKLDSMRSILRNHRYRRDARTLEDEEEMWFNTDEDDMEDGEAVV  568
            KGLKLRFEQQRERQDNPKLDSMRSILRNHRYRRDARTLEDEEEMWFNTDEDDMEDGEAVV
Sbjct  399  KGLKLRFEQQRERQDNPKLDSMRSILRNHRYRRDARTLEDEEEMWFNTDEDDMEDGEAVV  458

Query  569  SPSDKTKNDDDIMDPISKFMerkklkeseekevllkTNLSGRQSPSFKLSLSSGtktnlt  748
            SPSDKTKNDDDIMDPISKFMERKKLKESEEKEVLLKTNLSGRQSPSFKLSLSSGTKTNLT
Sbjct  459  SPSDKTKNDDDIMDPISKFMERKKLKESEEKEVLLKTNLSGRQSPSFKLSLSSGTKTNLT  518

Query  749  sqssttnlpgspgspgspgspgspgaVPKNTSQTAAITTKGGLVGLVDYPdddedddede  928
            SQSSTTNLPGSPGSPGSPGSPGSPGSVPKNTSQTAAITTKGGLVGLVDYPDDDEDDDEDE
Sbjct  519  SQSSTTNLPGSPGSPGSPGSPGSPGSVPKNTSQTAAITTKGGLVGLVDYPDDDEDDDEDE  578

Query  929  dkedTLPLSKKAKFDS  976
            DKEDTLPLSKKAKFDS
Sbjct  579  DKEDTLPLSKKAKFDS  594
```

7F - Range 1: 376 to 594

Score	Expect	Method	Identities	Positives	Gaps	Frame
305 bits(781)	1e-96	Compositional matrix adjust.	219/219(100%)	219/219(100%)	0/219(0%)	+2

```
Query  20   SLTAHVIENYWKALEDVDYVQTFKGLKLRFEQQRERQDNPKLDSMRSILRNHRYRRDART  199
           SLTAHVIENYWKALEDVDYVQTFKGLKLRFEQQRERQDNPKLDSMRSILRNHRYRRDART
Sbjct  376  SLTAHVIENYWKALEDVDYVQTFKGLKLRFEQQRERQDNPKLDSMRSILRNHRYRRDART  435

Query  200  LEDEEEMWFNTDEDDMEDGEAVVSPSDKTKNDDDIMDPISKFMerkklkeseekevllkT  379
           LEDEEEMWFNTDEDDMEDGEAVVSPSDKTKNDDDIMDPISKFMERKKLKESEEKEVLLKT
Sbjct  436  LEDEEEMWFNTDEDDMEDGEAVVSPSDKTKNDDDIMDPISKFMERKKLKESEEKEVLLKT  495

Query  380  NLSGRQSPSFKLSLSSGtktnltsqssttnlpgspgspgspgspgspgsVPKNTSQTAAI  559
           NLSGRQSPSFKLSLSSGTKTNLTSQSSTTNLPGSPGSPGSPGSPGSPGSVPKNTSQTAAI
Sbjct  496  NLSGRQSPSFKLSLSSGTKTNLTSQSSTTNLPGSPGSPGSPGSPGSPGSVPKNTSQTAAI  555

Query  560  TTKGGLVGLVDYPdddedddededkedTLPLSKKAKFDS  676
           TTKGGLVGLVDYPDDDEDDDEDEDKEDTLPLSKKAKFDS
Sbjct  556  TTKGGLVGLVDYPDDDEDDDEDEDKEDTLPLSKKAKFDS  594
```

8F - Range 1: 495 to 594

Score	Expect	Method	Identities	Positives	Gaps	Frame
91.7 bits(226)	7e-19	Compositional matrix adjust.	100/100(100%)	100/100(100%)	0/100(0%)	+1

```
Query  76   TNLSGRQSPSFKLSLSSGtktnltsqssttnlpgspgspgspgspgspgsVPKNTSQTAA  255
           TNLSGRQSPSFKLSLSSGTKTNLTSQSSTTNLPGSPGSPGSPGSPGSPGSVPKNTSQTAA
Sbjct  495  TNLSGRQSPSFKLSLSSGTKTNLTSQSSTTNLPGSPGSPGSPGSPGSPGSVPKNTSQTAA  554

Query  256  ITTKGGLVGLVDYPdddedddededkedTLPLSKKAKFDS  375
           ITTKGGLVGLVDYPDDDEDDDEDEDKEDTLPLSKKAKFDS
Sbjct  555  ITTKGGLVGLVDYPDDDEDDDEDEDKEDTLPLSKKAKFDS  594
```

The FASTA sequence obtained from Sanger sequencing was copied and pasted into BLAST@NCBI (https://blast.ncbi.nlm.nih.gov/Blast.cgi) to translate nucleotides into peptides. A smaller isoform of sMEK1 also known as serine/threonine-protein phosphatase 4 regulatory subunit 3A isoform 3, appeared at the top of the list with the highest overall percentage similarity after aligning and comparing the region covered by each forward primer 1F-9F, designed for the full-length endogenous sMEK1 isoform of 833 amino acids (95.368 kDa). Only the primers 1F and 5F to 8F yielded positive results (as displayed above) while the remaining present zero-similarity hits. With reference to the UniProtKB database, this isoform (identifier: Q6IN85-4) differs from the canonical sequence by missing amino acid residues 67-305, as highlighted below in yellow.

Amino acid sequence of the endogenous sMEK1 isoform (833 amino acid residues)

```
        10         20         30         40         50
MTDTRRRVKV YTLNEDRQWD DRGTGHVSSG YVERLKGMSL LVRAESDGSL
        60         70         80         90        100
LLESKINPNT AYQKQQDTLI VWSEAENYDL ALSFQEKAGC DEIWEKICQV
       110        120        130        140        150
QGKDPSVDIT QDLVDESEEE RFDDMSSPGL ELPSCELSRL EEIAELVASS
       160        170        180        190        200
LPSPLRREKL ALALENEGYI KKLLELFHVC EDLENIEGLH HLYEIIKGIF
       210        220        230        240        250
LLNRTALFEV MFSEECIMDV IGCLEYDPAL SQPRKHREFL TKTAKFKEVI
       260        270        280        290        300
PISDPELKQK IHQTYRVQYI QDMVLPTPSV FEENMLSTLH SFIFFNKVEI
       310        320        330        340        350
VGMLQEDEKF LTDLFAQLTD EATDEEKRQE LVNFLKEFCA FSQTLQPQNR
       360        370        380        390        400
DAFFKTLSNM GILPALEVIL GMDDTQVRSA ATDIFSYLVE YNPSMVREFV
       410        420        430        440        450
MQEAQQNDDV SKKLTEQKIT SKDILLINLI IEHMICDTDP ELGGAVQLMG
       460        470        480        490        500
LLRTLVDPEN MLATANKTEK TEFLGFFYKH CMHVLTAPLL ANTTEDKPSK
       510        520        530        540        550
DDFQTAQLLA LVLELLTFCV EHHTYHIKNY IINKDILRRV LVLMASKHAF
       560        570        580        590        600
LALCALRFKR KIIGLKDEFY NRYIMKSFLF EPVVKAFLNN GSRYNLMNSA
       610        620        630        640        650
IIEMFEFIRV EDIKSLTAHV IENYWKALED VDYVQTFKGL KLRFEQQRER
       660        670        680        690        700
QDNPKLDSMR SILRNHRYRR DARTLEDEEE MWFNTDEDDM EDGEAVVSPS
       710        720        730        740        750
DKTKNDDDIM DPISKFMERK KLKESEEKEV LLKTNLSGRQ SPSFKLSLSS
       760        770        780        790        800
GTKTNLTSQS STTNLPGSPG SPGSPGSPGS PGSVPKNTSQ TAAITTKGGL
       810        820        830
VGLVDYPDDD EDDDEDEDKE DTLPLSKKAK FDS
```

Appendix 2

```
Alignment of Sequence_1:  [original plasmid_6F.xdna] with  Sequence_2: [K416R_1.xdna]

Similarity : 1073/1454 (73.80 %)

              A  L  C  A  L  R  F  K  R  K  I  I  G  L  K  D  E  F  Y  N
Seq_1  119    GCATTATGTGCCCTTCGTTTTAAAAGAAAGATTATTGGATTAAAAGATGAGTTTTACAAC  178
              ||||||||||||||||||||||||||||||||||||||||||||||||||||||||||||
Seq_2  117    GCATTATGTGCCCTTCGTTTTAAAAGAAAGATTATTGGATTAAAAGATGAGTTTTACAAC  176
              A  L  C  A  L  R  F  K  R  K  I  I  G  L  K  D  E  F  Y  N

              R  Y  I  M  K  S  F  L  F  E  P  V  V  K  A  F  L  N  N  G
Seq_1  179    CGCTACATAATGAAAAGTTTTTTGTTTGAACCAGTAGTGAAAGCATTTCTCAACAATGGA  238
              ||||||||||||||||||||||||||||||||||||||||||||||||||||||||||||
Seq_2  177    CGCTACATAATGAAAAGTTTTTTGTTTGAACCAGTAGTGAAAGCATTTCTCAACAATGGA  236
              R  Y  I  M  K  S  F  L  F  E  P  V  V  K  A  F  L  N  N  G

              S  R  Y  N  L  M  N  S  A  I  I  E  M  F  E  F  I  R  V  E
Seq_1  239    TCCCGCTACAATCTGATGAACTCTGCCATAATAGAGATGTTTGAATTTATTAGAGTGGAA  298
              ||||||||||||||||||||||||||||||||||||||||||||||||||||||||||||
Seq_2  237    TCCCGCTACAATCTGATGAACTCTGCCATAATAGAGATGTTTGAATTTATTAGAGTGGAA  296
              S  R  Y  N  L  M  N  S  A  I  I  E  M  F  E  F  I  R  V  E

              D  I  K  S  L  T  A  H  V  I  E  N  Y  W  K  A  L  E  D  V
Seq_1  299    GATATAAAATCATTAACTGCTCATGTAATTGAAAATTACTGGAAAGCACTGGAAGATGTA  358
              ||||||||||||||||||||||||||||||||||||||||||||||||||||||||||||
Seq_2  297    GATATAAAATCATTAACTGCTCATGTAATTGAAAATTACTGGAAAGCACTGGAAGATGTA  356
              D  I  K  S  L  T  A  H  V  I  E  N  Y  W  K  A  L  E  D  V

              D  Y  V  Q  T  F  K  G  L  K  L  R  F  E  Q  Q  R  E  R  Q
Seq_1  359    GATTATGTACAGACATTTAAAGGATTAAAACTGAGATTTGAACAACAAAGAGAAAGGCAA  418
              ||||||||||||||||||||||||||||||||||||||||||||||||||||||||||||
Seq_2  357    GATTATGTACAGACATTTAAAGGATTAAAACTGAGATTTGAACAACAAAGAGAAAGGCAA  416
              D  Y  V  Q  T  F  K  G  L  K  L  R  F  E  Q  Q  R  E  R  Q

              D  N  P  K  L  D  S  M  R  S  I  L  R  N  H  R  Y  R  R  D
Seq_1  419    GATAATCCCAAACTTGACAGTATGCGTTCCATTTTGAGGAATCACAGATATCGAAGAGAT  478
              |||||||||| ||||||||||||||||||||||||||||||||||||||||||||||||||
Seq_2  417    GATAATCCCAGACTTGACAGTATGCGTTCCATTTTGAGGAATCACAGATATCGAAGAGAT  476
              D  N  P  R  L  D  S  M  R  S  I  L  R  N  H  R  Y  R  R  D

              A  R  T  L  E  D  E  E  E  M  W  F  N  T  D  E  D  D  M  E
Seq_1  479    GCCAGAACACTAGAAGATGAAGAAGAGATGTGGTTTAACACAGATGAAGATGACATGGAA  538
              ||||||||||||||||||||||||||||||||||||||||||||||||||||||||||||
Seq_2  477    GCCAGAACACTAGAAGATGAAGAAGAGATGTGGTTTAACACAGATGAAGATGACATGGAA  536
              A  R  T  L  E  D  E  E  E  M  W  F  N  T  D  E  D  D  M  E

              D  G  E  A  V  V  S  P  S  D  K  T  K  N  D  D  D  I  M  D
Seq_1  539    GATGGAGAAGCTGTAGTGTCTCCATCTGACAAAACTAAAAATGATGATGATATTATGGAT  598
              ||||||||||||||||||||||||||||||||||||||||||||||||||||||||||||
Seq_2  537    GATGGAGAAGCTGTAGTGTCTCCATCTGACAAAACTAAAAATGATGATGATATTATGGAT  596
              D  G  E  A  V  V  S  P  S  D  K  T  K  N  D  D  D  I  M  D
```

The sequencing result of acetyl-dead variant (K416R) was copied and pasted into the Serial Cloner software for local alignment, followed by translation into peptides.

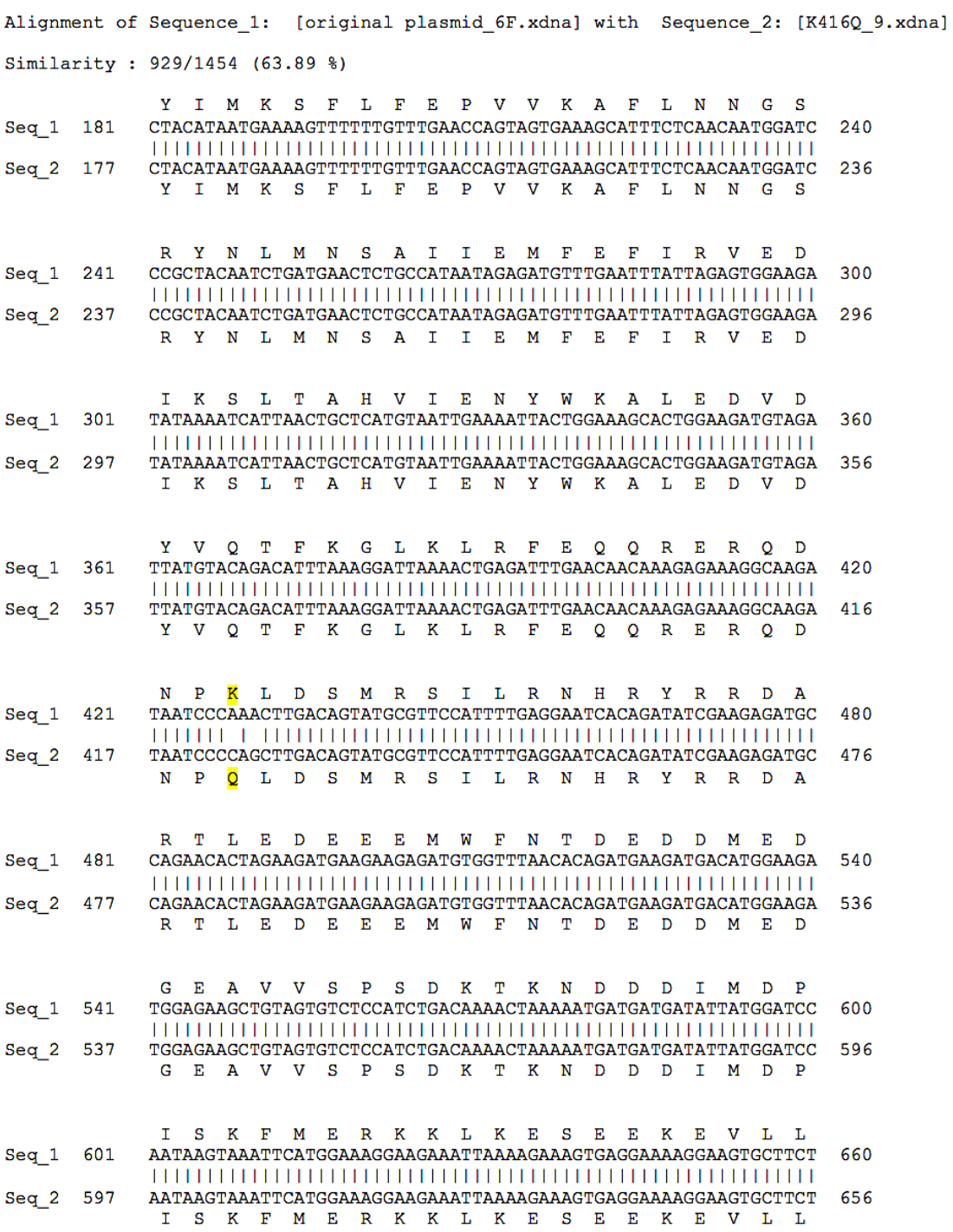

```
Alignment of Sequence_1:  [original plasmid_6F.xdna] with  Sequence_2: [K416Q_9.xdna]

Similarity : 929/1454 (63.89 %)

              Y  I  M  K  S  F  L  F  E  P  V  V  K  A  F  L  N  N  G  S
Seq_1  181   CTACATAATGAAAAGTTTTTTGTTTGAACCAGTAGTGAAAGCATTTCTCAACAATGGATC  240
             ||||||||||||||||||||||||||||||||||||||||||||||||||||||||||||
Seq_2  177   CTACATAATGAAAAGTTTTTTGTTTGAACCAGTAGTGAAAGCATTTCTCAACAATGGATC  236
              Y  I  M  K  S  F  L  F  E  P  V  V  K  A  F  L  N  N  G  S


              R  Y  N  L  M  N  S  A  I  I  E  M  F  E  F  I  R  V  E  D
Seq_1  241   CCGCTACAATCTGATGAACTCTGCCATAATAGAGATGTTTGAATTTATTAGAGTGGAAGA  300
             ||||||||||||||||||||||||||||||||||||||||||||||||||||||||||||
Seq_2  237   CCGCTACAATCTGATGAACTCTGCCATAATAGAGATGTTTGAATTTATTAGAGTGGAAGA  296
              R  Y  N  L  M  N  S  A  I  I  E  M  F  E  F  I  R  V  E  D


              I  K  S  L  T  A  H  V  I  E  N  Y  W  K  A  L  E  D  V  D
Seq_1  301   TATAAAATCATTAACTGCTCATGTAATTGAAAATTACTGGAAAGCACTGGAAGATGTAGA  360
             ||||||||||||||||||||||||||||||||||||||||||||||||||||||||||||
Seq_2  297   TATAAAATCATTAACTGCTCATGTAATTGAAAATTACTGGAAAGCACTGGAAGATGTAGA  356
              I  K  S  L  T  A  H  V  I  E  N  Y  W  K  A  L  E  D  V  D


              Y  V  Q  T  F  K  G  L  K  L  R  F  E  Q  Q  R  E  R  Q  D
Seq_1  361   TTATGTACAGACATTTAAAGGATTAAAACTGAGATTTGAACAACAAAGAGAAAGGCAAGA  420
             ||||||||||||||||||||||||||||||||||||||||||||||||||||||||||||
Seq_2  357   TTATGTACAGACATTTAAAGGATTAAAACTGAGATTTGAACAACAAAGAGAAAGGCAAGA  416
              Y  V  Q  T  F  K  G  L  K  L  R  F  E  Q  Q  R  E  R  Q  D


              N  P  K  L  D  S  M  R  S  I  L  R  N  H  R  Y  R  R  D  A
Seq_1  421   TAATCCCAAACTTGACAGTATGCGTTCCATTTTGAGGAATCACAGATATCGAAGAGATGC  480
             ||||||| | ||||||||||||||||||||||||||||||||||||||||||||||||||||
Seq_2  417   TAATCCCCAGCTTGACAGTATGCGTTCCATTTTGAGGAATCACAGATATCGAAGAGATGC  476
              N  P  Q  L  D  S  M  R  S  I  L  R  N  H  R  Y  R  R  D  A


              R  T  L  E  D  E  E  E  M  W  F  N  T  D  E  D  D  M  E  D
Seq_1  481   CAGAACACTAGAAGATGAAGAAGAGATGTGGTTTAACACAGATGAAGATGACATGGAAGA  540
             ||||||||||||||||||||||||||||||||||||||||||||||||||||||||||||
Seq_2  477   CAGAACACTAGAAGATGAAGAAGAGATGTGGTTTAACACAGATGAAGATGACATGGAAGA  536
              R  T  L  E  D  E  E  E  M  W  F  N  T  D  E  D  D  M  E  D


              G  E  A  V  V  S  P  S  D  K  T  K  N  D  D  D  I  M  D  P
Seq_1  541   TGGAGAAGCTGTAGTGTCTCCATCTGACAAAACTAAAAATGATGATGATATTATGGATCC  600
             ||||||||||||||||||||||||||||||||||||||||||||||||||||||||||||
Seq_2  537   TGGAGAAGCTGTAGTGTCTCCATCTGACAAAACTAAAAATGATGATGATATTATGGATCC  596
              G  E  A  V  V  S  P  S  D  K  T  K  N  D  D  D  I  M  D  P


              I  S  K  F  M  E  R  K  K  L  K  E  S  E  E  K  E  V  L  L
Seq_1  601   AATAAGTAAATTCATGGAAAGGAAGAAATTAAAAGAAAGTGAGGAAAAGGAAGTGCTTCT  660
             ||||||||||||||||||||||||||||||||||||||||||||||||||||||||||||
Seq_2  597   AATAAGTAAATTCATGGAAAGGAAGAAATTAAAAGAAAGTGAGGAAAAGGAAGTGCTTCT  656
              I  S  K  F  M  E  R  K  K  L  K  E  S  E  E  K  E  V  L  L
```

The sequencing result of acetyl-mimic variant (K416Q) was copied and pasted into the Serial Cloner software for local alignment, followed by translation into peptides.

Appendix 3

T24 control untreated

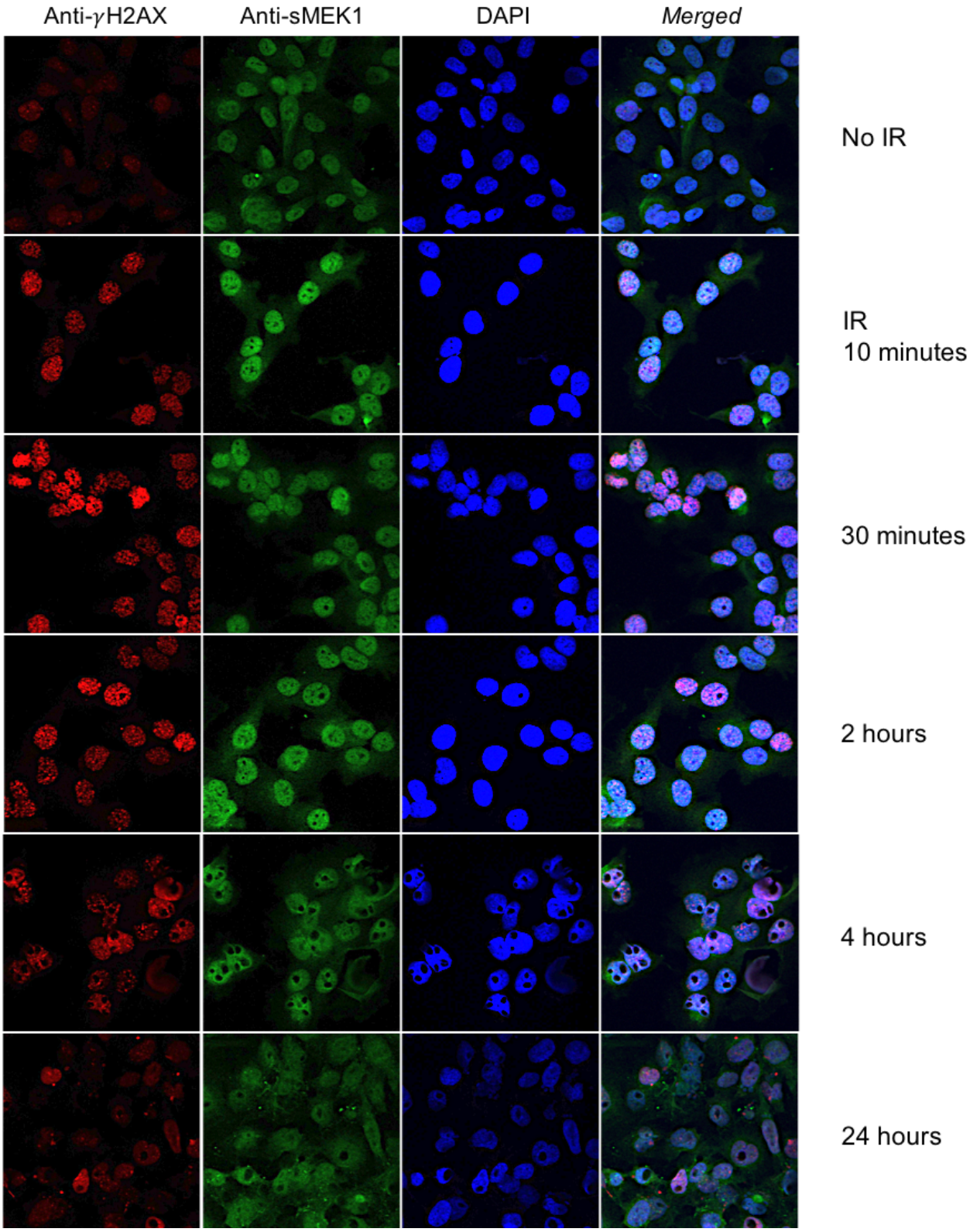

25 nM panobinostat

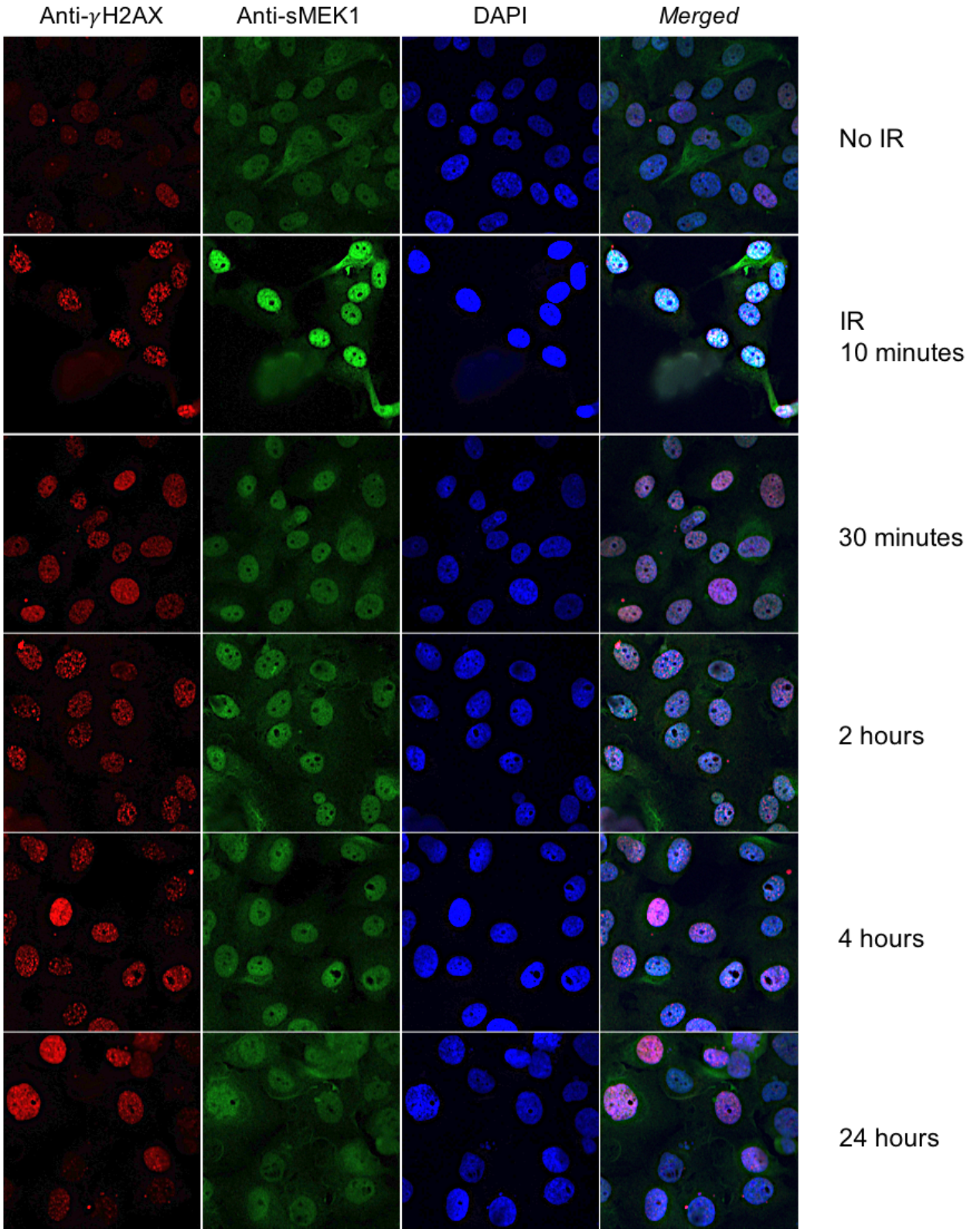

sMEK1 knockdown

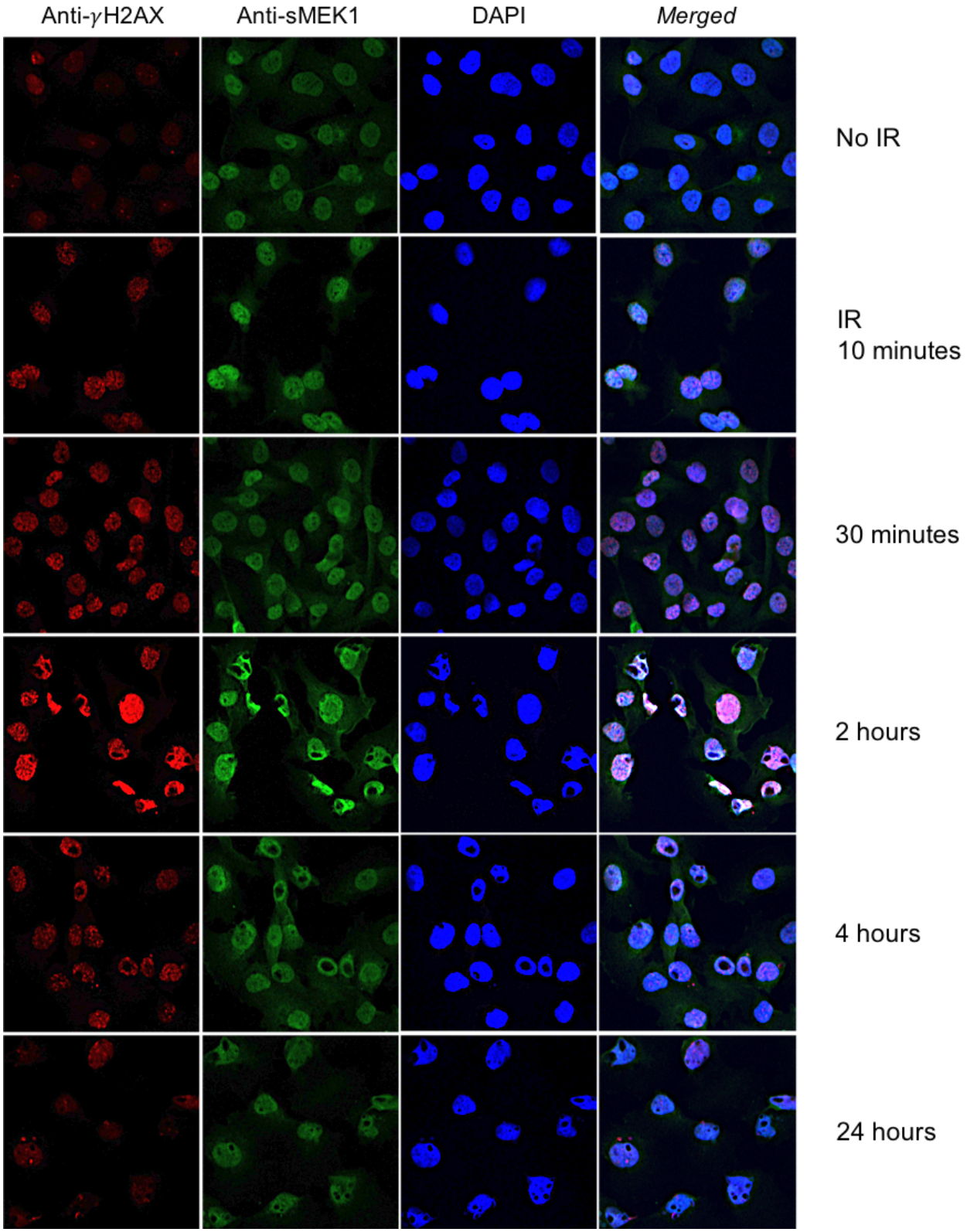

sMEK1 knockdown + K416Q re-transfection

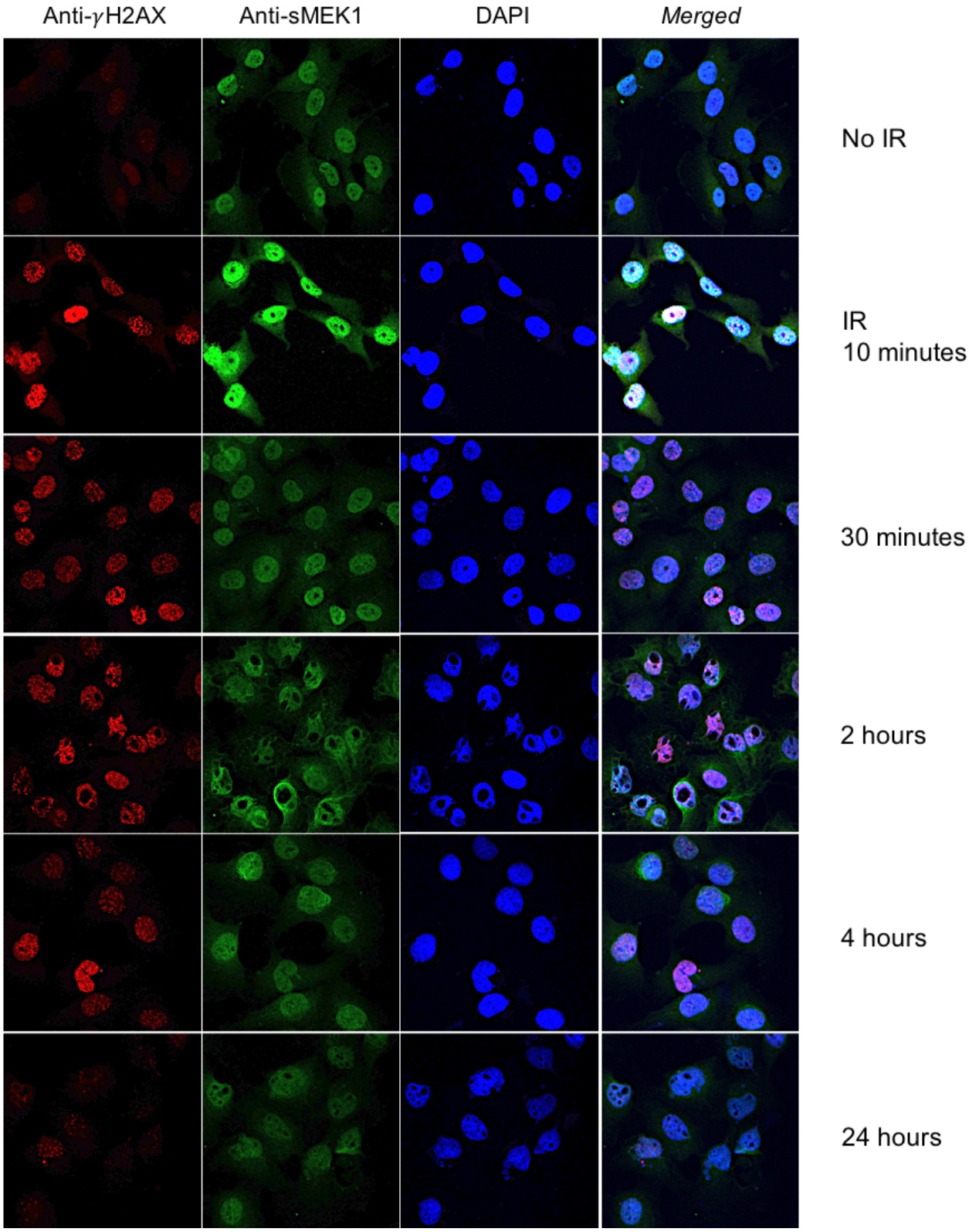

5. REFERENCES

ABRAHAM, J., KELLY, J., THIBAULT, P. & BENCHIMOL, S. 2000. Post-translational modification of p53 protein in response to ionizing radiation analyzed by mass spectrometry. *J Mol Biol,* 295**,** 853-64.

AHNESORG, P., SMITH, P. & JACKSON, S. P. 2006. XLF interacts with the XRCC4-DNA ligase IV complex to promote DNA nonhomologous end-joining. *Cell,* 124**,** 301-13.

ALT, F. W., ZHANG, Y., MENG, F. L., GUO, C. & SCHWER, B. 2013. Mechanisms of programmed DNA lesions and genomic instability in the immune system. *Cell,* 152**,** 417-29.

ANDREEVA, A. V. & KUTUZOV, M. A. 2001. PPP family of protein Ser/Thr phosphatases: two distinct branches? *Mol Biol Evol,* 18**,** 448-52.

ASANGANI, I. A., DOMMETI, V. L., WANG, X., MALIK, R., CIESLIK, M., YANG, R., ESCARA-WILKE, J., WILDER-ROMANS, K., DHANIREDDY, S., ENGELKE, C., IYER, M. K., JING, X., WU, Y. M., CAO, X., QIN, Z. S., WANG, S., FENG, F. Y. & CHINNAIYAN, A. M. 2014. Therapeutic targeting of BET bromodomain proteins in castration-resistant prostate cancer. *Nature,* 510**,** 278-82.

AUDEBERT, M., SALLES, B. & CALSOU, P. 2004. Involvement of poly(ADP-ribose) polymerase-1 and XRCC1/DNA ligase III in an alternative route for DNA double-strand breaks rejoining. *J Biol Chem,* 279**,** 55117-26.

BARTOCCI, C. & DENCHI, E. L. 2013. Put a RING on it: regulation and inhibition of RNF8 and RNF168 RING finger E3 ligases at DNA damage sites. *Front Genet,* 4**,** 128.

BELI, P., LUKASHCHUK, N., WAGNER, S. A., WEINERT, B. T., OLSEN, J. V., BASKCOMB, L., MANN, M., JACKSON, S. P. & CHOUDHARY, C. 2012. Proteomic investigations reveal a role for RNA processing factor THRAP3 in the DNA damage response. *Mol Cell,* 46**,** 212-25.

BELKINA, A. C. & DENIS, G. V. 2012. BET domain co-regulators in obesity, inflammation and cancer. *Nat Rev Cancer,* 12**,** 465-77.

BERGER, N. D., STANLEY, F. K. T., MOORE, S. & GOODARZI, A. A. 2017. ATM-dependent pathways of chromatin remodelling and oxidative DNA damage responses. *Philos Trans R Soc Lond B Biol Sci,* 372.

BERTRAM, P. G., CHOI, J. H., CARVALHO, J., AI, W., ZENG, C., CHAN, T. F. & ZHENG, X. F. 2000. Tripartite regulation of Gln3p by TOR, Ure2p, and phosphatases. *J Biol Chem,* 275**,** 35727-33.

BOLAND, C. R., LUCIANI, M. G., GASCHE, C. & GOEL, A. 2005. Infection, inflammation, and gastrointestinal cancer. *Gut,* 54**,** 1321-31.

BOLDEN, J. E., PEART, M. J. & JOHNSTONE, R. W. 2006. Anticancer activities of histone deacetylase inhibitors. *Nat Rev Drug Discov,* 5**,** 769-84.

BORBELY, G., HALDOSEN, L. A., DAHLMAN-WRIGHT, K. & ZHAO, C. 2015. Induction of USP17 by combining BET and HDAC inhibitors in breast cancer cells. *Oncotarget,* 6**,** 33623-35.

BRENNAN, P., BOGILLOT, O., GREISER, E., CHANG-CLAUDE, J., WAHRENDORF, J., CORDIER, S., JOCKEL, K. H., LOPEZ-ABENTE, G., TZONOU, A., VINEIS, P., DONATO, F., HOURS, M., SERRA, C., BOLM-AUDORFF, U., SCHILL, W., KOGEVINAS, M. & BOFFETTA, P. 2001. The contribution of cigarette smoking to bladder cancer in women (pooled European data). *Cancer Causes Control,* 12**,** 411-7.

BREWIS, N. D., STREET, A. J., PRESCOTT, A. R. & COHEN, P. T. 1993. PPX, a novel protein serine/threonine phosphatase localized to centrosomes. *Embo j,* 12**,** 987-96.

BUNTING, S. F., CALLEN, E., WONG, N., CHEN, H. T., POLATO, F., GUNN, A., BOTHMER, A., FELDHAHN, N., FERNANDEZ-CAPETILLO, O., CAO, L., XU, X., DENG, C. X., FINKEL, T., NUSSENZWEIG, M., STARK, J. M. & NUSSENZWEIG,

A. 2010. 53BP1 inhibits homologous recombination in Brca1-deficient cells by blocking resection of DNA breaks. *Cell,* 141**,** 243-54.
BYUN, H. J., KIM, B. R., YOO, R., PARK, S. Y. & RHO, S. B. 2012. sMEK1 enhances gemcitabine anti-cancer activity through inhibition of phosphorylation of Akt/mTOR. *Apoptosis,* 17**,** 1095-103.
CHANG, W. H., CHOI, S. H., MOON, B. S., CAI, M., LYU, J., BAI, J., GAO, F., HAJJALI, I., ZHAO, Z., CAMPBELL, D. B., WEINER, L. P. & LU, W. 2017. Smek1/2 is a nuclear chaperone and cofactor for cleaved Wnt receptor Ryk, regulating cortical neurogenesis. *Proc Natl Acad Sci U S A,* 114**,** E10717-e10725.
CHAPPELL, C., HANAKAHI, L. A., KARIMI-BUSHERI, F., WEINFELD, M. & WEST, S. C. 2002. Involvement of human polynucleotide kinase in double-strand break repair by non-homologous end joining. *Embo j,* 21**,** 2827-32.
CHEN, J., GHAZAWI, F. M. & LI, Q. 2010. Interplay of bromodomain and histone acetylation in the regulation of p300-dependent genes. *Epigenetics,* 5**,** 509-15.
CHEN, Y. & ZHU, W. G. 2016. Biological function and regulation of histone and non-histone lysine methylation in response to DNA damage. *Acta Biochim Biophys Sin (Shanghai),* 48**,** 603-16.
CHENG, Z., TEO, G., KRUEGER, S., ROCK, T. M., KOH, H. W., CHOI, H. & VOGEL, C. 2016. Differential dynamics of the mammalian mRNA and protein expression response to misfolding stress. *Mol Syst Biol,* 12**,** 855.
CHOI, J. Y., KO, J. H. & JO, S. A. 2018. HDAC1 regulates the stability of glutamate carboxypeptidase II protein by modulating acetylation status of lysine 479 residue. *Biochem Biophys Res Commun,* 497**,** 416-423.
CHOUDHURY, A., NELSON, L. D., TEO, M. T., CHILKA, S., BHATTARAI, S., JOHNSTON, C. F., ELLIOTT, F., LOWERY, J., TAYLOR, C. F., CHURCHMAN, M., BENTLEY, J., KNOWLES, M. A., HARNDEN, P., BRISTOW, R. G., BISHOP, D. T. & KILTIE, A. E. 2010. MRE11 expression is predictive of cause-specific survival following radical radiotherapy for muscle-invasive bladder cancer. *Cancer Res,* 70**,** 7017-26.
CHOWDHURY, D., KEOGH, M. C., ISHII, H., PETERSON, C. L., BURATOWSKI, S. & LIEBERMAN, J. 2005. gamma-H2AX dephosphorylation by protein phosphatase 2A facilitates DNA double-strand break repair. *Mol Cell,* 20**,** 801-9.
CHOWDHURY, D., XU, X., ZHONG, X., AHMED, F., ZHONG, J., LIAO, J., DYKXHOORN, D. M., WEINSTOCK, D. M., PFEIFER, G. P. & LIEBERMAN, J. 2008. A PP4-phosphatase complex dephosphorylates gamma-H2AX generated during DNA replication. *Mol Cell,* 31**,** 33-46.
COHEN, P. T., PHILP, A. & VAZQUEZ-MARTIN, C. 2005. Protein phosphatase 4--from obscurity to vital functions. *FEBS Lett,* 579**,** 3278-86.
CRIVAT, G. & TARASKA, J. W. 2012. Imaging proteins inside cells with fluorescent tags. *Trends Biotechnol,* 30**,** 8-16.
DE RUIJTER, A. J., VAN GENNIP, A. H., CARON, H. N., KEMP, S. & VAN KUILENBURG, A. B. 2003. Histone deacetylases (HDACs): characterization of the classical HDAC family. *Biochem J,* 370**,** 737-49.
DE SCHUTTER, H. & NUYTS, S. 2009. Radiosensitizing potential of epigenetic anticancer drugs. *Anticancer Agents Med Chem,* 9**,** 99-108.
DECOTTIGNIES, A. 2013. Alternative end-joining mechanisms: a historical perspective. *Front Genet,* 4**,** 48.
DEFAZIO, L. G., STANSEL, R. M., GRIFFITH, J. D. & CHU, G. 2002. Synapsis of DNA ends by DNA-dependent protein kinase. *Embo j,* 21**,** 3192-200.
DELMORE, J. E., ISSA, G. C., LEMIEUX, M. E., RAHL, P. B., SHI, J., JACOBS, H. M., KASTRITIS, E., GILPATRICK, T., PARANAL, R. M., QI, J., CHESI, M., SCHINZEL, A. C., MCKEOWN, M. R., HEFFERNAN, T. P., VAKOC, C. R.,

BERGSAGEL, P. L., GHOBRIAL, I. M., RICHARDSON, P. G., YOUNG, R. A., HAHN, W. C., ANDERSON, K. C., KUNG, A. L., BRADNER, J. E. & MITSIADES, C. S. 2011. BET bromodomain inhibition as a therapeutic strategy to target c-Myc. *Cell,* 146**,** 904-17.

DEVAIAH, B. N., GEGONNE, A. & SINGER, D. S. 2016. Bromodomain 4: a cellular Swiss army knife. *J Leukoc Biol,* 100**,** 679-686.

DEXHEIMER, T. S. 2013. *DNA Repair of Cancer Stem Cells*, Springer.

DONG, S. M., BYUN, H. J., KIM, B. R., LEE, S. H., TRINK, B. & RHO, S. B. 2012. Tumor suppressor BLU enhances pro-apoptotic activity of sMEK1 through physical interaction. *Cell Signal,* 24**,** 1208-14.

ELIA, A. E., BOARDMAN, A. P., WANG, D. C., HUTTLIN, E. L., EVERLEY, R. A., DEPHOURE, N., ZHOU, C., KOREN, I., GYGI, S. P. & ELLEDGE, S. J. 2015. Quantitative Proteomic Atlas of Ubiquitination and Acetylation in the DNA Damage Response. *Mol Cell,* 59**,** 867-81.

ESCRIBANO-DIAZ, C., ORTHWEIN, A., FRADET-TURCOTTE, A., XING, M., YOUNG, J. T., TKAC, J., COOK, M. A., ROSEBROCK, A. P., MUNRO, M., CANNY, M. D., XU, D. & DUROCHER, D. 2013. A cell cycle-dependent regulatory circuit composed of 53BP1-RIF1 and BRCA1-CtIP controls DNA repair pathway choice. *Mol Cell,* 49**,** 872-83.

FALKENBERG, K. J. & JOHNSTONE, R. W. 2014. Histone deacetylases and their inhibitors in cancer, neurological diseases and immune disorders. *Nat Rev Drug Discov,* 13**,** 673-91.

FERGUSON, L. R., CHEN, H., COLLINS, A. R., CONNELL, M., DAMIA, G., DASGUPTA, S., MALHOTRA, M., MEEKER, A. K., AMEDEI, A., AMIN, A., ASHRAF, S. S., AQUILANO, K., AZMI, A. S., BHAKTA, D., BILSLAND, A., BOOSANI, C. S., CHEN, S., CIRIOLO, M. R., FUJII, H., GUHA, G., HALICKA, D., HELFERICH, W. G., KEITH, W. N., MOHAMMED, S. I., NICCOLAI, E., YANG, X., HONOKI, K., PARSLOW, V. R., PRAKASH, S., REZAZADEH, S., SHACKELFORD, R. E., SIDRANSKY, D., TRAN, P. T., YANG, E. S. & MAXWELL, C. A. 2015. Genomic instability in human cancer: Molecular insights and opportunities for therapeutic attack and prevention through diet and nutrition. *Semin Cancer Biol,* 35 Suppl**,** S5-s24.

FILIPPAKOPOULOS, P. & KNAPP, S. 2014. Targeting bromodomains: epigenetic readers of lysine acetylation. *Nat Rev Drug Discov,* 13**,** 337-56.

FILIPPAKOPOULOS, P., PICAUD, S., MANGOS, M., KEATES, T., LAMBERT, J. P., BARSYTE-LOVEJOY, D., FELLETAR, I., VOLKMER, R., MULLER, S., PAWSON, T., GINGRAS, A. C., ARROWSMITH, C. H. & KNAPP, S. 2012. Histone recognition and large-scale structural analysis of the human bromodomain family. *Cell,* 149**,** 214-31.

FIRSANOV, D. V., SOLOVJEVA, L. V. & SVETLOVA, M. P. 2011. H2AX phosphorylation at the sites of DNA double-strand breaks in cultivated mammalian cells and tissues. *Clin Epigenetics,* 2**,** 283-97.

FORGET, A. L. & KOWALCZYKOWSKI, S. C. 2010. Single-molecule imaging brings Rad51 nucleoprotein filaments into focus. *Trends Cell Biol,* 20**,** 269-76.

FREEMAN, A. K. & MONTEIRO, A. N. 2010. Phosphatases in the cellular response to DNA damage. *Cell Commun Signal,* 8**,** 27.

FU, L. L., TIAN, M., LI, X., LI, J. J., HUANG, J., OUYANG, L., ZHANG, Y. & LIU, B. 2015. Inhibition of BET bromodomains as a therapeutic strategy for cancer drug discovery. *Oncotarget,* 6**,** 5501-16.

FURDAS, S. D., KANNAN, S., SIPPL, W. & JUNG, M. 2012. Small molecule inhibitors of histone acetyltransferases as epigenetic tools and drug candidates. *Arch Pharm (Weinheim),* 345**,** 7-21.

GALLAGHER, D. J., FEIFER, A. & COLEMAN, J. A. 2010. Genitourinary cancer predisposition syndromes. *Hematol Oncol Clin North Am,* 24**,** 861-83.
GAVIN, A. C., BOSCHE, M., KRAUSE, R., GRANDI, P., MARZIOCH, M., BAUER, A., SCHULTZ, J., RICK, J. M., MICHON, A. M., CRUCIAT, C. M., REMOR, M., HOFERT, C., SCHELDER, M., BRAJENOVIC, M., RUFFNER, H., MERINO, A., KLEIN, K., HUDAK, M., DICKSON, D., RUDI, T., GNAU, V., BAUCH, A., BASTUCK, S., HUHSE, B., LEUTWEIN, C., HEURTIER, M. A., COPLEY, R. R., EDELMANN, A., QUERFURTH, E., RYBIN, V., DREWES, G., RAIDA, M., BOUWMEESTER, T., BORK, P., SERAPHIN, B., KUSTER, B., NEUBAUER, G. & SUPERTI-FURGA, G. 2002. Functional organization of the yeast proteome by systematic analysis of protein complexes. *Nature,* 415**,** 141-7.
GINGRAS, A. C., CABALLERO, M., ZARSKE, M., SANCHEZ, A., HAZBUN, T. R., FIELDS, S., SONENBERG, N., HAFEN, E., RAUGHT, B. & AEBERSOLD, R. 2005. A novel, evolutionarily conserved protein phosphatase complex involved in cisplatin sensitivity. *Mol Cell Proteomics,* 4**,** 1725-40.
GLOZAK, M. A., SENGUPTA, N., ZHANG, X. & SETO, E. 2005. Acetylation and deacetylation of non-histone proteins. *Gene,* 363**,** 15-23.
GLOZAK, M. A. & SETO, E. 2007. Histone deacetylases and cancer. *Oncogene,* 26**,** 5420-32.
GNAD, F., GUNAWARDENA, J. & MANN, M. 2011. PHOSIDA 2011: the posttranslational modification database. *Nucleic Acids Res,* 39**,** D253-60.
GONG, F. & MILLER, K. M. 2013. Mammalian DNA repair: HATs and HDACs make their mark through histone acetylation. *Mutat Res,* 750**,** 23-30.
GOTTLICH, B., REICHENBERGER, S., FELDMANN, E. & PFEIFFER, P. 1998. Rejoining of DNA double-strand breaks in vitro by single-strand annealing. *Eur J Biochem,* 258**,** 387-95.
GROSELJ, B., KERR, M. & KILTIE, A. E. 2013. Radiosensitisation of bladder cancer cells by panobinostat is modulated by Ku80 expression. *Radiother Oncol,* 108**,** 429-33.
GRUNDY, G. J., RULTEN, S. L., ZENG, Z., ARRIBAS-BOSACOMA, R., ILES, N., MANLEY, K., OLIVER, A. & CALDECOTT, K. W. 2013. APLF promotes the assembly and activity of non-homologous end joining protein complexes. *Embo j,* 32**,** 112-25.
GU, W. & ROEDER, R. G. 1997. Activation of p53 sequence-specific DNA binding by acetylation of the p53 C-terminal domain. *Cell,* 90**,** 595-606.
HAINCE, J. F., MCDONALD, D., RODRIGUE, A., DERY, U., MASSON, J. Y., HENDZEL, M. J. & POIRIER, G. G. 2008. PARP1-dependent kinetics of recruitment of MRE11 and NBS1 proteins to multiple DNA damage sites. *J Biol Chem,* 283**,** 1197-208.
HALAZONETIS, T. D., GORGOULIS, V. G. & BARTEK, J. 2008. An oncogene-induced DNA damage model for cancer development. *Science,* 319**,** 1352-5.
HANAHAN, D. & WEINBERG, R. A. 2011. Hallmarks of cancer: the next generation. *Cell,* 144**,** 646-74.
HARPER, J. W. & ELLEDGE, S. J. 2007. The DNA damage response: ten years after. *Mol Cell,* 28**,** 739-45.
HOLSCHER, A. S., SCHULZ, W. A., PINKERNEIL, M., NIEGISCH, G. & HOFFMANN, M. J. 2018. Combined inhibition of BET proteins and class I HDACs synergistically induces apoptosis in urothelial carcinoma cell lines. *Clin Epigenetics,* 10**,** 1.
HUANG, X., CHENG, A. & HONKANEN, R. E. 1997. Genomic organization of the human PP4 gene encoding a serine/threonine protein phosphatase (PP4) suggests a common ancestry with PP2A. *Genomics,* 44**,** 336-43.
IP, S. C., RASS, U., BLANCO, M. G., FLYNN, H. R., SKEHEL, J. M. & WEST, S. C. 2008. Identification of Holliday junction resolvases from humans and yeast. *Nature,* 456**,** 357-61.

JAMES, N. D., HUSSAIN, S. A., HALL, E., JENKINS, P., TREMLETT, J., RAWLINGS, C., CRUNDWELL, M., SIZER, B., SREENIVASAN, T., HENDRON, C., LEWIS, R., WATERS, R. & HUDDART, R. A. 2012. Radiotherapy with or without chemotherapy in muscle-invasive bladder cancer. *N Engl J Med,* 366**,** 1477-88.

JEGGO, P. & O'NEILL, P. 2002. The Greek Goddess, Artemis, reveals the secrets of her cleavage. *DNA Repair (Amst),* 1**,** 771-7.

JUNG, K. H., NOH, J. H., KIM, J. K., EUN, J. W., BAE, H. J., XIE, H. J., CHANG, Y. G., KIM, M. G., PARK, H., LEE, J. Y. & NAM, S. W. 2012. HDAC2 overexpression confers oncogenic potential to human lung cancer cells by deregulating expression of apoptosis and cell cycle proteins. *J Cell Biochem,* 113**,** 2167-77.

JUNQUEIRA-NETO, S., VIEIRA, F. Q., MONTEZUMA, D., COSTA, N. R., ANTUNES, L., BAPTISTA, T., OLIVEIRA, A. I., GRACA, I., RODRIGUES, A., MAGALHAES, J. S., OLIVEIRA, J., HENRIQUE, R. & JERONIMO, C. 2015. Phenotypic impact of deregulated expression of class I histone deacetylases in urothelial cell carcinoma of the bladder. *Mol Carcinog,* 54**,** 523-31.

KAO, G. D., MCKENNA, W. G., GUENTHER, M. G., MUSCHEL, R. J., LAZAR, M. A. & YEN, T. J. 2003. Histone deacetylase 4 interacts with 53BP1 to mediate the DNA damage response. *J Cell Biol,* 160**,** 1017-27.

KEOGH, M. C., KIM, J. A., DOWNEY, M., FILLINGHAM, J., CHOWDHURY, D., HARRISON, J. C., ONISHI, M., DATTA, N., GALICIA, S., EMILI, A., LIEBERMAN, J., SHEN, X., BURATOWSKI, S., HABER, J. E., DUROCHER, D., GREENBLATT, J. F. & KROGAN, N. J. 2006. A phosphatase complex that dephosphorylates gammaH2AX regulates DNA damage checkpoint recovery. *Nature,* 439**,** 497-501.

KHANNA, K. K. & JACKSON, S. P. 2001. DNA double-strand breaks: signaling, repair and the cancer connection. *Nat Genet,* 27**,** 247-54.

KIM, B. R., SEO, S. H., PARK, M. S., LEE, S. H., KWON, Y. & RHO, S. B. 2015. sMEK1 inhibits endothelial cell proliferation by attenuating VEGFR-2-dependent-Akt/eNOS/HIF-1alpha signaling pathways. *Oncotarget,* 6**,** 31830-43.

KIM, G. D., CHOI, Y. H., DIMTCHEV, A., JEONG, S. J., DRITSCHILO, A. & JUNG, M. 1999. Sensing of ionizing radiation-induced DNA damage by ATM through interaction with histone deacetylase. *J Biol Chem,* 274**,** 31127-30.

KIRKALI, Z., CHAN, T., MANOHARAN, M., ALGABA, F., BUSCH, C., CHENG, L., KIEMENEY, L., KRIEGMAIR, M., MONTIRONI, R., MURPHY, W. M., SESTERHENN, I. A., TACHIBANA, M. & WEIDER, J. 2005. Bladder cancer: epidemiology, staging and grading, and diagnosis. *Urology,* 66**,** 4-34.

KLOEKER, S. & WADZINSKI, B. E. 1999. Purification and identification of a novel subunit of protein serine/threonine phosphatase 4. *J Biol Chem,* 274**,** 5339-47.

KOTWAL, S., CHOUDHURY, A., JOHNSTON, C., PAUL, A. B., WHELAN, P. & KILTIE, A. E. 2008. Similar treatment outcomes for radical cystectomy and radical radiotherapy in invasive bladder cancer treated at a United Kingdom specialist treatment center. *Int J Radiat Oncol Biol Phys,* 70**,** 456-63.

LAGGER, G., O'CARROLL, D., REMBOLD, M., KHIER, H., TISCHLER, J., WEITZER, G., SCHUETTENGRUBER, B., HAUSER, C., BRUNMEIR, R., JENUWEIN, T. & SEISER, C. 2002. Essential function of histone deacetylase 1 in proliferation control and CDK inhibitor repression. *Embo j,* 21**,** 2672-81.

LEE, J. H., CHOY, M. L., NGO, L., FOSTER, S. S. & MARKS, P. A. 2010. Histone deacetylase inhibitor induces DNA damage, which normal but not transformed cells can repair. *Proc Natl Acad Sci U S A,* 107**,** 14639-44.

LEE, K. J., SAHA, J., SUN, J., FATTAH, K. R., WANG, S. C., JAKOB, B., CHI, L., WANG, S. Y., TAUCHER-SCHOLZ, G., DAVIS, A. J. & CHEN, D. J. 2016. Phosphorylation

of Ku dictates DNA double-strand break (DSB) repair pathway choice in S phase. *Nucleic Acids Res,* 44**,** 1732-45.

LESSEL, D., VAZ, B., HALDER, S., LOCKHART, P. J., MARINOVIC-TERZIC, I., LOPEZ-MOSQUEDA, J., PHILIPP, M., SIM, J. C., SMITH, K. R., OEHLER, J., CABRERA, E., FREIRE, R., POPE, K., NAHID, A., NORRIS, F., LEVENTER, R. J., DELATYCKI, M. B., BARBI, G., VON AMELN, S., HOGEL, J., DEGORICIJA, M., FERTIG, R., BURKHALTER, M. D., HOFMANN, K., THIELE, H., ALTMULLER, J., NURNBERG, G., NURNBERG, P., BAHLO, M., MARTIN, G. M., AALFS, C. M., OSHIMA, J., TERZIC, J., AMOR, D. J., DIKIC, I., RAMADAN, K. & KUBISCH, C. 2014. Mutations in SPRTN cause early onset hepatocellular carcinoma, genomic instability and progeroid features. *Nat Genet,* 46**,** 1239-44.

LIEBER, M. R., LU, H., GU, J. & SCHWARZ, K. 2008. Flexibility in the order of action and in the enzymology of the nuclease, polymerases, and ligase of vertebrate non-homologous DNA end joining: relevance to cancer, aging, and the immune system. *Cell Res,* 18**,** 125-33.

LIN, K. T., YEH, S. H., CHEN, D. S., CHEN, P. J. & JOU, Y. S. 2005. Epigenetic activation of alpha4, beta2 and beta6 integrins involved in cell migration in trichostatin A-treated Hep3B cells. *J Biomed Sci,* 12**,** 803-13.

LINDAHL, T. & BARNES, D. E. 2000. Repair of endogenous DNA damage. *Cold Spring Harb Symp Quant Biol,* 65**,** 127-33.

LINDOR, N. M., MCMASTER, M. L., LINDOR, C. J. & GREENE, M. H. 2008. Concise handbook of familial cancer susceptibility syndromes - second edition. *J Natl Cancer Inst Monogr***,** 1-93.

LINGER, J. G. & TYLER, J. K. 2007. Chromatin disassembly and reassembly during DNA repair. *Mutat Res,* 618**,** 52-64.

LIU, C., SRIHARI, S., CAO, K. A., CHENEVIX-TRENCH, G., SIMPSON, P. T., RAGAN, M. A. & KHANNA, K. K. 2014. A fine-scale dissection of the DNA double-strand break repair machinery and its implications for breast cancer therapy. *Nucleic Acids Res,* 42**,** 6106-27.

LOBRICH, M., SHIBATA, A., BEUCHER, A., FISHER, A., ENSMINGER, M., GOODARZI, A. A., BARTON, O. & JEGGO, P. A. 2010. gammaH2AX foci analysis for monitoring DNA double-strand break repair: strengths, limitations and optimization. *Cell Cycle,* 9**,** 662-9.

LOEB, L. A., SPRINGGATE, C. F. & BATTULA, N. 1974. Errors in DNA replication as a basis of malignant changes. *Cancer Res,* 34**,** 2311-21.

LOSSON, H., SCHNEKENBURGER, M., DICATO, M. & DIEDERICH, M. 2016. Natural Compound Histone Deacetylase Inhibitors (HDACi): Synergy with Inflammatory Signaling Pathway Modulators and Clinical Applications in Cancer. *Molecules,* 21.

LUIJSTERBURG, M. S., ACS, K., ACKERMANN, L., WIEGANT, W. W., BEKKER-JENSEN, S., LARSEN, D. H., KHANNA, K. K., VAN ATTIKUM, H., MAILAND, N. & DANTUMA, N. P. 2012. A new non-catalytic role for ubiquitin ligase RNF8 in unfolding higher-order chromatin structure. *Embo j,* 31**,** 2511-27.

MADHURANTAKAM, C., VARADAMSETTY, G., GRUTTER, M. G., PLUCKTHUN, A. & MITTL, P. R. 2012. Structure-based optimization of designed Armadillo-repeat proteins. *Protein Sci,* 21**,** 1015-28.

MAILAND, N., BEKKER-JENSEN, S., FAUSTRUP, H., MELANDER, F., BARTEK, J., LUKAS, C. & LUKAS, J. 2007. RNF8 ubiquitylates histones at DNA double-strand breaks and promotes assembly of repair proteins. *Cell,* 131**,** 887-900.

MARKS, P., RIFKIND, R. A., RICHON, V. M., BRESLOW, R., MILLER, T. & KELLY, W. K. 2001. Histone deacetylases and cancer: causes and therapies. *Nat Rev Cancer,* 1**,** 194-202.

MARTIN, R. M., KERR, M., TEO, M. T., JEVONS, S. J., KORITZINSKY, M., WOUTERS, B. G., BHATTARAI, S. & KILTIE, A. E. 2014. Post-transcriptional regulation of MRE11 expression in muscle-invasive bladder tumours. *Oncotarget,* 5**,** 993-1003.
MARTINEZ-BALBAS, M. A., BAUER, U. M., NIELSEN, S. J., BREHM, A. & KOUZARIDES, T. 2000. Regulation of E2F1 activity by acetylation. *Embo j,* 19**,** 662-71.
MCCULLOCH, S. D. & KUNKEL, T. A. 2008. The fidelity of DNA synthesis by eukaryotic replicative and translesion synthesis polymerases. *Cell Res,* 18**,** 148-61.
MCILWRAITH, M. J., VAISMAN, A., LIU, Y., FANNING, E., WOODGATE, R. & WEST, S. C. 2005. Human DNA polymerase eta promotes DNA synthesis from strand invasion intermediates of homologous recombination. *Mol Cell,* 20**,** 783-92.
MIHINDUKULASURIYA, K. A., ZHOU, G., QIN, J. & TAN, T. H. 2004b. Protein phosphatase 4 interacts with and down-regulates insulin receptor substrate 4 following tumor necrosis factor-alpha stimulation. *J Biol Chem,* 279**,** 46588-94.
MIMITOU, E. P. & SYMINGTON, L. S. 2009. Nucleases and helicases take center stage in homologous recombination. *Trends Biochem Sci,* 34**,** 264-72.
MISHINA, Y., DUGUID, E. M. & HE, C. 2006. Direct reversal of DNA alkylation damage. *Chem Rev,* 106**,** 215-32.
MISHRA, V. K., WEGWITZ, F., KOSINSKY, R. L., SEN, M., BAUMGARTNER, R., WULFF, T., SIVEKE, J. T., SCHILDHAUS, H. U., NAJAFOVA, Z., KARI, V., KOHLHOF, H., HESSMANN, E. & JOHNSEN, S. A. 2017. Histone deacetylase class-I inhibition promotes epithelial gene expression in pancreatic cancer cells in a BRD4- and MYC-dependent manner. *Nucleic Acids Res,* 45**,** 6334-6349.
MOTYCKA, T. A., BESSHO, T., POST, S. M., SUNG, P. & TOMKINSON, A. E. 2004. Physical and functional interaction between the XPF/ERCC1 endonuclease and hRad52. *J Biol Chem,* 279**,** 13634-9.
MOURTADA-MAARABOUNI, M. & WILLIAMS, G. T. 2008. Protein phosphatase 4 regulates apoptosis, proliferation and mutation rate of human cells. *Biochim Biophys Acta,* 1783**,** 1490-502.
MUNOZ, M. C., LAULIER, C., GUNN, A., CHENG, A., ROBBIANI, D. F., NUSSENZWEIG, A. & STARK, J. M. 2012. RING finger nuclear factor RNF168 is important for defects in homologous recombination caused by loss of the breast cancer susceptibility factor BRCA1. *J Biol Chem,* 287**,** 40618-28.
MUNSHI, A., HOBBS, M. & MEYN, R. E. 2005. Clonogenic cell survival assay. *Methods Mol Med,* 110**,** 21-8.
NAKADA, S., CHEN, G. I., GINGRAS, A. C. & DUROCHER, D. 2008. PP4 is a gamma H2AX phosphatase required for recovery from the DNA damage checkpoint. *EMBO Rep,* 9**,** 1019-26.
NAKANISHI, K., CAVALLO, F., BRUNET, E. & JASIN, M. 2011. Homologous recombination assay for interstrand cross-link repair. *Methods Mol Biol,* 745**,** 283-91.
NETWORK, C. G. A. R. 2014. Comprehensive molecular characterization of urothelial bladder carcinoma. *Nature,* 507**,** 315-22.
NICHOLSON, J., JEVONS, S. J., GROSELJ, B., ELLERMANN, S., KONIETZNY, R., KERR, M., KESSLER, B. M. & KILTIE, A. E. 2017. E3 Ligase cIAP2 Mediates Downregulation of MRE11 and Radiosensitization in Response to HDAC Inhibition in Bladder Cancer. *Cancer Res,* 77**,** 3027-3039.
NICHOLSON, J., VENDRELL, I., YEO, X. Y., KESSLER, B. M. & KILTIE, A. E. submitted. Identification and Validation of Non-Histone Acetylation Sites and Their Regulation of the DNA Damage Response.
NICK MCELHINNY, S. A., HAVENER, J. M., GARCIA-DIAZ, M., JUAREZ, R., BEBENEK, K., KEE, B. L., BLANCO, L., KUNKEL, T. A. & RAMSDEN, D. A.

2005. A gradient of template dependence defines distinct biological roles for family X polymerases in nonhomologous end joining. *Mol Cell,* 19**,** 357-66.
NIEGISCH, G., KNIEVEL, J., KOCH, A., HADER, C., FISCHER, U., ALBERS, P. & SCHULZ, W. A. 2013. Changes in histone deacetylase (HDAC) expression patterns and activity of HDAC inhibitors in urothelial cancers. *Urol Oncol,* 31**,** 1770-9.
NIMONKAR, A. V., OZSOY, A. Z., GENSCHEL, J., MODRICH, P. & KOWALCZYKOWSKI, S. C. 2008. Human exonuclease 1 and BLM helicase interact to resect DNA and initiate DNA repair. *Proc Natl Acad Sci U S A,* 105**,** 16906-11.
NISHI, R., WIJNHOVEN, P., LE SAGE, C., TJEERTES, J., GALANTY, Y., FORMENT, J. V., CLAGUE, M. J., URBE, S. & JACKSON, S. P. 2014. Systematic characterization of deubiquitylating enzymes for roles in maintaining genome integrity. *Nat Cell Biol,* 16**,** 1016-26, 1-8.
NOWELL, P. C. 1976. The clonal evolution of tumor cell populations. *Science,* 194**,** 23-8.
OCHI, T., BLACKFORD, A. N., COATES, J., JHUJH, S., MEHMOOD, S., TAMURA, N., TRAVERS, J., WU, Q., DRAVIAM, V. M., ROBINSON, C. V., BLUNDELL, T. L. & JACKSON, S. P. 2015. DNA repair. PAXX, a paralog of XRCC4 and XLF, interacts with Ku to promote DNA double-strand break repair. *Science,* 347**,** 185-188.
OLIVE, P. L. 2011. Retention of gammaH2AX foci as an indication of lethal DNA damage. *Radiother Oncol,* 101**,** 18-23.
PAUL, K., WANG, M., MLADENOV, E., BENCSIK-THEILEN, A., BEDNAR, T., WU, W., ARAKAWA, H. & ILIAKIS, G. 2013. DNA ligases I and III cooperate in alternative non-homologous end-joining in vertebrates. *PLoS One,* 8**,** e59505.
PEARL, L. H., SCHIERZ, A. C., WARD, S. E., AL-LAZIKANI, B. & PEARL, F. M. 2015. Therapeutic opportunities within the DNA damage response. *Nat Rev Cancer,* 15**,** 166-80.
PICAUD, S., LEONARDS, K., LAMBERT, J. P., DOVEY, O., WELLS, C., FEDOROV, O., MONTEIRO, O., FUJISAWA, T., WANG, C. Y., LINGARD, H., TALLANT, C., NIKBIN, N., GUETZOYAN, L., INGHAM, R., LEY, S. V., BRENNAN, P., MULLER, S., SAMSONOVA, A., GINGRAS, A. C., SCHWALLER, J., VASSILIOU, G., KNAPP, S. & FILIPPAKOPOULOS, P. 2016. Promiscuous targeting of bromodomains by bromosporine identifies BET proteins as master regulators of primary transcription response in leukemia. *Sci Adv,* 2**,** e1600760.
REDON, C. E., DICKEY, J. S., BONNER, W. M. & SEDELNIKOVA, O. A. 2009. gamma-H2AX as a biomarker of DNA damage induced by ionizing radiation in human peripheral blood lymphocytes and artificial skin. *Adv Space Res,* 43**,** 1171-1178.
RENODON-CORNIÈRE, A., WEIGEL, P., BRETON, M. L. & F., F. 2013. New Potential Therapeutic Approaches by Targeting Rad51- Dependent Homologous Recombination. IntechOpen.
ROGAKOU, E. P., PILCH, D. R., ORR, A. H., IVANOVA, V. S. & BONNER, W. M. 1998. DNA double-stranded breaks induce histone H2AX phosphorylation on serine 139. *J Biol Chem,* 273**,** 5858-68.
RONNE, H., CARLBERG, M., HU, G. Z. & NEHLIN, J. O. 1991. Protein phosphatase 2A in Saccharomyces cerevisiae: effects on cell growth and bud morphogenesis. *Mol Cell Biol,* 11**,** 4876-84.
ROTHENBERG, E., GRIMME, J. M., SPIES, M. & HA, T. 2008. Human Rad52-mediated homology search and annealing occurs by continuous interactions between overlapping nucleoprotein complexes. *Proc Natl Acad Sci U S A,* 105**,** 20274-9.
SARTORI, A. A., LUKAS, C., COATES, J., MISTRIK, M., FU, S., BARTEK, J., BAER, R., LUKAS, J. & JACKSON, S. P. 2007. Human CtIP promotes DNA end resection. *Nature,* 450**,** 509-14.
SCUTO, A., KIRSCHBAUM, M., KOWOLIK, C., KRETZNER, L., JUHASZ, A., ATADJA, P., PULLARKAT, V., BHATIA, R., FORMAN, S., YEN, Y. & JOVE, R. 2008. The

novel histone deacetylase inhibitor, LBH589, induces expression of DNA damage response genes and apoptosis in Ph- acute lymphoblastic leukemia cells. *Blood,* 111**,** 5093-100.

SEKI, M., NAKAGAWA, T., SEKI, T., KATO, G., TADA, S., TAKAHASHI, Y., YOSHIMURA, A., KOBAYASHI, T., AOKI, A., OTSUKI, M., HABERMANN, F. A., TANABE, H., ISHII, Y. & ENOMOTO, T. 2006. Bloom helicase and DNA topoisomerase IIIalpha are involved in the dissolution of sister chromatids. *Mol Cell Biol,* 26**,** 6299-307.

SENESE, S., ZARAGOZA, K., MINARDI, S., MURADORE, I., RONZONI, S., PASSAFARO, A., BERNARD, L., DRAETTA, G. F., ALCALAY, M., SEISER, C. & CHIOCCA, S. 2007. Role for histone deacetylase 1 in human tumor cell proliferation. *Mol Cell Biol,* 27**,** 4784-95.

SHAHBAZI, J., LIU, P. Y., ATMADIBRATA, B., BRADNER, J. E., MARSHALL, G. M., LOCK, R. B. & LIU, T. 2016. The Bromodomain Inhibitor JQ1 and the Histone Deacetylase Inhibitor Panobinostat Synergistically Reduce N-Myc Expression and Induce Anticancer Effects. *Clin Cancer Res,* 22**,** 2534-44.

SHAO, M., HE, L., ZHENG, L., HUANG, L., ZHOU, Y., WANG, T., CHEN, Y., SHEN, M., WANG, F., YANG, Z. & CHEN, L. 2017. Structure-based design, synthesis and in vitro antiproliferative effects studies of novel dual BRD4/HDAC inhibitors. *Bioorg Med Chem Lett,* 27**,** 4051-4055.

SHARMA, S., JAVADEKAR, S. M., PANDEY, M., SRIVASTAVA, M., KUMARI, R. & RAGHAVAN, S. C. 2015. Homology and enzymatic requirements of microhomology-dependent alternative end joining. *Cell Death Dis,* 6**,** e1697.

SHIBATA, A., MOIANI, D., ARVAI, A. S., PERRY, J., HARDING, S. M., GENOIS, M. M., MAITY, R., VAN ROSSUM-FIKKERT, S., KERTOKALIO, A., ROMOLI, F., ISMAIL, A., ISMALAJ, E., PETRICCI, E., NEALE, M. J., BRISTOW, R. G., MASSON, J. Y., WYMAN, C., JEGGO, P. A. & TAINER, J. A. 2014. DNA double-strand break repair pathway choice is directed by distinct MRE11 nuclease activities. *Mol Cell,* 53**,** 7-18.

STARK, C., BREITKREUTZ, B. J., REGULY, T., BOUCHER, L., BREITKREUTZ, A. & TYERS, M. 2006. BioGRID: a general repository for interaction datasets. *Nucleic Acids Res,* 34**,** D535-9.

STARK, J. M., PIERCE, A. J., OH, J., PASTINK, A. & JASIN, M. 2004. Genetic steps of mammalian homologous repair with distinct mutagenic consequences. *Mol Cell Biol,* 24**,** 9305-16.

STENZL, A., COWAN, N. C., DE SANTIS, M., KUCZYK, M. A., MERSEBURGER, A. S., RIBAL, M. J., SHERIF, A. & WITJES, J. A. 2011. Treatment of muscle-invasive and metastatic bladder cancer: update of the EAU guidelines. *Eur Urol,* 59**,** 1009-18.

STUCKI, M., CLAPPERTON, J. A., MOHAMMAD, D., YAFFE, M. B., SMERDON, S. J. & JACKSON, S. P. 2005. MDC1 directly binds phosphorylated histone H2AX to regulate cellular responses to DNA double-strand breaks. *Cell,* 123**,** 1213-26.

SUBRAMANIAN, C., HADA, M., OPIPARI, A. W., JR., CASTLE, V. P. & KWOK, R. P. 2013. CREB-binding protein regulates Ku70 acetylation in response to ionization radiation in neuroblastoma. *Mol Cancer Res,* 11**,** 173-81.

TAMKUN, J. W., DEURING, R., SCOTT, M. P., KISSINGER, M., PATTATUCCI, A. M., KAUFMAN, T. C. & KENNISON, J. A. 1992. brahma: a regulator of Drosophila homeotic genes structurally related to the yeast transcriptional activator SNF2/SWI2. *Cell,* 68**,** 561-72.

TEO, G., VOGEL, C., GHOSH, D., KIM, S. & CHOI, H. 2014. PECA: a novel statistical tool for deconvoluting time-dependent gene expression regulation. *J Proteome Res,* 13**,** 29-37.

TRUONG, L. N., LI, Y., SHI, L. Z., HWANG, P. Y., HE, J., WANG, H., RAZAVIAN, N., BERNS, M. W. & WU, X. 2013. Microhomology-mediated End Joining and Homologous Recombination share the initial end resection step to repair DNA double-strand breaks in mammalian cells. *Proc Natl Acad Sci U S A,* 110**,** 7720-5.

VENKATARAMAN, S., ALIMOVA, I., BALAKRISHNAN, I., HARRIS, P., BIRKS, D. K., GRIESINGER, A., AMANI, V., CRISTIANO, B., REMKE, M., TAYLOR, M. D., HANDLER, M., FOREMAN, N. K. & VIBHAKAR, R. 2014. Inhibition of BRD4 attenuates tumor cell self-renewal and suppresses stem cell signaling in MYC driven medulloblastoma. *Oncotarget,* 5**,** 2355-71.

VIRSHUP, D. M. & SHENOLIKAR, S. 2009. From promiscuity to precision: protein phosphatases get a makeover. *Mol Cell,* 33**,** 537-45.

WALKER, J. R., CORPINA, R. A. & GOLDBERG, J. 2001. Structure of the Ku heterodimer bound to DNA and its implications for double-strand break repair. *Nature,* 412**,** 607-14.

WANG, H., WANG, M., BOCKER, W. & ILIAKIS, G. 2005. Complex H2AX phosphorylation patterns by multiple kinases including ATM and DNA-PK in human cells exposed to ionizing radiation and treated with kinase inhibitors. *J Cell Physiol,* 202**,** 492-502.

WEICHERT, W., ROSKE, A., GEKELER, V., BECKERS, T., EBERT, M. P., PROSS, M., DIETEL, M., DENKERT, C. & ROCKEN, C. 2008a. Association of patterns of class I histone deacetylase expression with patient prognosis in gastric cancer: a retrospective analysis. *Lancet Oncol,* 9**,** 139-48.

WEICHERT, W., ROSKE, A., GEKELER, V., BECKERS, T., STEPHAN, C., JUNG, K., FRITZSCHE, F. R., NIESPOREK, S., DENKERT, C., DIETEL, M. & KRISTIANSEN, G. 2008b. Histone deacetylases 1, 2 and 3 are highly expressed in prostate cancer and HDAC2 expression is associated with shorter PSA relapse time after radical prostatectomy. *Br J Cancer,* 98**,** 604-10.

WEICHERT, W., ROSKE, A., NIESPOREK, S., NOSKE, A., BUCKENDAHL, A. C., DIETEL, M., GEKELER, V., BOEHM, M., BECKERS, T. & DENKERT, C. 2008c. Class I histone deacetylase expression has independent prognostic impact in human colorectal cancer: specific role of class I histone deacetylases in vitro and in vivo. *Clin Cancer Res,* 14**,** 1669-77.

WRIGHT, W. D. & HEYER, W. D. 2014. Rad54 functions as a heteroduplex DNA pump modulated by its DNA substrates and Rad51 during D loop formation. *Mol Cell,* 53**,** 420-32.

WU, S. Y., LEE, A. Y., LAI, H. T., ZHANG, H. & CHIANG, C. M. 2013. Phospho switch triggers Brd4 chromatin binding and activator recruitment for gene-specific targeting. *Mol Cell,* 49**,** 843-57.

WU, X., LIU, D., TAO, D., XIANG, W., XIAO, X., WANG, M., WANG, L., LUO, G., LI, Y., ZENG, F. & JIANG, G. 2016. BRD4 Regulates EZH2 Transcription through Upregulation of C-MYC and Represents a Novel Therapeutic Target in Bladder Cancer. *Mol Cancer Ther,* 15**,** 1029-42.

XIE, A., HARTLERODE, A., STUCKI, M., ODATE, S., PUGET, N., KWOK, A., NAGARAJU, G., YAN, C., ALT, F. W., CHEN, J., JACKSON, S. P. & SCULLY, R. 2007. Distinct roles of chromatin-associated proteins MDC1 and 53BP1 in mammalian double-strand break repair. *Mol Cell,* 28**,** 1045-57.

YAMAGUCHI, T., CUBIZOLLES, F., ZHANG, Y., REICHERT, N., KOHLER, H., SEISER, C. & MATTHIAS, P. 2010. Histone deacetylases 1 and 2 act in concert to promote the G1-to-S progression. *Genes Dev,* 24**,** 455-69.

YAN, Y., YANG, F. Q., ZHANG, H. M., LI, J., LI, W., WANG, G. C., CHE, J. P., ZHENG, J. H. & LIU, M. 2014. Bromodomain 4 protein is a predictor of survival for urothelial carcinoma of bladder. *Int J Clin Exp Pathol,* 7**,** 4231-8.

YOO, S. & DYNAN, W. S. 1999. Geometry of a complex formed by double strand break repair proteins at a single DNA end: recruitment of DNA-PKcs induces inward translocation of Ku protein. *Nucleic Acids Res,* 27**,** 4679-86.

YOON, Y. S., LEE, M. W., RYU, D., KIM, J. H., MA, H., SEO, W. Y., KIM, Y. N., KIM, S. S., LEE, C. H., HUNTER, T., CHOI, C. S., MONTMINY, M. R. & KOO, S. H. 2010. Suppressor of MEK null (SMEK)/protein phosphatase 4 catalytic subunit (PP4C) is a key regulator of hepatic gluconeogenesis. *Proc Natl Acad Sci U S A,* 107**,** 17704-9.

ZHANG, F., FAN, Q., REN, K. & ANDREASSEN, P. R. 2009. PALB2 functionally connects the breast cancer susceptibility proteins BRCA1 and BRCA2. *Mol Cancer Res,* 7**,** 1110-8.

ZHANG, X., OZAWA, Y., LEE, H., WEN, Y. D., TAN, T. H., WADZINSKI, B. E. & SETO, E. 2005. Histone deacetylase 3 (HDAC3) activity is regulated by interaction with protein serine/threonine phosphatase 4. *Genes Dev,* 19**,** 827-39.

ZHAO, Z. F., WANG, K., GUO, F. F. & LU, H. 2017. Inhibition of T24 and RT4 Human Bladder Cancer Cell Lines by Heterocyclic Molecules. *Med Sci Monit,* 23**,** 1156-1164.

ZHOU, G., MIHINDUKULASURIYA, K. A., MACCORKLE-CHOSNEK, R. A., VAN HOOSER, A., HU, M. C., BRINKLEY, B. R. & TAN, T. H. 2002. Protein phosphatase 4 is involved in tumor necrosis factor-alpha-induced activation of c-Jun N-terminal kinase. *J Biol Chem,* 277**,** 6391-8.

ZUBER, J., SHI, J., WANG, E., RAPPAPORT, A. R., HERRMANN, H., SISON, E. A., MAGOON, D., QI, J., BLATT, K., WUNDERLICH, M., TAYLOR, M. J., JOHNS, C., CHICAS, A., MULLOY, J. C., KOGAN, S. C., BROWN, P., VALENT, P., BRADNER, J. E., LOWE, S. W. & VAKOC, C. R. 2011. RNAi screen identifies Brd4 as a therapeutic target in acute myeloid leukaemia. *Nature,* 478**,** 524-8.